THESIS

STUDY OF EXHAUST GAS RECIRCULATION (EGR) ON THE OPERATION OF LIQUID-FUELED GAS TURBINES

Submitted by

Kingsley Essuman Atomboh

Department of Mechanical Engineering

In partial fulfillment of the requirements

For the Degree of Master of Science

Colorado State University

Fort Collins, Colorado

Summer 2025

Master's Committee:

Advisor: Bret C. Windom

Todd Bandhauer
Dan Wise
Daniel Herber

ABSTRACT

STUDY OF EXHAUST GAS RECIRCULATION (EGR) ON THE OPERATION OF LIQUID-FUELED GAS TURBINES

Gas turbines, one of the main producers of electricity, and propulsion for transportation, are significant contributors to the US greenhouse gas (GHG) inventory. The goal of this thesis is to study the process of removing GHGs (i.e., CO_2) from industrial/marine propulsion scale gas turbines by leveraging carbon capture while maintaining low NOx and CO emissions. Recirculating the exhaust gas back into the intake of the gas turbine, in a process termed Exhaust Gas Recirculation (EGR) poses a pathway to reduce the scale of industrial and shipboard carbon capture and storage, where weight, space, power, and cost are significant constraints, by enriching the CO_2 concentration in the exhaust. However, the amount of EGR and the associated exhaust CO_2 concentrations are limited by the onset of combustion instabilities. This occurs because EGR displaces intake air with oxygen-depleted exhaust, reducing the oxygen available for stable and efficient combustion. Earlier works have studied the incorporation of EGR in natural gas-fired turbines. The industrial and maritime sectors have demonstrated growing interest in integrating carbon capture systems with gas turbines operating on liquid hydrocarbon fuels, including diesel, and emerging sustainable fuel alternatives. This study is the initial attempt to understand EGR limits on gas turbine combustion with liquid fuels through the development of a chemical reactor model (CRN) comprised of a series of joined perfectly stirred reactors (PSR), representing different flame and flow zones within the combustor. The CRN is a numerical investigation tool that provides plenary species composition and temperature data at a fraction of the time and cost

of conventional reacting flow computational fluid dynamics (CFD) simulations. Chemical reactor networks (CRNs) typically developed for gaseous fuel applications have shown potential to predict gas turbine emissions and operational limits and have been incorporated into gas turbine technology Research and Development (R&D). Nonetheless, challenges exist with implementing CRN approaches with liquid fuels due to the inherent multi-dimensional nature of liquid fuel evaporation and combustion. To incorporate liquid fuels in a CRN model, a stratification method was employed, where a PSR was created to model a portion of the fuel flow as a lean mixture representing the premixed/vaporized fraction of the fuel in parallel with a PSR operating at stoichiometric mixture fractions to simulate the portion of the non-premixed/vaporized fuel flow and its combustion. The C3 chemical mechanism was implemented in this modeling approach to simulate the diesel fuel chemistry (using a simple surrogate) while incorporating chemical reactions to predict NOx and CO emissions. This approach provided an avenue of control within the reactor network to predict emission levels, which was compared and validated against Solar Turbines Centaur 40 (SoLoNOx combustor) engine test emissions data. Following model validation, Exhaust Gas Recirculation (EGR) was introduced, revealing a decreasing trend in NOx emissions with increasing EGR rates, accompanied by a corresponding rise in CO emissions. At elevated EGR levels, CO concentrations reached thresholds associated with significant combustion instability and eventual flameout. The findings indicate that the SoLoNOx (Dry Low Emissions) liquid-fueled combustor exhibits greater EGR tolerance compared to the conventional liquid-fueled combustor.

ACKNOWLEDGEMENTS

I would like to express my deepest gratitude to Dr. Bret Windom for his invaluable guidance, steadfast support, and inspiring mentorship throughout my master's studies. His expertise, encouragement, and unwavering belief in my abilities have been instrumental in shaping this thesis and fostering my academic and professional growth. Thank you for consistently challenging me to excel and for providing the direction I needed to succeed.

My sincere thanks also go to Dr. Dan Wise, whose insightful lectures, constructive feedback, and engaging discussions significantly deepened my understanding of thermodynamics and turbomachinery. His enthusiasm for teaching has been a continuous source of inspiration. I would also like to extend my appreciation to Dr. Todd Bandhauer and Dr. Daniel Herber, along with Dr. Wise, for serving on my advisory committee and for their valuable insights and contributions to this work.

I am especially grateful to the Office of Naval Research (ONR) for funding this research through the Decarbonization Research Consortium, under award number N00014-23-S-B001. This thesis would not have been possible without their generous support and commitment to advancing sustainable energy technologies.

To my family, thank you for your unconditional love, support, and encouragement every step of the way. Your belief in me has been a constant source of strength. To my friends, your companionship, motivation, and countless shared memories made this journey not only possible but hugely enjoyable. A heartfelt thank you to Dr. George Asafo, Dr. Paul Lartey, Mr. Andy Halm, Daniel Reitz, and Dang Lee for always being there during the most challenging moments, offering support and perspective.

This thesis is a product of the collective support, mentorship, and encouragement I have been fortunate to receive. I am deeply thankful to all who have played a role in this journey.

DEDICATION

"To God Almighty for preserving my life. And to my parents (Mr. Kingsford Essuman Atomboh and Mrs. Doris Essuman), whose love and sacrifices have been my constant pillar."

TABLE OF CONTENTS

LIST OF TABLES

LIST OF FIGURES

NOMENCLATURE

Symbols

Δ	Change in
ρ	Density
∇	Gradient
ω	Source term
τ_{chem}	Chemical time scale
τ_{mix}	Mixing time
τ_{res}	Residence time
$\emptyset$	Equivalence ratio
η_{th}	Thermal efficiency of a gas turbine
χ	Scalar dissipation rate
ϵ	Turbulent diffusion rate
Ar	Argon
AC	After Combustion
B.C	Boundary Condition
C	Carbon - element
CCS	Carbon Capture and Sequestration/Storage
CH_4	Methane
CO	Carbon monoxide
CO_2	Carbon dioxide
C_p	Specific heat at constant pressure

CRN	Chemical Reactor Network
D	Diffusion co-efficient/Diffusivity
DLE	Dry Low Emission
EGR	Exhaust Gas Recirculation
EES	Engineering Equation Solver
EQR	Equivalence ratio
F	Fuel
F_{st}	Stoichiometric Fuel/Air ratio
g	gravitational acceleration
GHG	Greenhouse Gases
GT	Gas Turbine
H	Hydrogen – element
h	enthalpy
h_{fg}	enthalpy of vaporization
H_2O	Water
i.e.	That is.
IGV	Inlet Guide Vane
in	Inlet
K	Kelvin
L_F	Length of the flame
LHV_D	Lower heating value of diesel
LHV_{NG}	Lower heating value of natural gas
MW	Molecular weight

$\dot{m}_F$	Mass flow rate of fuel
$\dot{m}_i$	Mass flow rate of species
$\dot{m}_O$	Mass flow rate of oxidizer
N_2	Diatomic Nitrogen
NG	Natural gas
NO	Nitric oxide
NO_2	Nitrogen dioxide
NOx	Nitric Oxides
O	Oxygen - element
O_2	Diatomic Oxygen
out	outlet
p	Pressure
P	Power
PC	Pre-Combustion
PCD	Compressor Discharge Pressure
ppmv	parts per million (volumetric)
ppmvd	dry ppmv
PR	Pressure ratio
PFR	Plug flow reactor
PSR	Perfectly Stirred Reactor
R	Radius
R_u	Universal Gas Constant
R&D	Research and Development

SG	Specific Gravity
st	stoichiometric
T	Temperature
TRIT	Turbine rotor inlet temperature
UHC	Unburned Hydrocarbons
u	Velocity
V	Volume
W	Gas Flow
Wf	Fuel Flow
X	Mole Fraction
Y	Mass Fraction
Z	Mixture Fraction

Subscript

act	Actual
ad	Adiabatic
amb	Ambient
comp	Compressor
ref	Reference
turb	Turbine

CHAPTER 1 - INTRODUCTION

1.1 Motivation

In this era of heightened environmental awareness and increasingly stringent emissions regulations, the energy industry is under significant pressure to develop cleaner, more efficient power generation technologies. Gas turbines, which are extensively employed in various sectors such as industrial power generation, marine propulsion, and combined-cycle power plants, play a critical role in meeting global energy demands. However, these turbines are often challenged by high NOx and other greenhouse gases emissions, which not only have adverse effects on air quality and human health but also contribute to the broader issues of climate change. In this context, innovative strategies that can mitigate pollutant formation without compromising system efficiency are of paramount importance. These emissions concerns gave rise to the rapid development and deployment of renewable energy technologies like wind turbines, solar panels, geothermal, and biomass. Although there is an increase in renewable energy, these technologies are not fully dependable and cannot be used for base load purposes. Gas turbines remain the primary source of electricity production, industrial energy source and the engine that propels the aviation sector. Even though the use of renewable energy technologies has increased significantly, so has the demand for gas turbines increased drastically to the extent that manufacturers are not able to catch up with demand [1]. The high demand for gas turbines is due to high volumes of data centers and artificial intelligence that require a constant and reliable energy supply. The global gas turbine market was projected to increase at a compound annual growth rate of 4% in 2030. GE Vernova, the largest gas turbine manufacturer, saw a significant increase in gas turbine orders that has created a backlog of about USD 119 billion, which was reported in their 2024 annual report

[2]. As the demand for gas turbines increases due to their reliability, it is imperative to find innovative ways to deal with the emissions they emit, especially NOx and carbon dioxide.

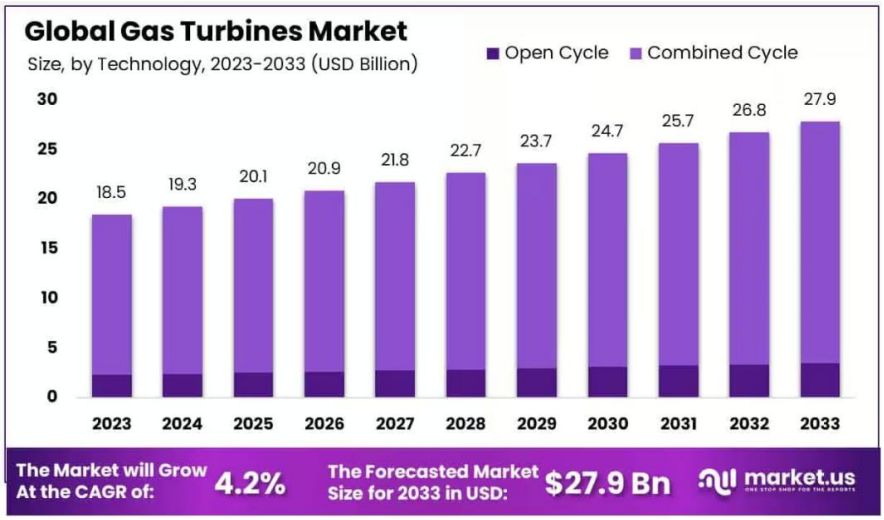

Figure 1.1 A graph of the global gas turbine market trend. [3]

Exhaust gas recirculation (EGR) has emerged as a promising technique for reducing NOx and carbon dioxide emissions in combustion systems. EGR works by redirecting a portion of the turbine's exhaust gas back into the combustion chamber. This recirculated gas acts as a diluent, lowering the oxygen concentration and specific combustion temperature. Since thermal NOx formation is extremely sensitive to temperature, a reduction in peak flame temperatures can significantly suppress the generation of these pollutants. While EGR has been widely applied and studied in automotive engines, its effects in the context of gas turbines, especially liquid-fueled gas turbines, remain less explored. This issue warrants a thorough investigation given the critical role that liquid-fueled gas turbines play across multiple sectors, including power generation, marine propulsion, data centers, and the petrochemical industry. In many regions, particularly those rich in oil resources, access to natural gas and the necessary distribution infrastructure is either limited or entirely unavailable, rendering liquid fuels the only viable energy source for gas

turbine operation. However, combustion of liquid fuels typically results in significantly higher emissions of carbon monoxide (CO) and nitrogen oxides (NOx) compared to natural gas. This elevated emission profile underscores the importance of exploring emission reduction strategies, such as exhaust gas recirculation (EGR), specifically tailored to liquid-fueled gas turbine systems. Liquid fuels exhibit distinct combustion characteristics compared to gaseous fuels, including differences in atomization, mixing, and vaporization. These factors fundamentally alter the combustion dynamics and, consequently, the pathways for NOx and CO formation.

Liquid-fueled gas turbines present a multi-phase process that affects flame stability, heat release rates, and the overall chemical kinetics of the combustion reaction. Therefore, a detailed understanding of these interactions is essential for designing EGR systems that are both effective and dependable.

The primary motivation for this thesis stems from the need to address this knowledge gap. Understanding how EGR influences the operation of liquid-fueled gas turbines (in both lean premixed and conventional combustors) could lead to breakthroughs in turbine design and operation strategies, enabling a more environmentally friendly and efficient energy sector. The lean premixed combustor, commonly referred to as a Dry Low Emissions (DLE) combustor, is designated by Solar Turbines as the SoLoNOx combustor within their product line. By integrating numerical investigations and computational modeling, this research aims to unravel the complex interplay between EGR, combustion dynamics, and emissions formation in liquid-fueled systems. The insights derived from this study could pave the way for optimized turbine performance, where reduced pollutant emissions are achieved without relinquishing thermal efficiency and/or power output. The outcomes of this research have the potential to significantly impact both the academic

field of combustion engineering and the practical implementation of emissions control technologies in the power industry.

1.2 Objectives

Understanding the influence of Exhaust Gas Recirculation (EGR) on the chemical pathways leading to NOx and CO formation in premixed and non-premixed combustion is essential for the effective mitigation of these emissions in gas turbine systems. This thesis aims to address the following research questions:

- How can Chemical Reactor Network (CRN) be used to model premixed and non-premixed liquid fuel combustion in gas turbines?
- What are the emission characteristics of premixed and non-premixed combustion in a gas turbine operating with and without Exhaust Gas Recirculation (EGR)?
- How sensitive are combustion parameters like residence time, mass flowrate, and mole fraction of flue gases to emissions?
- What is an appropriate balance between combustion stability and emission reduction?
- How will the Chemical Reactor Network (CRN) models for premixed and non-premixed liquid fuel combustion be validated using experimental engine test data?

CHAPTER 2 - THEORY AND LITERATURE REVIEW

2.1 Brayton cycle and gas turbines.

The Brayton cycle forms the thermodynamic basis of gas turbine operation, which has become a cornerstone in power generation and propulsion systems. Named after George Brayton, this cycle describes the operation of a constant-pressure heat engine which is characterized by its simplicity, efficiency, and adaptability to various applications [4]. Over the past decades, the Brayton cycle has been refined to maximize performance, reduce emissions, and adapt to changing fuel sources.

The ideal Brayton cycle consists of four reversible processes: two adiabatic (isentropic) and two isobaric (constant-pressure) processes [5]. During the isentropic compression (process 1–2), air is compressed in a compressor, raising its pressure and temperature. In the combustion chamber (process 2–3), fuel is added and combusted at nearly constant pressure, significantly increasing the temperature. The high-energy gas then expands isentropically in the turbine (process 3–4), producing work. Finally, the cycle is completed by rejecting heat at constant pressure (process 4–1) [6].

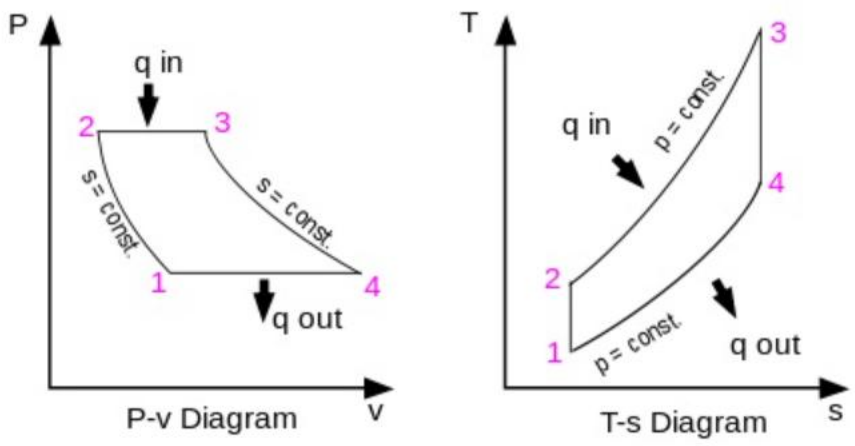

Figure 2.1 PV & TS diagram of the Brayton cycle. [7]

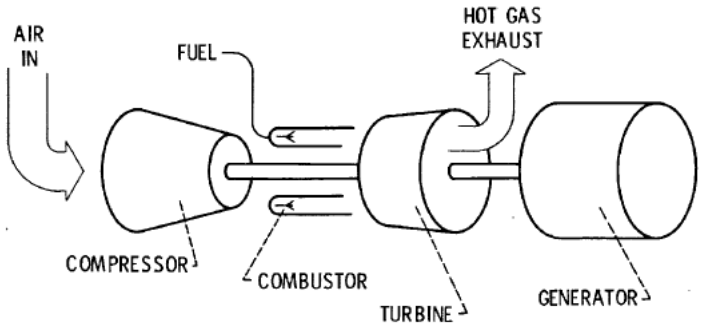

Figure 2.2 Schematic of the Brayton cycle. [4]

The Brayton cycle's maximum efficiency is defined in **Eq(2.1)**

$$\eta_{max} = 1 - (\frac{P_2}{P_1})^{\frac{1-\gamma}{\gamma}} \qquad Eq(2.1)$$

2.1.1 Gas turbine parts and functions

A gas turbine consists of three main components: the compressor, the combustor, and the turbine.

- Compressor: The function of the compressor is to increase the pressure and density of airflow. Based on isentropic relations, as the air pressure increases, the air temperature also increases. Compressors can be categorized into two: axial or centrifugal, and single stage or multi-stage. Most gas turbines run on multistage axial compressors.

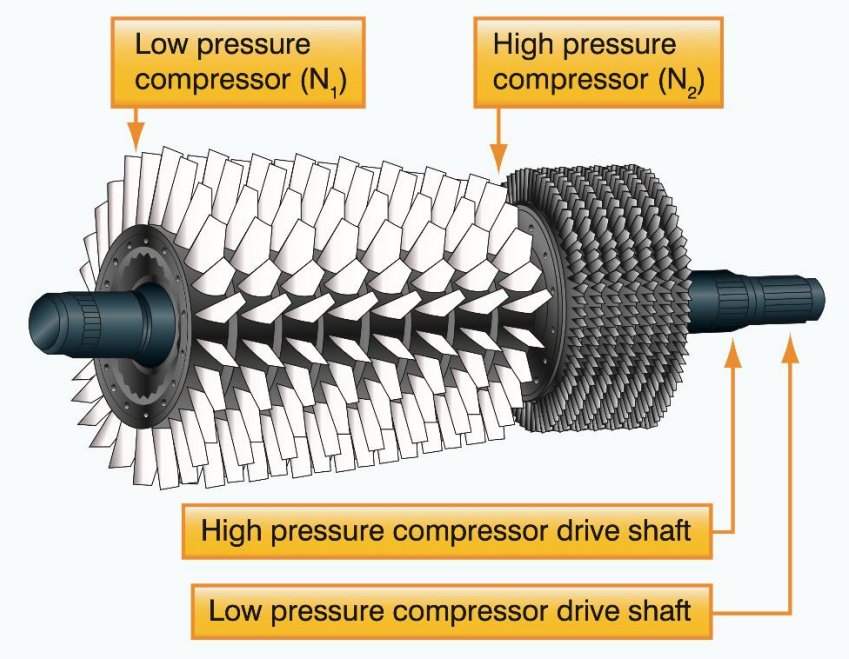

Figure 2.3 An image of a multistage axial compressor. [8]

$$\eta_c = \frac{Ideal\ (isentropic) head}{Actual\ head} = \frac{h\_2^* - h_1}{h_2 - h_1} = \frac{T\_2^* - T_1}{T_2 - T_1} \qquad Eq(2.2)$$

$$\frac{P_n}{P_1} = \left(1 + \frac{\eta}{C_p \cdot T_1} \cdot H\right)^{\frac{\gamma}{\gamma-1}} = \left(1 + \frac{\eta}{T_1} \cdot n\frac{\omega^2 r^2}{C_p}\right)^{\frac{\gamma}{\gamma-1}} \qquad Eq(2.3)$$

- Combustor: The function of a combustor is to add heat energy to the compressor airflow [9]. This heat addition significantly increases the temperature of the airflow [10]. Gas turbine combustion is a steady state flow process in which a hydrocarbon fuel is burned with air to achieve a desired combustor firing temperature. This combustion process is exothermic and that leads to enormous heat release [11]. Some of the combustors are turboannular, can and annular.

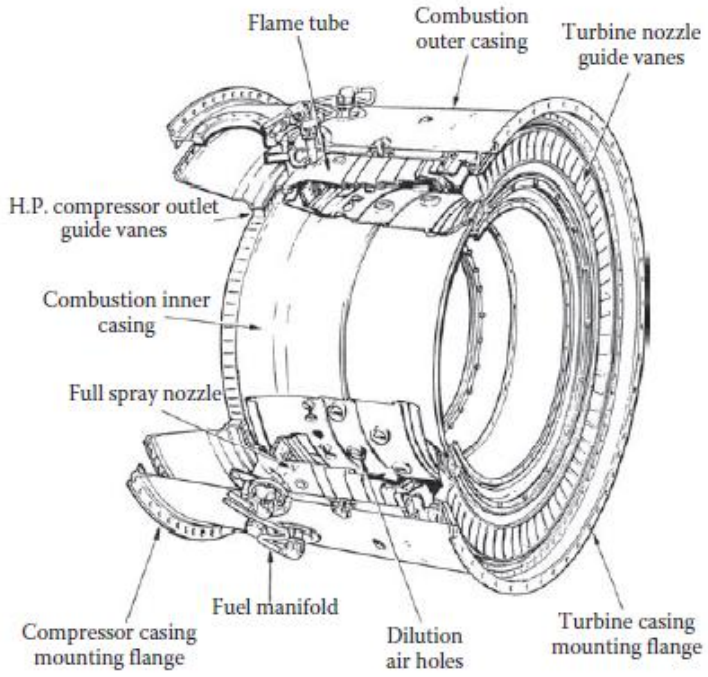

Figure 2.4 An image of a gas turbine combustor. [11]

$$\eta_b = \frac{Energy\_out}{Fuel\_energy} = \frac{W_{air} \cdot C_p \cdot (T_e - T_i)}{W_{fuel} \cdot Q_R} \qquad Eq(2.4)$$

$$W_{fuel} \cdot Q_R = W_{air} \cdot (h_3 - h_2)\eta_B \qquad Eq(2.5)$$

$$C_xH_y + (x + y/4)\ O_2 \rightarrow {}_xCO_2 + (m/2)\ H_2O + 3.76{*}N_2 \qquad Eq(2.6)$$

- Turbine: the turbine is in two sections; the gas producing turbine and the power turbine. The gas mixture exiting from the combustor contains potential energy mainly in two forms: heat and pressure. The function of the turbine is to convert these fluid energies into mechanical shaft energy [12]. The gas producer is to absorb only enough energy from the flow to drive the compressor, while the power turbine is supposed to convert the remaining flow energy into shaft rotational output energy [13]. The turbine can be a reaction or an impulse type.

Figure 2.5 An image of the turbine section of a GE frame 9E gas turbine.

$$P = W \cdot H = W \cdot C_p \cdot (T_{combustor} - T_{exit}) \qquad Eq(2.7)$$

$$\eta_{gt} = \frac{Actual\ head}{Ideal(isentropic)\ head} = \frac{h_2 - h_1}{h\_2^* - h_1} = \frac{T_2 - T_1}{T\_2^* - T_1} \qquad Eq(2.8)$$

2.1.2 Ancillary & auxiliary systems

Gas turbine ancillary and auxiliary systems, including fuel, lubrication, control, cooling, Auxiliary Power unit (APU), and exhaust systems, form an integrated network that is vital to the gas turbine's operation [13]. Advances in these systems have led to significant improvements in turbine efficiency, durability, and environmental performance. As gas turbine technology continues to evolve, further integration and optimization of these subsystems will remain critical to meeting future energy demands and environmental challenges [13].

These systems are critical to ensuring the safe, efficient, and reliable operation of gas turbines. These systems encompass a range of subsystems that support the primary engine functions, such as fuel delivery, lubrication, control, cooling, and exhaust management. Their integrated operation is essential for optimizing performance, reducing emissions, and prolonging equipment life [14].

- Fuel systems**:**

  The fuel system is responsible for storing, processing, and delivering fuel to the combustion chamber under controlled conditions. It typically includes storage tanks, filters, metering devices, and atomizers. Proper fuel conditioning is crucial for maintaining consistent combustion and preventing contaminants that can lead to efficiency losses or component damage. Advanced fuel systems now incorporate

redundancy and safety features, ensuring uninterrupted operation during transients and startup [15].

- Lubrication systems:

  A well-designed lubrication system minimizes friction between moving parts, reduces wear, and dissipates heat generated by high-speed components [16]. This system includes oil pumps, coolers, filters, and reservoirs that ensure an adequate and continuous supply of high-quality lubricants. Maintaining optimal oil temperature and pressure is vital for preventing bearing failures and extending turbine life. Modern systems often feature auxiliary oil cooling circuits to manage excess thermal loads [13].

- Control systems:

  Modern gas turbines employ sophisticated digital control systems (DCS) that monitor and manage various engine parameters in real time [17]. These systems use a network of sensors to track temperature, pressure, speed, and vibration. Advanced algorithms process this data to regulate fuel flow, adjust cooling air distribution, and coordinate startup and shutdown sequences. Integrated fault-detection and diagnostic features allow operators to anticipate potential issues and optimize turbine performance, leading to increased reliability and efficiency [18].

- Cooling systems:

  High turbine inlet temperatures necessitate robust cooling strategies to protect critical components such as turbine blades and vanes. Air, steam, or advanced film cooling methods are used to control the operating temperature [19]. Cooling air is usually extracted from the compressor, ensuring that turbine components remain within safe thermal limits. Improvements in cooling design not only enhance the durability of turbine

parts but also contribute to overall efficiency by allowing higher operating temperatures [20].

- Auxiliary power units (APU) and startup systems:

  Auxiliary systems, such as APUs/electrical motor/IC engines, are essential for providing the initial energy required to start the turbine and to operate ancillary equipment when the main engine is offline [21]. These systems often include dedicated generators, batteries, and ignition systems that facilitate reliable startup, especially under varying ambient conditions [22]. The coordination between the APU and the main control system is critical during both startup and shutdown operations, ensuring smooth transitions and minimal wear on the turbine [13].

- Exhaust and emissions control systems:

  The exhaust system manages the turbine's waste gases and is instrumental in reducing the environmental impact of turbine operations [13]. Technologies such as Exhaust Gas Recirculation (EGR) and Heat Recovery Steam Generators (HRSG) are employed to lower combustion temperatures and recover waste heat for additional power generation [23]. These systems not only improve overall efficiency but also help meet stringent emission standards by minimizing the formation of NOx and CO [24].

- Fire and gas detection systems:

  Modern gas turbines have very robust gas detection and firefighting systems that help in sustaining fire before external help comes through [25].

2.2 Gas turbine applications

Gas turbines are versatile machines with applications across diverse sectors. Gas turbines are one of the key engines used in the aviation industry. They are used to power commercial airliners and military aircraft, offering high thrust and fuel efficiency essential for long-haul flights [26]. Their robustness makes them an ideal choice for fighter jets and other high demand military activities. They also serve as auxiliary power units on aircraft. Their compact design and rapid response capabilities make them ideal for turbojet, turbofan, and turboprop engines [27].

In power generation, gas turbines form the backbone of base load power in the world. There has been significant increase in the demand for combined cycle power plants due to an increase in power output, where gas turbine exhaust heat is used as a source of energy for boilers to produce steam to drive steam turbines [28]. This configuration significantly enhances overall efficiency while reducing emissions. They also operate in simple cycle mode to meet peak load demands in industrial and utility settings, offering quick start-up and reliable performance.

In the oil and gas industry, gas turbines drive compressors in pipelines and gas processing facilities, ensuring the continuous flow of natural gas and other crude products [29]. Additionally, they are employed in marine propulsion systems for commercial vessels and naval ships due to their high power-to-weight ratio and robust reliability under challenging conditions.

Recent advancements have expanded their use in data centers, distributed generation systems, supporting decentralized power supply in remote or rapidly growing urban areas. Furthermore, hybrid energy systems integrate gas turbines with renewable sources, balancing intermittent

outputs and ensuring grid stability. This diversity of applications underscores the critical role of gas turbines in modern energy and transportation infrastructure.

2.3 Fuels for gas turbines

Gas turbines are widely recognized for their versatility, efficiency, and rapid responsiveness, making them indispensable in power generation, aviation, marine propulsion, and industrial applications [13]. A critical aspect of gas turbine performance is the type of fuel used, which influences combustion efficiency, emissions, and overall operational reliability [30]. This thesis provides an in-depth discussion of the fuels used in gas turbines, their characteristics, and the challenges associated with their utilization. Fuels used are either liquid or gaseous and are mostly hydrocarbons.

- Gaseous Fuels: Natural gas is the most common fuel for gas turbines, especially in power generation. Its high hydrogen-to-carbon ratio contributes to cleaner combustion with lower emissions of sulfur oxides (SO_x) and particulate matter [31]. The primary components of natural gas are methane, ethane, and other light hydrocarbons, which combust rapidly and efficiently under high-temperature conditions. Due to its high calorific value and low viscosity, natural gas promotes efficient fuel-air mixing and complete combustion, leading to high thermal efficiencies [26].

  However, the composition of natural gas can vary geographically, which affects its calorific value and combustion characteristics. Modern gas turbines incorporate sophisticated control systems and fuel conditioning units to cater for these variations, ensuring stable operation under varying load conditions. Moreover, the infrastructure for natural gas supply and distribution is well established, making it a preferred fuel in most parts of the world.

- Liquid fuels: A sizable portion of gas turbine applications, especially in remote areas or in regions lacking a natural gas pipeline network, liquid fuels such as distillate fuels and diesel are used. Distillate fuels, including Jet-A and diesel, are refined products with low sulfur content and high energy density. They offer logistical advantages, such as ease of storage and transportation, and are particularly common in aviation and marine applications [13]. Liquid fuels require atomization for efficient combustion. In gas turbines, fuel is introduced into the combustor where it is atomized into fine droplets. The subsequent evaporation of these droplets is critical for achieving a homogeneous fuel-air mixture. However, the atomization process adds complexity to the combustion dynamics compared to gaseous fuels. Challenges such as fuel film formation on combustor walls, incomplete vaporization, and flashback can impact performance and emissions [32]. The combustion of liquid fuels typically produces higher levels of carbon monoxide (CO) and unburned hydrocarbons due to the challenges associated with droplet evaporation and mixing. To mitigate these issues, modern combustor designs incorporate advanced fuel injection systems and staged combustion techniques. These improvements help to ensure complete combustion, thereby enhancing efficiency and reducing pollutant emissions [33].
- Heavy fuel oils: Heavy fuel oils (HFOs) are used in gas turbines where economic considerations and fuel availability dictate their use, particularly in industrial and marine sectors [34]. HFOs are residual fuels characterized by high viscosity, high sulfur content, and significant amounts of contaminants such as metals and asphaltenes. The use of HFOs present challenges, including difficult atomization, poor combustion stability, and high emissions of SO_x and particulate matter. Gas turbines operating on heavy fuel oils typically require preheating and extensive fuel treatment to reduce viscosity and remove

contaminants. Preheating ensures that the fuel can be atomized effectively, while fuel treatment systems remove impurities that could lead to fouling and corrosion of turbine components. Despite these challenges, the low cost of HFOs in certain regions makes them an attractive option, and research continues into improving turbine design and combustion techniques to better accommodate these fuels [35].

- Alternative and synthetic fuels: In response to environmental concerns and the fluctuating price of fossil fuels, alternative fuels, including biofuels and synthetic fuels, are gaining attention in gas turbine applications. Biofuels, derived from renewable resources such as vegetable oils, animal fats, or waste products, offer the advantage of lower carbon emissions. However, their chemical and physical properties differ from conventional fuels, requiring modifications to turbine design and fuel handling systems [36]. These fuels can be engineered to have low sulfur content and a consistent chemical composition, making them attractive for use in gas turbines. Nonetheless, challenges remain in scaling up production and ensuring that the overall environmental footprint of synthetic fuel production is minimized [37].
- Fuel blending and future trends: An emerging trend in gas turbine operation is the blending of different fuels to optimize performance and emissions. For example, mixing natural gas with a small percentage of biofuel can reduce greenhouse gas emissions while maintaining combustion stability [38]. Fuel blending allows operators to take advantage of the beneficial properties of different fuels while mitigating some of the drawbacks.

  Moreover, as the global energy landscape shifts towards decarbonization, gas turbines are increasingly being adapted to operate on hydrogen-enriched fuels. Hydrogen offers the promise of near-zero carbon emissions during combustion, although it poses challenges

related to flame speed and combustion dynamics [39]. Research is ongoing to develop advanced combustor designs and fuel injection systems that can effectively manage hydrogen-rich fuel blends [40].

2.4 Types of combustion

Combustion is a chemical process in which a fuel reacts with an oxidizer, releasing heat and light in the form of flames [13]. This exothermic reaction is fundamental to numerous energy systems, from internal combustion engines and industrial furnaces to power plants and jet engines. The study of combustion encompasses not only chemical kinetics and thermodynamics but also fluid mechanics, heat transfer, and pollutant formation [41]. Combustion can be premixed, non-premixed, partially premixed, and flameless combustion. Combustion processes lead to flame formation and this flame can be premixed or diffusion flame. A flame is a self-sustaining propagation of a localized combustion zone at subsonic velocities[41]. Certain factors affect the formation and quality of flame in a combustion process and these are temperature, pressure, equivalence ratio and fuel type. But this research studies both premixed and non-premixed combustion in gas turbines.

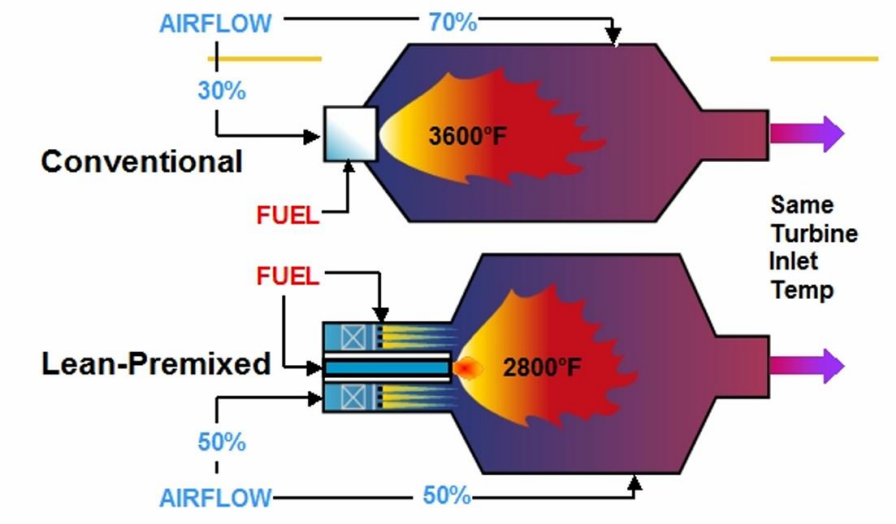

Figure 2.6 An image of a conventional and a premixed combustion. [13]

- Premixed combustion: This is a type of combustion where the fuel and oxidizer are mixed prior to the combustion process. This leads to the formation of a flame which can be either laminar or turbulent [41]. This combustion type ensures proper mixing of fuel and oxidizer, which helps in the reduction of pollutant formation. Its homogeneity of the mixture facilitates rapid flame propagation. For this type of combustion, once the process is initiated it is self-sustained [42]. How this type of combustion process takes place is shown in Figure 2.6.

Figure 2.7 An image of a premixed flame. [43]

- Non-premixed combustion: With this type of combustion, the fuel and oxidizer are separately introduced into the combustion chamber [44]. The fuel and oxidizer are mixed at molecular stoichiometric proportion inside the combustion chamber where the flame is formed at the stoichiometric interface [41]. This combustion process is seen in Figure 2.6.

Figure 2.8 An image of a non-premixed flame. [43]

- Partially premixed combustion: Partially premixed combustion represents a hybrid between premixed and non-premixed modes. In this process, some degree of mixing occurs

prior to ignition, but the mixture is not completely homogeneous. This can lead to a flame with characteristics of both premixed and diffusion flames [45].

Figure 2.9 An image of a partially premixed flame. [46]

- Flameless combustion: Flameless combustion is an advanced combustion technique that aims to reduce thermal NO_x emissions by eliminating the visible flame. In this process, exhaust gas recirculation (EGR) is used to dilute the reactants, resulting in a distributed, volumetric reaction zone with lower peak temperatures [47].

2.5 Stoichiometric fuel-to- air ratio

Fuel to air ratio is one of the key parameters that affect a combustion process [48]. It is the ratio of the amount of fuel engaging in the combustion process to the amount of oxidizer (air) partaking in the combustion process [49]. There are situations where the amount of fuel equals the amount of air. With this dynamic the ratio between the air and fuel becomes one (1) and it is termed stoichiometric fuel to air ratio [49]. The equation for calculating the stoichiometric air fuel ratio is done based on a mole of each fuel species contained in the fuel [41]. To burn 1 mole of dodecane, 18.5 moles of air is required, which can be seen in **Eq(2.9)**.

$$C_{12}H_{26} + 18.5\ (O_2 + 3.76N_2) \rightarrow CO_2 + 2H_2O + (3.76 * 18.5)N_2 \qquad Eq(2.9)$$

$$F_{st} = \frac{MW_F}{MW_O * total\ air\ requirement\ (mol/mol)} \qquad Eq(2.10)$$

F_{st} = stoichiometric fuel to air ratio, MW_i = molecular weight of the species.

$$\emptyset = \frac{\dot{m}_F/\dot{m}_O}{F_{st}} \qquad Eq(2.11)$$

2.6 Emissions and emission regulations

While combustion is highly effective at releasing energy from fuels, it is also responsible for producing a variety of emissions that have significant environmental and health impacts [13]. For a combustion process that involves hydrocarbon, ideally carbon dioxide, and water is the byproduct of a combustion process [32]. However, combustion is rarely perfect. Factors such as incomplete mixing, insufficient oxygen supply, or low temperature regions can lead to incomplete combustion [50]. As a result, a range of pollutants are produced, including carbon monoxide (CO), unburned hydrocarbons (UHC), particulate matter (PM), nitrogen oxides (NO_x), and sulfur oxides (SO_x) [23]. The two main emissions that are of concern to this research are carbon monoxide (CO) and oxides of nitrogen (NOx).

2.6.1 Oxides of nitrogen (NOx)

Oxides of nitrogen are one of the emissions produced by gas turbines' combustion [13]. It can be produced in diverse ways and are described below:

- Thermal NOx or Zeldovich mechanism

This type of NOx is produced by the oxidation of atmospheric nitrogen in an elevated temperature region of the flame and in the post-flame gases [41]. The thermal NOx is an endothermic reaction, and it happens at a significant rate only at temperatures above and around 1800 K [51]. The reaction schemes for thermal NO uses the extended Zeldovich mechanism [41]. It peaks on the fuel-lean side of stoichiometric [41]. This happens because of the competition between fuel and nitrogen for the available oxygen. While the combustion temperature is higher on the slightly rich side of stoichiometric, the available oxygen is consumed by the fuel.

$$O_2 \rightleftharpoons 2O \qquad \textit{Eq(2.12)}$$

$$N_2 + O \rightleftharpoons NO + N \qquad \textit{Eq(2.13)}$$

$$N + O_2 \rightleftharpoons NO + O \qquad \textit{Eq(2.14)}$$

$$N + OH \rightleftharpoons NO + H \qquad \textit{Eq(2.15)}$$

- Prompt nitric oxide / Fenimore mechanism.

  This type of NOx is found early in the flame region. It contrasts with the idea of a kinetically controlled process. The initiating reaction for prompt nitric oxide is [52].

$$N_2 + CH \rightleftharpoons HCN + N \qquad \textit{Eq(2.16)}$$

It usually occurs at low temperatures and pressures. The balance of the prompt NO mechanism involves the oxidation of HCN molecules and N atoms. HCN oxidizes to NO by a sequence of reactions involving HCN → CN → NCO → NO. The N atom usually reacts by the second Zeldovich reaction [53]. The influence of pressure is important because prompt NO can be a

significant contributor to NO emissions in lean premix combustion [41]. Conversion of HCN to NO for equivalence ratios less than 1.2 are shown below:

$$HCN + O \rightleftharpoons NCO + H \qquad Eq(2.17)$$

$$NCO + H \rightleftharpoons NH + CO \qquad Eq(2.18)$$

$$NH + H \rightleftharpoons N + H_2 \qquad Eq(2.19)$$

$$N + OH \rightleftharpoons NO + H \qquad Eq(2.20)$$

- NNH Mechanism

  The NNH Mechanism involves a reaction of NNH with oxygen atoms due to the vast availability of oxygen radicals, especially during lean premixed combustion. This mechanism was originally identified by Dean and Bozzelli in 1995 [54]. This happens when there is a reaction between nitrogen and H radical at low flame temperatures [55]. NNH formation is presented below:

$$N_2 + H \rightleftharpoons NNH \qquad Eq(2.21)$$

$$NNH + O \rightleftharpoons NO + NH \qquad Eq(2.22)$$

$$NNH + O \rightleftharpoons N_2O + H \qquad Eq(2.23)$$

$$NNH + O \rightleftharpoons N_2 + OH \qquad Eq(2.24)$$

- N_2O or Nitrous oxide

Oxygen radical and N_2 molecules usually react with fuel at low temperatures (T < 1800K), giving rise to the species N_2O. The formation of nitrous oxide is given as a three-reaction pathway and as a third body reaction [41]. This mechanism was first introduced by Malte and Pratt in 1974 [56].

$$N_2 + O + M \rightleftharpoons N_2O(\cdot) + M \qquad \textit{Eq(2.25)}$$

$$N_2O(\cdot) + M \rightleftharpoons N_2O + M \qquad \textit{Eq(2.26)}$$

$$N_2O + M \rightleftharpoons N_2 + O + M \qquad \textit{Eq(2.27)}$$

The above reaction always happens in the presence of a third body, M. N_2 and O react with the third body, M to form an unstable intermediate N_2O (*) which subsequently forms N_2O. Nicol et al presented an argument that the above three-step reaction pathway initiates the formation of NO [57]. This mechanism often happens in combustion because of the higher nitrogen concentrations. N_2O is a precursor to NO formation in a combustion process. The production of NO happens when N_2O reacts with O and H radicals, it can also happen with CO [32]:

$$N_2O + O \rightleftharpoons NO + NO \qquad \textit{Eq(2.28)}$$

$$N_2O + H \rightleftharpoons NO + NH \qquad \textit{Eq(2.29)}$$

$$N_2O + CO \rightleftharpoons NO + NCO \qquad \textit{Eq(2.30)}$$

2.6.2 Nox and residence time

Residence time, τ is a combustion parameter that defines the period reactants stay in a combustion zone to allow heat transfer, mixing, and chemical reaction [58]. In 1975, Anderson revealed the impact of residence time on NOx emissions, especially on combustion processes with equivalence ratio higher than 0.4 ($\emptyset \geq 0.4$) [59]. For very lean combustion, the rate of formation is so low that NOx emission becomes insensitive to time.

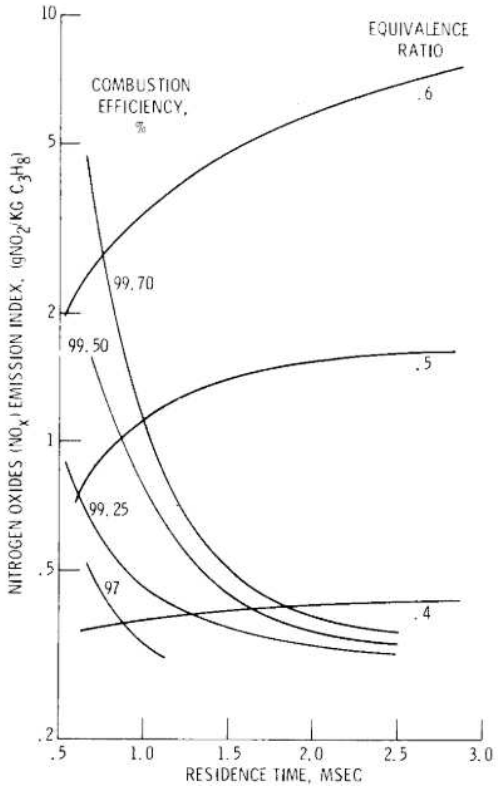

Figure 2.10 An image of the influence of residence time on NOx production at different equivalence ratio. [60]

One of the primary factors contributing to the increase in emission is the primary zone residence time [32]. An increase in NOx emissions is directly proportional to combustor volume and residence time in the primary zone. However, increasing the primary zone combustor volume helps

in reducing CO emissions [61]. This presents a need to balance things to achieve reasonable NOx and CO while designing the combustion chamber.

2.6.3 Carbon monoxide (CO)

In combustion systems, CO formation is closely tied to the local oxygen concentration, temperature, and the mixing quality of the fuel and air [61]. In an ideal, fully premixed flame, sufficient oxygen is available to convert all carbon into CO_2 [42]. However, under conditions where the air-to-fuel ratio is lower than the stoichiometric requirement, or where flame quenching occurs, some carbon atoms fail to oxidize completely, resulting in the production of CO. This phenomenon is common in diffusion flames [62], such as those found in diesel engines, where the mixing of fuel and air is governed by molecular diffusion rather than complete pre-mixing [41].

Causes for the formation of CO are:

- Improper mixing: this is the situation where there is an improper mixing of the fuel and oxidizer. There is spatial and temporal unmixedness in the combustion chamber. The uneven mixing creates hot and cold spots in the combustion chamber that favors the formation of CO [41].
- Residence time/Incomplete combustion: chemical process between the fuel and oxidizer needs time for it to be efficient. Under low residence time, there is not enough time for the fuel and oxidizer to fully/completely combust [13]. In conditions where oxygen is deficient, especially in the primary zone, it leads to the formation of CO [63].
- Flame quenching: Local quenching of flames can occur when flames suddenly refuse to sustain itself. Leading to high CO formations. CO is oxidation resistant and the conversion to CO_2 can be a rate determining step. The dissociation of CO_2 to CO and O_2 can be understood from the following equations [41]

$$CO_2 \rightleftharpoons CO + 0.5O_2 \qquad Eq\ (2.31)$$

Overall oxidation of CO can be split into 4 steps [41]

$$CO + O_2 \rightleftharpoons CO_2 + O \qquad Eq(2.32)$$

$$O + H_2O \rightleftharpoons OH + OH \qquad Eq(2.33)$$

$$CO + OH \rightleftharpoons CO_2 + H \qquad Eq(2.34)$$

$$O_2 + H \rightleftharpoons OH + O \qquad Eq(2.35)$$

The rate determining step is the first equation and acts as the initiation reaction [41]. The formation of CO_2 from the oxidation of CO is hastened by the presence of OH, O, and H radicals.

2.6.4 NOx reduction techniques

NOx is one of the key emissions that affect our environment. Unfortunately, it is a prominent emission from a gas turbine, and as we continue to expand the usage of gas turbines it is imperative to reduce NOx emissions being released into the atmosphere. Figure 2.11 shows the different ways to control NOx formation in a combustion process.

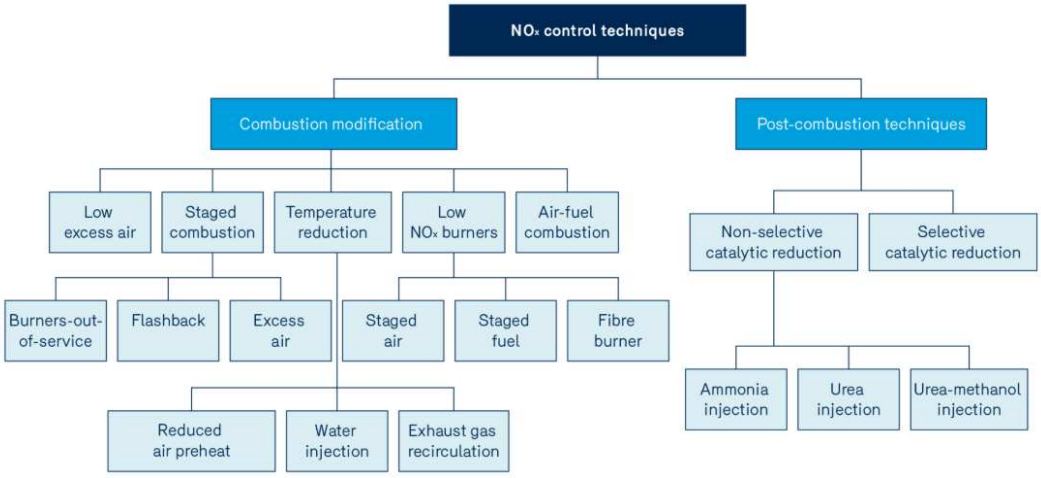

Figure 2.11 An image of NOx control techniques. [64]

Exhaust gas recirculation (EGR) is one of the ways to achieve NOx reduction and that is the heart and soul of this thesis.

2.6.5 Evaluation of emissions levels/emissions characterization

Emissions can be evaluated by direct methods or by calculation. For comparison and standardization purposes, it is important to quantify emissions. By quantifying, a common scale is used in comparing emissions with other technical results from system measurements or experiments.

- Emission index: this is the ratio of the mass of the pollutant to the mass of fuel. Different unit scales are used to account for the order of magnitude difference between the two quantities. This type of emission quantification is used in the aviation sector [65].

$$Emission\ Index = \frac{mass\ of\ pollutant\ (g)}{mass\ of\ fuel\ (kg)} \qquad Eq(2.36)$$

- O_2 correction: The O_2 correction is done to have a standard form of comparison between emissions. To achieve this, all water contents from the exhaust products are removed first before the correction is applied. Oxygen is diluted at various degrees in a combustion process.

$$X_{dry} = \frac{X_{wet}}{1 - X_{H_2O,wet}} \qquad Eq(2.37)$$

Generally, the correction is done for 15%, typically a combustion process has about 21% oxygen pre-combustion (0.21 mole fraction O_2), as seen in **Eq(2.38)**.

$$NO_{x_{15\%O_2}} = NO_{x_{dry}} \frac{0.21 - 0.15}{0.21 - X_{O_2,dry}} \qquad Eq(2.38)$$

- To measure the emission index of nitrogen oxides (EINOx). It is the mass of NO_2 produced per kg of fuel. The fraction of NO in the exhaust stream is considered as NO_2 mass-related because NO is oxidized into NO_2 in the atmosphere.

$$EINOx = \frac{(X_{NO,exhaust} + X_{NO_2,exhaust}) \cdot \frac{MW_{NO_2}}{MW_{exhaust}} \cdot \dot{m}_{exhaust}}{\dot{m}_{fuel}} \qquad Eq(2.39)$$

2.6.6 Modeling emissions

Modeling emissions is an essential part of designing a gas turbine. Emissions modeling helps in developing energy efficient and clean combustion systems. This is a guide to meeting regulatory compliance for a better environment in terms of air quality. Emissions are modelled in diverse ways, which are:

- Chemical kinetics models: Chemical kinetics involve chemical and molecular species and lots of chemical reactions. It describes the rate at which chemical reactions take place [65]. Chemical kinetic models are used to understand NOx, CO, and UHC formation. It is represented as systems of ordinary differential equations which describe the time evolution of chemical species concentrations. This model can be computational demanding and expensive when coupled with spatially resolved fluid dynamics [66]. It uses reaction rate coefficients which are determined experimentally and or through mechanical quantum calculations to solve the ordinary differential equations.
- Computational fluid dynamics (CFD): CFD presents a high-fidelity representation of complex interactions between chemical reactions. It is one of the powerful tools for modelling emissions [67]. It achieves that by solving the Navier-Stokes equation along with species conservation and energy equations. CFD captures temporal and spatial variations in temperature, velocity, and species concentrations within the combustion chamber. It incorporates detailed chemical mechanisms to simulate the formation of pollutants under the most realistic conditions possible [68].
- Empirical models: This is when emissions are modelled based on extended periods of trends in experimental data [69]. The emissions are often related to parameters like temperature, air-fuel ratio, and pressure. Empirical models are inexpensive and simple

compared to the others. This makes it the preferred choice for initial design studies. There are times theoretical understanding is derived from empirical data. Based on theoretical understanding, predictions with correction factors are derived from empirical data.

There is a future of emission modelling where integration of experimental diagnostics and advanced computational techniques will drive the modelling. Machine learning promises to reduce computational cost while maintaining accuracy. Emission modeling is a multi-faceted problem that combines fluid dynamics, chemical kinetics, and advanced computational methods. As environmental and regulatory concerns heightened, advances in emissions modelling will play a crucial role in designing combustion-efficient systems.

2.7 Carbon capture

As emissions standards become stringent and pollution levels increase it is important to develop new and innovative ways to deal with them. One such innovative way is carbon capture. Carbon captures aim to capture CO_2 from industrial sources and utilize it in various processes or store it underground [70]. Carbon capture now presents a complementary solution alongside renewable energy. The processes involved are capturing, transport, and storage or utilization [71]. Chemical solvents such as anime are used in the process of absorbing CO2. After the capturing process, CO2 is transported via pipes, ships, and trucks to geological storage sites [70]. At geological storage sites the captured CO2 is injected into deep rock formation, depleted oil and gas reservoirs, non-mineable coal seams, and saline aquifers. It can also be used in enhanced oil recovery where it is injected into aging oil fields to boost extraction while simultaneously storing the CO2 underground [72]. The three ways in which carbon can be captured in a combustion process are as follows:

- Post combustion capture: This is when CO_2 is captured from flue gases emitted by industrial facilities and gas turbines. This type of capture is most suitable for existing industrial machines and is retrofitted into existing gas turbines [73].
- Pre combustion capture: This is when fuels undergo a gasification process to produce a syn gas composed of CO and H_2. CO reacts with steam to CO_2. The CO2 is separated before the commencement of the combustion process. This is a highly effective capture process but it is expensive and requires imminent infrastructure investment [74]
- Oxy-fuel process: This is when fuel is combusted in only pure oxygen instead of air. This kind of combustion only produces CO_2 and water vapor. After the water is condensed, a concentrated CO2 stream that can be easily captured [75]. The production of oxygen for this type of combustion is energy intensive.

Carbon capture presents lots of great benefits. It is a process that will help in the reduction of greenhouse gases and support a just energy transition. With industries like steel, chemical and cement which are hard to decarbonize, will benefit from CCS which will in turn help in the reduction of the release of greenhouse gases into the atmosphere. Reducing the usage of fossil fuels gives an opportunity to energy intensive industries to transition to cleaner alternative energy sources without disrupting the energy economy. It ensures preservation of energy security and jobs. When CCS is combined with bioenergy (BECCS) or direct air capture (DAC), it can result in negative emissions and help in achieving climate targets [76][77]. The future of CCS looks like we are developing new materials for more efficient and effective CO2 separation [70]. Also, captured CO2 can be converted into

products such as synthetic fuels, building materials, and chemicals which can provide incentives for CCS adoption [78].

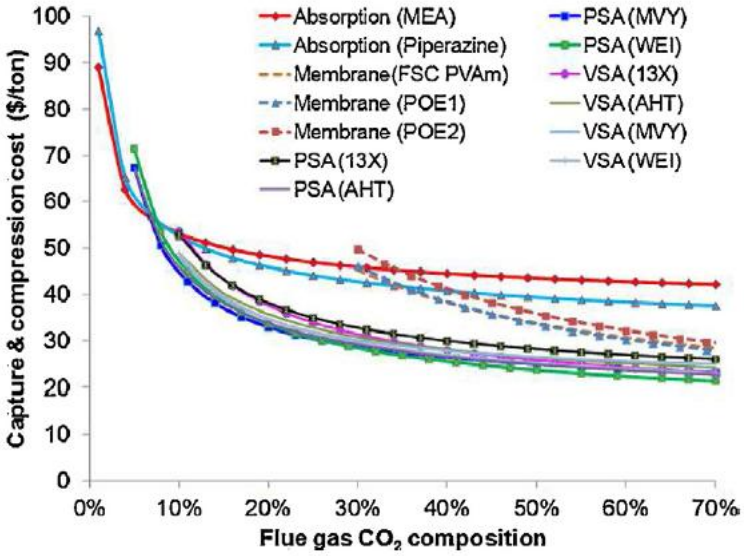

Figure 2.12 Carbon capture and compression cost trends as a function of flue gas CO2 concentrations for various materials and technologies. [70]

2.8 Exhaust gas recirculation.

Exhaust gas recirculation is when portions of the exhaust gas (flue gas) are recirculated back into the system for combustion. This process has been in existence for many years with reciprocating engines [79]. With gas turbines there is an option for it to be recirculated back into the compressor or the combustion chamber after its pressure has been increased to match the compressor exit pressure. It has primarily been used as an emission control technique aiming at reducing NOx emissions in reciprocating engines [80]. It lowers the combustion temperature and alters the air-fuel mixture. The reduced peak cylinder temperature contributes to reduction in engine knock in gasoline and enhances engine durability in diesel engines [79]. EGR also helps with fuel efficiency. It helps in reducing pumping losses by allowing partial throttle operation [81].

The introduction of inert gases such as carbon dioxide and water vapor into the cylinder reduces the concentration of oxygen available for combustion. The EGR system consists of some key components like the EGR divergent valve, heat exchanger (cooler), and control system to regulate and ensure some synchronization between engine speed, engine load and amount of exhaust gas to be recirculated [82]. It can be done internally or externally[83]. The internal EGR is done by altering the valve timing to retain some exhaust gases within the combustion chamber without the need for external piping [84]. This is prevalent in gasoline engines. For external EGR, the exhaust gas is piped and routed into the intake manifold. This is prevalent with diesel engines, and the flue gas is cooled before being introduced into the intake manifold. In as much as EGR presents many advantages it equally presents some drawbacks. EGR leads to increased particulate matter and soot production which if not dealt with blocks the intake manifold and EGR valves [85]. It also increases engine deposits and creates maintenance issues. The inception of carbon rich deposits in the flue gas leads to building up carbon in the intake system which will eventually affect engine performance if not maintained on time [86].

2.8.1 EGR in gas turbines

Gas turbines have been examined to see the possibility of inculcating EGR. This efforts dates back as far as the 1980s. The early studies were aimed at theoretical assessment of the possibility of EGR implementation on gas turbines [87]. Experiments were conducted on small scale turbines. As the initial studies of EGR on gas turbines continue, certain challenges were realized. Most of the challenges faced were associated with combustion efficiency and stability, material integrity and cycle efficiency. With some suggesting the use of highly oxygenated fuel to make up for the reduction in oxygen in the combustion process [88]. To investigate the effects of EGR in gas turbines, the gas turbine is often modeled using a CFD, CRN both to establish how EGR affects

gas turbine overall performance, power output and emissions. This thesis seeks to explore how CRN can be used to understand the effects of EGR of both conventional and premixed combustor of the Centaur 40 gas turbine.

2.9 CRN for combustion system

Combustion reactor network is a modeling approach used to analyze a combustion process in complex systems like industrial furnaces, gas turbines, and internal combustion engines [89]. This is done by breaking down the combustion system into a network of idealized reactors that is used in the study of pollutant formation, flame characteristics, and combustion efficiency [90]. It is also used to understand the NOx and CO emissions pathway. CRN is used to represent a physical combustion system as a series of interconnected ideal reactors. CRN is inexpensive and uses less time compared to traditional CFD. The reactors used for CRN models are 0-D dimensional; perfectly stirred reactors (PSR) and plug flow reactor (PFR) [91]. One inexpensive and accurate way to model emissions in gas turbines in this era is the use of chemical reactor networks [92].

2.9.1 Perfectly stirred reactor (PSR)

For this type of reactor, there is an assumption that mixing occurs in molecular scale and is instantaneous compared to the chemical reaction in the controlled volume. These types of reactors are also called continuously stirred tank/well-stirred reactors [41]. The mixing and molecular scale is assumed to be instantaneous[93]. The flow conditions corresponding to the PSR can be calculated based on the dissipation gradient method, which is when the pressure drops and the volumetric flow rate meets a critical condition, the reactor element is treated as perfectly stirred [94]. With this type of reactor, it is assumed that chemical reactions occur homogeneously. Since it is assumed to operate in steady state conditions it has no dependence on time [41]. There are mass, species, and energy conservation equations that define the functionality of this reactor.

Mass Conservation: Mass conservation in a control volume of a PSR is given by [41],

$$\frac{dm}{dt} = \sum \dot{m}_{in} - \sum \dot{m}_{out} + \dot{m}_{wall} \qquad \textit{Eq(2.40)}$$

Since there are no penetrable walls $\dot{m}_{wall}$ will be neglected [41].

Species Conservation: The governing equation is the rate at which the species k is generated and is as follows [41]:

$$\dot{m}_{k,generated} = V\dot{\omega}MW \qquad \textit{Eq(2.41)}$$

The rate at which the mass is changed for each species is as follows.

$$\frac{d(mY_k)}{dt} = \sum \dot{m}_{in}Y_{k,in} - \sum \dot{m}_{out}Y_{k,out} + \dot{m}_{k,generated} \qquad \textit{Eq(2.42)}$$

Y_k is the mass fraction of species, V is the reactor volume in m^3, MW is the molecular weight of the species k in kg/mol and $\dot{\omega}$ is the chemical source term in mol/m^3sec. The mean residence time used in the CRN is as follows.

$$\tau_{res} = \frac{\rho V}{\dot{m}} \qquad \textit{Eq(2.43)}$$

Where ρ is the density of the species is, V the combustor volume, and $\dot{m}$ the mass flowrate of the species through the reactor.

Energy conservation: Apart from mass and species conservation energy is also conserved as every species entering the reactor is destroyed and a new one is formed [41]. The governing equations for energy conservation are as follows:

$$U = m \sum_{k} Y_k \, U_k(T) \qquad \textit{Eq(2.44)}$$

$$\frac{dU}{dt} = u\frac{dm}{dt} + mc_v\frac{dT}{dt} + m\sum_{k} u_k \frac{Y_k}{dt} \qquad \textit{Eq(2.45)}$$

Where U is the total internal energy and m is the mass in kg. The equations given are for an ideal gas case.

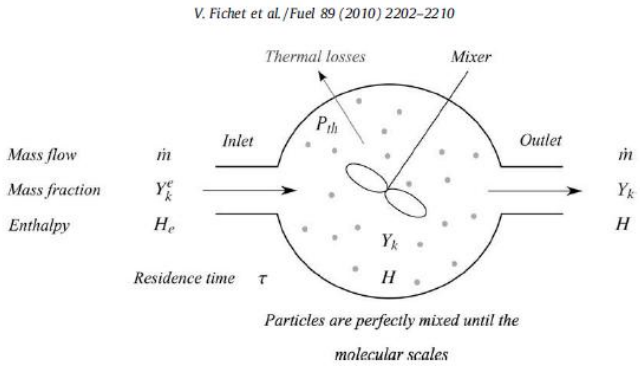

Figure 2.13 A perfectly stirred reactor.[95]

2.9.2 Plug flow reactor.

This reactor is mostly used to model the exhaust of the combustor where gases complete the combustion process and move out of the exhaust [89]. With this type of model there is no mixing in the axial direction. Which implies that molecular and/or turbulent mass diffusion is negligible in the flow direction [41]. This reactor presents a uniform property in the direction perpendicular to the flow, i.e., one dimensional flow [96]. With this assumption it means the reactor only considers radial diffusion and not axial diffusion with a steady state condition. The governing equations are seen in Figure 2.14. Since it is a one-dimensional flow, only the x direction of equations is considered:

$$\frac{d(\rho U_x A)}{dx} = 0 \qquad \textit{Eq(2.46)}$$

$$\frac{dY_i}{dx} = \frac{\omega \dot{M} W A}{\dot{m}} \qquad \textit{Eq(2.47)}$$

$$\frac{d(h + \frac{v_x^2}{2})}{dx} + \frac{\dot{Q}"P}{\dot{m}} = 0 \qquad \textit{Eq(2.48)}$$

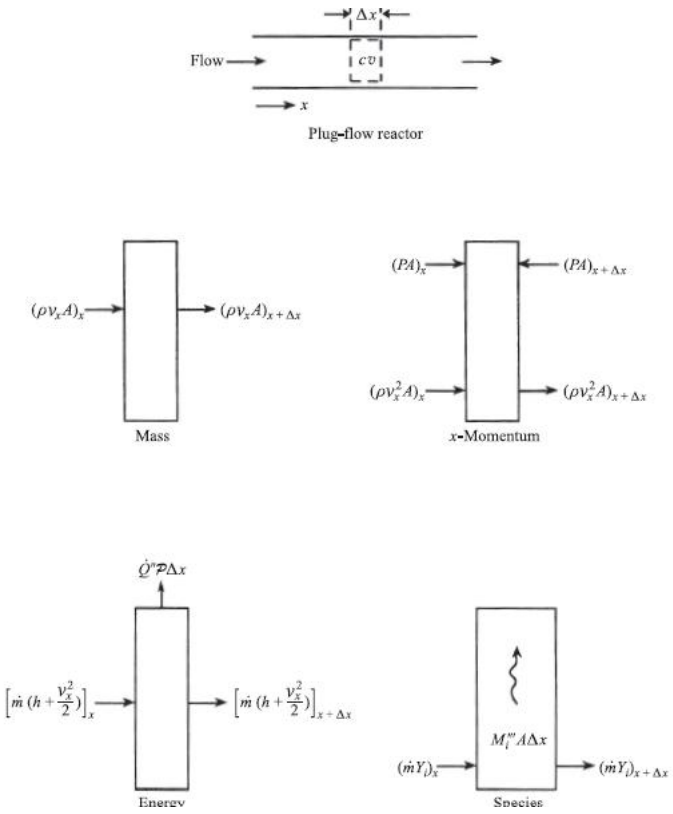

Figure 2.14 A plug Flow reactor.[41]

2.10 Modeling tools

There are many tools used in the study of chemical kinetics, but for this thesis ANSYS Chemkin Pro was used. Chemkin Pro was used to solve the problems associated with thermodynamics, transport processes, and chemical kinetics [97]. There must be an input for Chemkin Pro to be able to solve the thermodynamic and transport processes. The input must contain NOx, CO kinetics for Chemkin Pro to be able to predict the formation of such pollutants. A simple reaction as seen in **Eq(2.9)** is what is used to represent a reaction but that is an oversimplification but there is a lot of complex chemistry that happens in between. This is because combustion is not a single step reaction but a sequence of different reactions coming together to

form the final product [41]. The collection of all these chemical reactions is known as a chemical mechanism [98]. There are many chemical mechanisms available for modeling and some are.

- C3 mechanism
- GRI-Mech
- San Diego mechanism
- LLNL mechanism
- Konnov mechanism

2.10.1 Gas turbine modeling using CRN.

Modeling gas turbines using CRN approach is something that has been explored for at least seven decades (1950s). There are technical papers that describe the working of CRN model for a premixed and a non-premixed combusted gas turbine. Different papers described the various zones in the combustor based on diffusive properties of the flame and mixture fraction gradients mostly from 3-D CFD simulations. Modeling gas turbine combustors with PSRs and PFRs was initially introduced by S.L. Bragg [99]. Longwell and Weiss later experimentally validated it [100] with an experiment where back mixing of recirculated gas was assumed fast compared to the controlling chemical reaction rate. Swithenbank proposed the zonal combustion model [94]. With the zonal modeling approach the combustor volume is divided into zones represented by idealized reactor elements such as PSR, PFR, or a mix of the two. Rutar and Malte modeled the experimental jet stirred reactor with a simple two or three idealized reactors scheme [101]. Schlegel et al., and Feitelberg et al., also performed similar experiments using simple idealized reactor elements for predicting emission production in gas turbines [102][51]. The CRN approach is a quick and remarkably effective way of evaluating emission and the effects of parameters of interest using

detailed chemical kinetic mechanisms. There are instances where a more complicated CRN model will be required due to the complexities of the flow field and boundary conditions. Sturgess et al also did a lean blow out model for an aircraft engine using the zonal modeling approach [103]. Sturgess in 1996 developed a CRN model based on post-processing CFD simulation [104]. The fuel used for these studies was Jet-A/JP-5/JP-8 by comparing the CRN predictions with experimental emissions data. NOx emissions are highly influenced by injector boundary conditions. The CRN model built by Nicol et al had the fuel-air stream divided into five parallel flows with the discrete fuel-air equivalence ratio obtained from a Gaussian distribution function [57]. Different research challenges can be incorporated into CRN just as Tonouchi and Pratt had a finite rate mixing model used to incorporate the effects of large and small scale mixing into the chemical reactor scheme [105]. The idea of splitting flows into different numbers of streams to account for imperfect mixing was done by Nguyen et al in 2013 [106] . Employing a CRN Nguyen and his team modeled the experimental results of Mellor with the pre-mixer outlet flow split into two streams to describe the imperfection in the mixing process. In 2001, Novosselov also used a CRN to predict NOx and CO emissions of the lean premixed combustor [107] of Mellor. This was based on the CFD results of combustor eight step global chemistry. Over the years the methodology for building CRN is different from author to author. There is a gap in analyzing interactions between chemistry, mixing, and complex boundary conditions. The CRN models are used to study emissions and perform parametric studies on gas turbine combustor performance as well. Below is an extensive look into combustion studies using CRN.

- A.B. Lebedev et al.

  Lebedev and his team developed an improved reactor model for predicting emissions (NOx, CO, unburned hydrocarbons, and sulfur oxides) in gas turbine combustor operating in diffusion

mode. A CIAM-M combustor was used for the model. The studies were done for both methane and kerosene-fueled combustors. A three-dimensional CFD was used to analyze the combustor flow fields [108]. The combustor volume was then divided into reactors with uniform mixture fractions (mixture fraction gradient). PSRs models were used to simulate fuel-rich zones near the injectors, flame front region, and cooling system region near walls. The flame front region is an almost stoichiometric region [108]. Each flame front was giving a residence time as seen in Eq(2.49). GRI-Mech 3.0, Konnovo's mechanism, and DS reaction mechanism were the detailed kinetic mechanism used. Emission indices for NOx, CO, SO_2, and SO_3 were calculated at different operating conditions. The model was validated using data from the CIAM-M combustor, like the PC-90A gas turbine. The measurement taken included NOx concentrations at 1MPa for methane and 1.16MPa for kerosene.

$$\tau_{res} = \frac{Flame\ front\ thickness}{Flow\ velocity} \qquad Eq(2.49)$$

$$Flame\ front\ thickness = \sqrt{\frac{D_T \Delta Z^2}{\chi}} \qquad Eq(2.50)$$

D_T is the diffusion coefficient and ΔZ is 0.01, which is the difference in mixture fraction that determines if the region is above or below the stoichiometric mixture fraction (rich or lean). The CRN was able to validate the NOx values obtained from the model with experimental data.

Some insights from the experiments were:

- The GRI-Mech 3.0 and Konnov's mechanism underestimated the NOx emissions by 50% whereas the DS kinetic model provided the most accurate NOx predictions.
- The GRI-Mech 3.0 relied on the Zeldovich mechanism whereas the DS model predicted a stronger influence of prompt NO formation in the fuel-rich zones.
- Kerosene combustion produced 50% more NOx than methane. CO and unburned hydrocarbons emissions were also higher for kerosene due to its higher C/H ratio.
- Air temperature and residence time are directly proportional to NOx emissions but inversely proportional to CO emissions.
- At full load power, NOx emissions were 36.4 g/kg and at 7% load there was a sharp rise in CO from 0.72 g/kg to 105 g/kg.

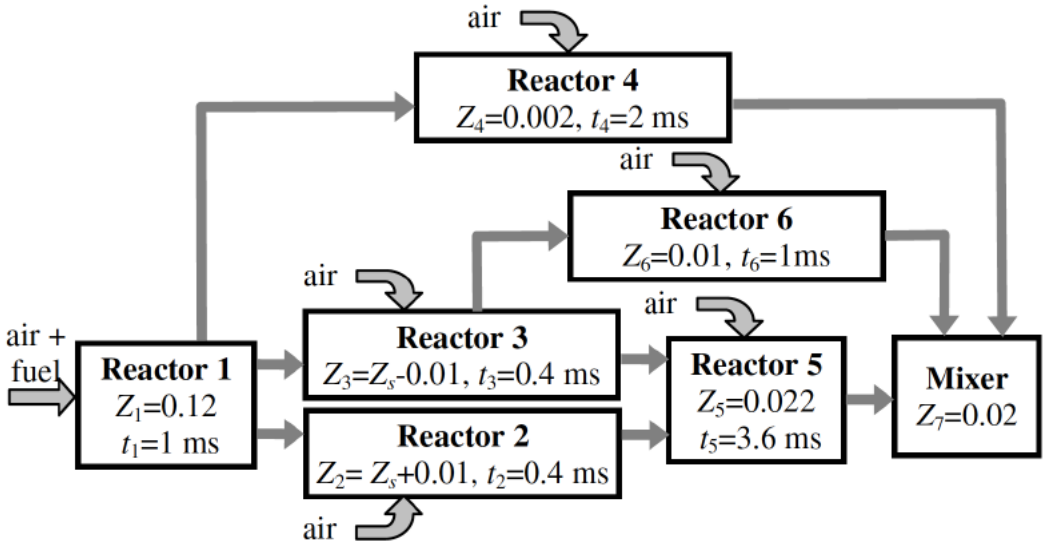

Figure 2.15 An image of Lebedev CRN. [108]

- I.V. Novosselov et al.

Novosselov and his team developed a CRN and applied it to a DLE industrial gas turbine engine with the aim of studying exhaust emissions. The CRN creation was based on the CFD

work by the University of Washington [107]. The University of Washington used the eight-step global mechanism. The CRN that was created was made up of thirty-one chemical reactor elements representing the different flow and reaction zones of the combustor. The experiment was conducted at full-load engine conditions with varying pilot flows ranging from 35% to 200% of the neutral pilot [90]. The detailed GRI-Mech 3.0 kinetic mechanism was used in the prediction of NOx and CO emissions. CFD results of the flow fields and reaction space were a guide in creating the CRN. The experiment was performed on Solar Turbine's Centaur 40 SoLoNOx injector, which has a main and a pilot flow. Fuel used was 2.35% by volume of nitrogen dilution of methane, and emission prediction was done at full load engine operating conditions [90]. For this test, the actual engine test rig pressure, temperature, and flow rates were simulated by using the K-epsilon turbulence closure model. A rate limiting approach was used in determining the effective reaction rate, i.e., the smaller turbulent mixing reaction rate and chemical kinetic rate were selected [90]. The turbulent mixing reaction rate was computed with the eddy break-up (EBU) of Magnussen and Hjertager [109]. The University of Washington's eight-step process, global kinetic mechanism and pressure-sensitive approach were used in calculating the chemical kinetic rate [90]. The eight steps used in building this model are:

- Fuel-air distribution in the pre-mixer/injector main circuit.
- Fluctuations in flame temperature.
- Temperatures, fuel-air ratios, and volumes, of the main regions of the burning flow field.
- Interaction and mixing of the pilot gas with the main recirculation zone and the main flame.

- Crossflow turbulent mixing within the injector main circuit outlet stream and the resultant main flame.
- Rate of entrainment of the main recirculation zone and the dome recirculation zone gases into the main flame.
- Mixing gas from neighboring injectors/flames into the main flame.
- Velocity profile in the pre-mixer/injector main circuit.

The CRN comprised thirty-one elements, made up of PSR, PFR, and mix. The mix stands for an element where the inlet streams are uniformly mixed without chemical reaction [90]. The thirty-one elements represented different distinct zones and regions in the combustor: the main flame zone - consisting of the inner, center, and outer fuel-air input streams as provided by the pre-mixer/injector main circuit. The pilot flame zone which is made up of the pilot flow input stream as provided by the injector pilot circuit. The center recirculation zone is made up of the back-mixed hot product gas flow. The dome recirculation zone is made up of the combustor dome air input stream. The post-flame zone consisted of the CO burnout zones and secondary dilution input stream. The flow parameters for each region were determined based on CFD temperature, species field, and flow. The pre-mixer outlet stream and resultant main flame were divided into three streams: outer, center, and inner. Combustion was initiated in the center stream by using a single PSR element. PFRs were used to model the parts of the flow that do not satisfy the conditions required for a PSR, and those parts that are used to complete the combustion process in post flame zones, allowing the carbon monoxide concentration to relax and reach the local equilibrium value. As the secondary dilution air enters the combustor, the CO chemistry is quenched. This brings CO close to the engine emission. Using PSRs in series to model a flame yields a residence time

distribution like that of a one-dimensional chemical reactor with longitudinal diffusion [110]. Some insights from the experiments are:

- CO levels were at chemical equilibrium conditions before the injection of secondary cooling air into the combustor.
- CRN helps understand the pathways and zones that contribute to NOx and CO emissions. And they may change with modification to combustor setup (liner, injector) and/or boundary conditions (load, pressure, and fuel-air ratio)
- Prompt and NNH nitrogen oxide form in the early part of the flame and then their rates reduce sharply as the flame continues. N_2O and flame Zeldovich routes are highly active in the heart of the flame and continue into the near post flame zone. The low contributions of the prompt and NNH pathways are a result of part of the pressure assumed, which is engine pressure. High pressure tends to diminish these pathways.

Burns et al.:

- Burnes et al at Solar Turbines in 2020 conducted research to explore the use of EGR in industrial gas turbines to facilitate the efficiency of carbon capture while maintaining turbine performance [71]. CRN was used for this exploration. The studies were done on a single-shaft turbine (Titan 130) and a two-shaft turbine (Titan 250). Performance analysis on the gas turbines was done using a Numerical Propulsion System Simulation (NPSS) model. The residence time was evaluated from the CFD model by the University of Washington [90]. EGR was simulated at varying EGR levels. Seventy-five percent EGR was a point of interest in the studies. The studies were done at 75% EGR with and without supplemental O_2 injection [71]. NOx, CO, and unburned hydrocarbons emissions under different oxygen levels were

investigated. Flame stability and laminar flame speed at varying EGR levels were studied. Some of the key findings from the studies were:

- The two-shaft turbines showed better performance with EGR compared to the single-shaft turbines.
- Compressors' characteristics improved as EGR levels increased; this phenomenon led to efficient power generation.
- At 75% EGR, the carbon dioxide level increased to about 13% mole fraction, which presents a wonderful opportunity for carbon capture.
- Thermal efficiency of the gas turbine reduces slightly as EGR is introduced.
- The density of the oxidizer increases as EGR levels increase, which results in higher power output.
- There was a 50% decrease in NOx emissions at 14 – 16% O_2 due to lowered flame temperature.
- It was realized that the optimal oxygen concentration levels that supports robust combustion is between 14 – 16% O_2.
- Five percent supplemental O_2 is required at 75%.
- There is a potential of 25,000 gallons/day from condensed exhaust.

2.11 Literature review summary

This chapter provides a foundational understanding of the theoretical principles underlying gas turbine operation. As revealed through the literature review, the Chemical Reactor Network (CRN) modeling approach has been employed in gas turbine research since the 1950s. This method offers a simplified yet robust framework for analyzing complex combustion processes by representing various combustion zones using idealized reactor elements—namely, Perfectly

Stirred Reactors (PSRs) and Plug Flow Reactors (PFRs). The CRN methodology facilitates efficient evaluation of emissions characteristics, combustion performance, and the impact of operational parameters by leveraging both detailed and global chemical kinetic mechanisms.

Pioneering contributions by researchers such as S.L. Bragg, Longwell, and Swithenbank laid the groundwork for zonal modeling and assumptions of back-mixed gas flow. Subsequent advancements by Rutar, Malte, and others further refined the approach by developing simplified CRN schemes for emission prediction and flame behavior characterization. The integration of CRN modeling with computational fluid dynamics (CFD)-derived flow field data has significantly enhanced the accuracy and predictive capabilities of these models.

Notably, studies by A.B. Lebedev et al. and I.V. Novosselov et al. utilized idealized reactor networks to investigate combustion stability and emission formation in both Dry Low Emission (DLE) and diffusion-mode combustors. These investigations demonstrated that NOx emissions are strongly influenced by residence time and flame temperature, and that fuels with higher carbon-to-hydrogen (C/H) ratios tend to produce greater quantities of CO and NOx. Other critical factors affecting emission formation include pilot fuel flow rates, mixing quality, fuel composition, combustor boundary conditions, and operating pressure.

Further contributions by Burnes et al. of Solar Turbines explored the application of Exhaust Gas Recirculation (EGR) in natural gas-fueled industrial gas turbines. Their findings indicate that, at elevated EGR levels, supplemental oxygen must be introduced to sustain stable combustion.

Building upon these established studies, the present thesis aims to investigate the effects of EGR on liquid-fueled gas turbines utilizing both DLE and conventional combustor configurations through CRN modeling. To the best of the author’s knowledge, this represents a novel contribution

in the field. The successful completion of this work is expected to provide significant advancements in gas turbine design and manufacturing, contribute to emission mitigation strategies, and support the broader objectives of carbon capture and environmental sustainability.

CHAPTER 3 - METHODOLOGY

3.1 Model development

The preceding chapter provided an insight into how CRN is developed and optimized. This chapter will capture how a non-premixed and a premixed flame inside a Centaur 40 gas turbine can be modeled using CRN with the incorporation of EGR. The CRN will be used to capture emissions and blowout conditions in the different zones in the combustor. The CRN model consists of several PSRs connected in series to represent the different combustor zones. The natural gas model was built off slight alterations from what Burnes et al did [71]. The combustor is segmented into three distinct zones: the primary combustion zone, the secondary combustion zone, and the cooling/dilution zone. The primary zone serves as the flame initiation and anchoring region, where fuel and air mixing begin and stable combustion is established. This zone operates under high-temperature conditions, typically ranging between 1200 K and 2000 K, facilitating rapid chemical reactions necessary for ignition and sustained flame stability [32]. There is sufficient time and turbulence in this zone to achieve complete combustion of the air-fuel mixture. Air flow patterns in the primary zone are key contributors to sustaining combustion in the zone [13]. Combustor designers have the responsibility to create this airflow pattern to sustain combustion by creating toroidal flow reversal that entrains and recirculates a portion of the hot combustion gases to provide continuous ignition to the incoming fuel air mixture [32]. A good flow pattern in the primary zone helps in preventing combustion pulsation and noise. Some of the ways combustor designers create this desired airflow patterns are the use of air swirlers or creating holes in combustion liner walls at the upstream end of the liner [32]. The intermediate zone provides an avenue for some amount of air to be added in pursuit of complete combustion of intermediates and other products like CO.

If gases move directly from the primary zone to the dilution zone and are cooled suddenly, the gas composition will be affected and will lead to elevated levels of CO passing through the exhaust. The dilution zone makes room for the rest of the air after the combustion and wall cooling process. It also serves as an outlet with a temperature distribution that proceeds to the turbine section of a gas turbine[13]. Between 20% - 40% of the total combustor air flow is consumed in the dilution zone [111]. Air is introduced into the dilution zone through distinct size and shape holes in the liner walls with the sole aim of optimizing effective mixing of the air with the fuel air mixture coming from the intermediate zone. An effective design of the dilution zone impacts the turbine section, especially the first stage turbine blades, thus affecting the total power production [32].

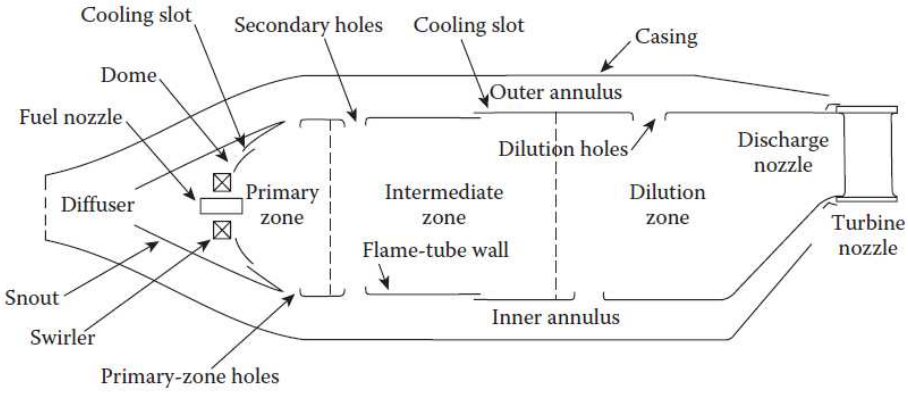

Figure 3.1 An image of the different zones of a gas turbine combustor.[32]

The combustor under scrutiny is both the dry low emission (DLE) and conventional combustor of the Centaur 40 gas turbine. PSRs are used to represent these zones in the main and pilot sections of the combustor. The main section of the combustor has a premixed flame feature as shown in Figure 2.8, whereas the pilot section has a diffusion flame that anchors the main flame for the premixed combustor type as seen in Figure 2.7. Before a CRN model can be developed, key design

parameters of the combustion system must be known as this drives the development process. These key design parameters are presented in Table 1 and Table 2.

Before CRN can be developed for a gas turbine combustor the different flow fields, temperature, and species profile in the combustor must be identified. This information can be analyzed and achieved through a CFD model. The flow will be taken from work already done by Priyank et al and Novosselov [71][90]. It is based on the work of these two that my CRN was developed.

In the construction of CRN, information regarding the geometry of the combustor and the flow patterns in the combustor play a huge role in zoning the combustor and calculating the residence time [32]. One reliable and effective way of defining the flow patterns is performing a three-dimensional study on the combustor. CFD modeling of combustors helps to provide information about the temperature, flow, and species profiles in the combustor. These profiles help the visualization and interpretation of the reaction space and flow patterns that will play a key guide in accurately developing a CRN to represent the different zones. This model was built based on CFD predicted flame behavior and combustor boundary conditions and engine test results [112].

Table 1: Key combustor parameters for a Centaur 40 dual fuel dry low emission (SoLoNOx) combustor.

Parameters	**Values**
Number of Injectors	12
Secondary air flow	0.10

There are some assumptions that were made during the construction of the CRN. The assumptions are in place to reduce computational complexity, enable parametric studies and mechanism

reduction, and bridge the gap between detailed chemistry and realistic flow dynamics. These assumptions are:

- A perfect mixture of recirculated air and ambient air for the EGR process.
- No losses due to fluid friction.
- Equal velocity of air and fuel.
- Chemical reaction time is greater than mixing time ($\tau_{chem} > \tau_{mixing}$).
- No molecular transport of species, thermal energy, and momentum.
- No spatial gradient (no variation in properties from one point to another within the reactor).
- The net rate of accumulation of mass and energy is zero.
- In transient situations, changes over time are allowed and tracked until equilibrium or steady conditions are reached.
- Constant pressure assumptions.
- Heat losses, wall reactions, and mass transfer to and from walls are neglected.
- The gas mixture follows the ideal gas law, simplifying thermodynamic calculations.
- Gas phase is assumed (no droplets, soot, or condensed phase).
- All reactions take place within the bulk fluid and not on surfaces.
- Flow between reactors is idealized.
- The residence time allocated to each PSR is based on CFD data, geometry, and engineering estimates.
- Real turbulent mixing and flame propagation are not resolved; instead, mixing is lumped into the residence time and reactor volume.

- Residence time is the same for both the liquid fuel and the gaseous fuel because the atomization and evaporation of the fuel is accounted for in **Eq(**3.4) but the mixing time is assumed to be the same.
- Assuming the conventional combustor has the same geometry and flow conditions as the DLE combustor

Table 2: Key combustor parameters for a Centaur 40 conventional combustor.

Parameters	**Values**
Number of Injectors	10
Secondary air flow	0.10

3.1.1 Air distribution for combustion and the combustion process.

Following compression, the total airflow from the compressor progresses to the next phase of the Brayton cycle, the combustor. However, not all the compressed air is directed into the combustion chamber. A portion of this air is diverted, or scavenged, for essential auxiliary functions such as cooling high-temperature components, sealing rotating parts, valve actuation, and atomization of liquid fuel. The fraction of air diverted for non-combustion purposes is an engineering design parameter, typically determined by the Original Equipment Manufacturer (OEM). This diverted air fraction is denoted by the Greek symbol β (Beta). Consequently, the effective combustion air that is, the portion of air available for the combustion process is calculated as the total compressor discharge air minus Beta.

In advanced dry low emission systems such as the SoLoNOx combustor, a further subdivision of the combustion air occurs. A proportion of the available combustion air is routed through the fuel injectors to facilitate premixing, which enhances fuel-air uniformity and helps achieve reduced NOx emissions. The ratio of the airflow entering the injector to the total combustion air is defined as α (Alpha). The Alpha value is strongly influenced by the effective flow areas of both the injector and combustor liner and is typically provided by the OEM based on proprietary combustor design specifications.

The remaining combustion air, after accounting for injector flow, is then distributed among the various zones within the combustor, specifically the primary combustion zone, intermediate (or secondary) combustion zone, and the dilution zone. This distribution is determined based on the geometric configuration of the combustor, including the location and size of the air admission holes on the liner walls. These design features govern the staged mixing of air and fuel, combustion stability, flame anchoring, and influence emissions and efficiency.

This airflow partitioning framework using β and α forms the basis for modeling combustion dynamics, flame stability, and pollutant formation in complex systems such as the dual-fuel Centaur 40 SoLoNOx gas turbine under Exhaust Gas Recirculation (EGR) conditions.

$$Combustion_{air} = Total_{comp_{air}} - \beta \qquad Eq(3.1)$$

$$\alpha = \frac{amount\ of\ Combustion_{air}\ in\ injector}{Combustion_{air}} \qquad Eq(3.2)$$

Since PSRs assume a perfect mixture, it helps isolate the effects of reaction kinetics from the complexities of mass and heat transfer limitation. This makes every fluid element inside the reactor experience the same temperature, pressure, and concentration conditions throughout the reactor volume. With this uniformity assumption, the residence time is hence characterized by a single average value rather than a distribution thereby avoiding complexities associated with non-ideal flow patterns and spatial gradient. CO wall quenching effect is not modeled in the CRN.

Residence time, τ, is a combustion parameter that defines the period reactants stay in a combustion zone to allow heat transfer, mixing, and chemical reaction [113]. This parameter plays a crucial role in the development of CRN combustion studies and emission prediction. It is the ratio of the volume of the combustor and the volumetric flow rates of the reactants.

$$\tau_{res}\,(sec) = \frac{\rho V}{\dot{m}} \qquad \textit{Eq(3.3)}$$

Where V(m^3) is the combustor volume, $\dot{m}$(kg/sec) is the mass flow rate, and ρ(kg/m^3) is the density.

The thesis built out a model for the Centaur 40 dry low emission (SoLoNOx) combustor that runs on natural gas, the Centaur 40 dry low emission (SoLoNOx) combustor that runs on liquid fuel (diesel), and the conventional Centaur 40 combustor that runs on liquid fuel (diesel). The PSRs selected to represent the combustor were the same as the dual fuel dry low emission (SoLoNOx) combustor (both liquid fuel and gas fuel). It was 7 PSRs in total to represent the primary, secondary, and dilution zone.

Figure 3.2 is a graphical representation of the CRN model for Centaur 40 dry low emission (SoLoNOx) combustor that runs on natural gas. The model is comprised of two fuel/air inlets (main and pilot) that are connected to a gas mixture. Each of these gas mixtures is connected to a PSR to model the primary zone of the combustor at 1800K. Each PSR in the primary zone has a residence time of 3msec which was chosen based on flow patterns observed from CFD studies [91]. The PSRs for the primary zone join another set of PSR which joins a PSR (R5) to make up the secondary zone. The R5 is the PSR where the main and the pilot flow meet. The secondary zone has a total residence time of 13msec and temperature of 1783K. The stream is then mixed with the remainder of the combustion air and passed through a final set of perfectly stirred reactors to model the dilution zone of the combustor at a temperature of 1478K and 8msec residence time. The total residence time set for the whole combustion process is 30msec which was derived from **Eq(3.3**) based on the mass flowrate from engine test data and the combustor volume.

After the various PSRs and residence times were identified and calculated, the necessary boundary conditions were applied to the model. The applied boundary conditions can be seen in Table 1, the mole fractions for oxidizer and fuel for DLE combustor (both gas and liquid fuel) are seen in

In this study, the boundary conditions for the combustor model, specifically, the compressor discharge pressure and temperature, as well as the total air and fuel flow rates were selected to reflect the gas turbine's full-load operating conditions. The objective was to capture representative behavior under steady-state, high-power scenarios. Accordingly, only full-load operation was considered in the thermodynamic and chemical reactor network (CRN) analysis presented in this thesis.

The fuel and air flows entering the combustor were split into two distinct inlet streams: the main flow and the pilot flow. These flow splits are crucial in defining flame stability, ignition

characteristics, and emissions. The split ratios between the pilot and main flows were obtained from Solar Turbines (OEM) and represent typical operational values optimized for low-NOx performance. It is important to note that different pilot-to-main split values are used for natural gas and liquid (diesel) fuels, reflecting their distinct combustion characteristics.

For natural gas, the injection into the combustor facilitates homogeneous premixing with the incoming air, a critical requirement for lean-premixed combustion strategies such as those employed in the SoLoNOx combustor. This promotes uniform flame propagation, reduces flame temperature gradients, and significantly minimizes thermal NO_x formation. In contrast, diesel fuel, being a liquid, undergoes atomization and vaporization, resulting in a fundamentally different mixing and combustion behavior that necessitates a different fuel split strategy and zone-specific combustion modeling.

Table 3 and Table 4. The applied boundary conditions were selected to match those provided on the Centaur 40 dry low emission (SoLoNOx) dual fuel gas turbine test results [112].

In this study, the boundary conditions for the combustor model, specifically, the compressor discharge pressure and temperature, as well as the total air and fuel flow rates were selected to reflect the gas turbine's full-load operating conditions. The objective was to capture representative behavior under steady-state, high-power scenarios. Accordingly, only full-load operation was considered in the thermodynamic and chemical reactor network (CRN) analysis presented in this thesis.

The fuel and air flows entering the combustor were split into two distinct inlet streams: the main flow and the pilot flow. These flow splits are crucial in defining flame stability, ignition characteristics, and emissions. The split ratios between the pilot and main flows were obtained from Solar Turbines (OEM) and represent typical operational values optimized for low-NOx performance. It is important to note that different pilot-to-main split values are used for natural gas and liquid (diesel) fuels, reflecting their distinct combustion characteristics.

For natural gas, the injection into the combustor facilitates homogeneous premixing with the incoming air, a critical requirement for lean-premixed combustion strategies such as those employed in the SoLoNOx combustor. This promotes uniform flame propagation, reduces flame temperature gradients, and significantly minimizes thermal NO_x formation. In contrast, diesel fuel, being a liquid, undergoes atomization and vaporization, resulting in a fundamentally different mixing and combustion behavior that necessitates a different fuel split strategy and zone-specific combustion modeling.

Table 3: Fuel and oxidizer mole fraction for liquid-fueled combustion.

Fuel and oxidizer (mole fraction)		
	Diesel Surrogate	**Air**
$nC_{12}H_{26}$	0.902	
$nC_{11}H_{24}$	0.07	
$nC_{10}H_{22}$	0.028	
N_2		0.777
O_2		0.2084
H_2O		0.0054
CO_2		0.0003
Ar		0.0093

Table 4: Fuel and oxidizer mole fraction for natural gas combustion.

Fuel and oxidizer (mole fraction)		
	Gas Fuel	**Air**

CH_4 (Methane)	1.0	
N_2		0.777
O_2		0.2084
H_2O		0.0054
CO_2		0.0003
Ar		0.0093

Table 5: Gas fuel boundary conditions for Centaur 40 dry low emission (SoLoNOx) combustor.

Gas fuel boundary conditions		
Variable	**Value**	**SI Unit**
T_amb	229.04	K
P_amb	101.01	kPa
Mass flowrate Air	17.96	Kg/s
Mass flowrate Fuel	0.258	Kg/s
AFR		-

The detailed C3 chemical mechanism [114] was implemented to model all hydrocarbons oxidation and emissions chemistry in the CRN model. The C3 detailed chemical kinetic mechanism was selected for modeling both the Dry Low Emissions (DLE) and conventional liquid-fueled combustors due to its comprehensive representation of oxidation chemistry for large hydrocarbon molecules, along with nitrogen oxide (NOx) formation pathways. Among the available

mechanisms, the C3 mechanism stands out for its ability to simulate a wide range of combustion phenomena relevant to both gaseous and liquid fuels used in gas turbines.

This mechanism was chosen for the current study because it provides detailed reaction pathways for key fuels such as dodecane, methanol, dimethyl ether, hydrogen, and syngas, making it highly applicable to simulations involving both conventional and alternative fuels. Additionally, it includes surrogate components that accurately represent the chemical behavior of diesel, gasoline, and jet fuels, enabling more realistic combustion modeling under industrial gas turbine conditions.

Critically, the C3 mechanism incorporates comprehensive sub-mechanisms for NOx formation, including thermal (Zeldovich), prompt, and fuel-bound pathways, as well as polycyclic aromatic hydrocarbon (PAH) formation, which are essential for accurate prediction of pollutant emissions. The mechanism consists of 3,761 chemical species and 16,522 elementary reactions, making it one of the most detailed and robust mechanisms suitable for chemical reactor network (CRN) modeling of complex combustion processes [114]. The C3 mechanism was first published on December 28, 2021, and developed by Computational Chemistry Consortium, a collaboration involving the Lawrence Livermore National Laboratory (LLNL) NUI Galway, Politecnico di Milano, RWTH Aachen University, and the Argonne National Laboratory.

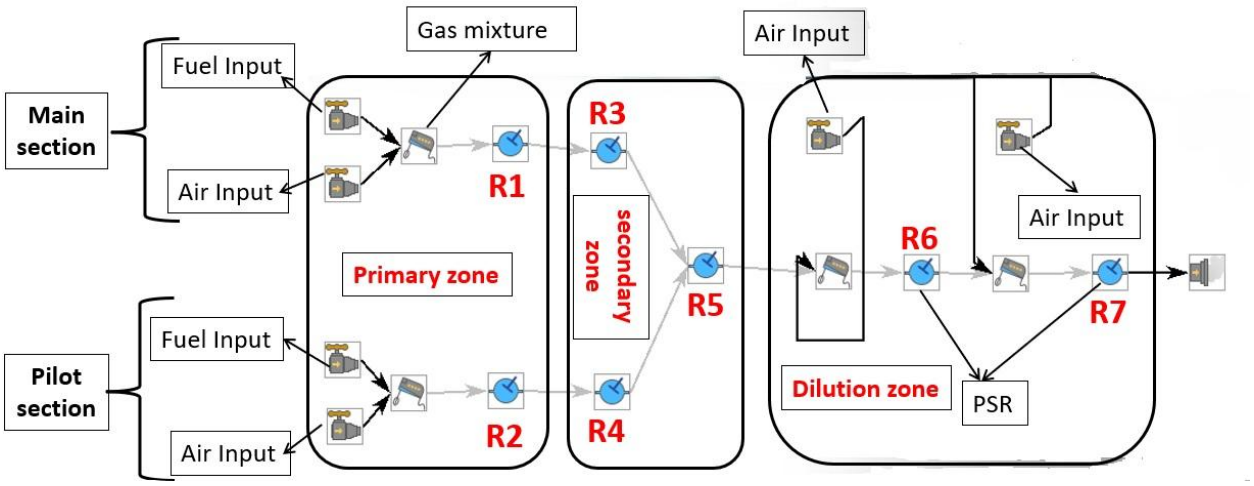

Figure 3.2 CRN model for Centaur 40 SoLoNOx gas-fueled gas turbine.

Figure 3.3 is a graphical representation of the CRN model for Centaur 40 dry low emission (SoLoNOx) combustor that runs on liquid fuel (diesel). The model is comprised of three fuel/air inlets (stoic, lean, and pilot) that are connected to gas mixtures. The subdivision of the main combustion section into lean and stoichiometric zones was implemented to address the distinct characteristics of liquid fuel combustion. This differentiation is a key factor that sets the liquid-fueled combustion model apart from the natural gas model and is examined in greater detail throughout this thesis. The global equivalence ratio for this combustion was 0.231. Each of these gas mixtures is connected to a PSR to model the primary zone of the combustor at 1800K. Each PSR in the primary zone has a residence time of 3msec which was chosen based on flow patterns observed from CFD studies [91] and residence time sensitivity analysis performed on the model. The stoic and the lean region of the primary zone is then joined together into a PSR with the products from the pilot flame section to form the secondary zone with a residence time of 13msec and temperature of 1783K. The stream is then mixed with the rest of the combustion air and passed

through a final set of perfectly stirred reactors to model the dilution zone of the combustor at a temperature of 1478K and 8msec residence time. The total residence time set for the whole combustion process is 30msec and was derived from **Eq(3.3)**. The residence time of each PSR was independently varied; for the primary zone (stoic, lean, and pilot), the residence times were independently varied from 1msec to 6msec, the secondary zone was varied from 1msec to 13msec, and the dilution zone varied from 1msec to 9msec. As seen in Figure 3.4, Figure 3.5, and Figure 3.6 the primary zone indicated the highest degree of sensitivity to residence time, as noted by variations in NOx production. The primary zone is the hottest region (1800K) in the reactor and the thermal NOx is highly influenced by temperature and time according to the Zeldovich mechanism [32]. Within the primary zone, the stoic section was the most sensitive to residence time with a slope of 5.788, followed by the lean section with a slope of 1.06 as seen in Figure 3.4.

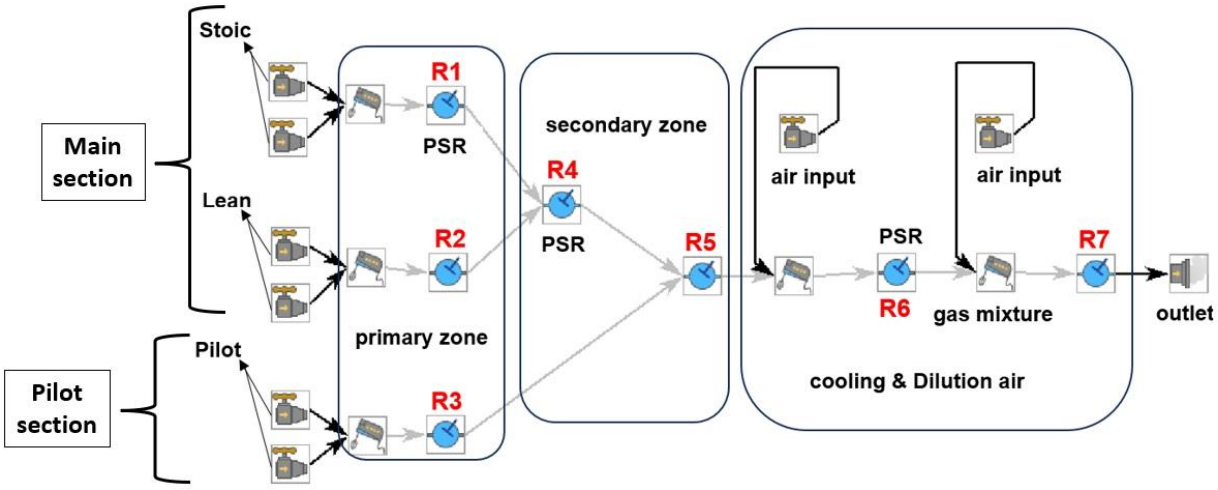

Figure 3.3 CRN model for Centaur 40 dry low emission (SoLoNOx) liquid-fueled gas turbine.

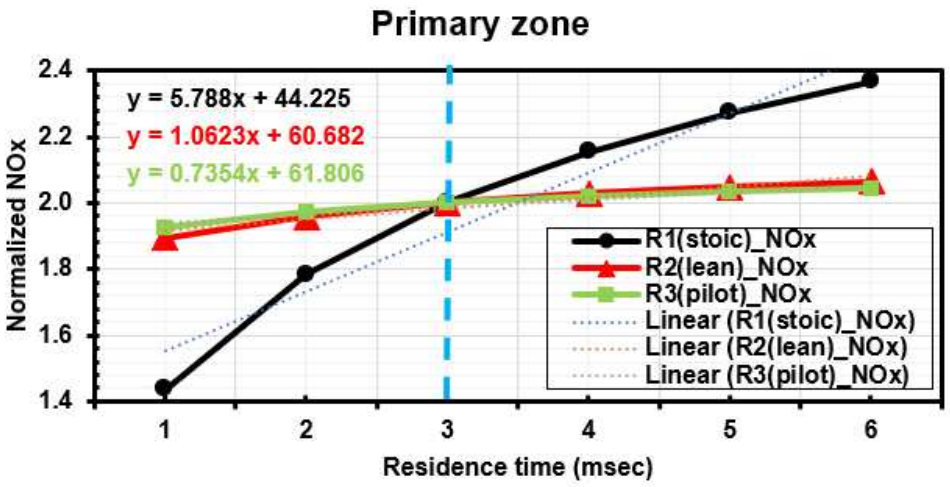

Figure 3.4 Residence time sensitivity analysis for primary zone diesel-fueled gas turbine (blue line representing the chosen residence time).

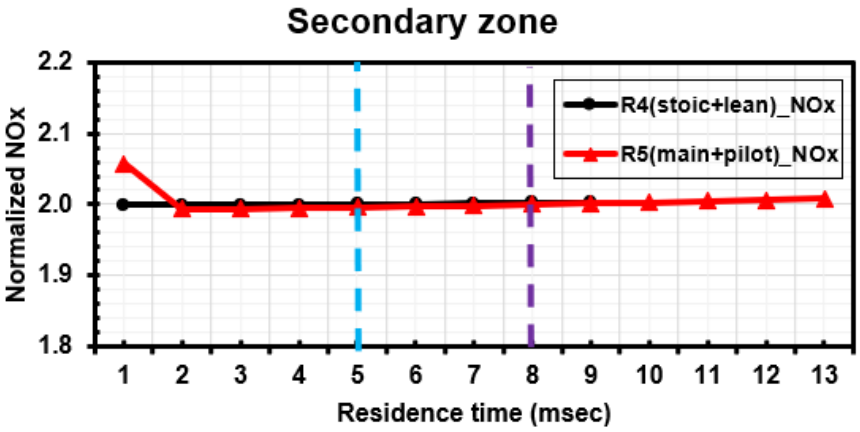

Figure 3.5 Residence time sensitivity analysis for secondary zone diesel-fueled gas turbine (blue and purple line representing chosen residence time for R4 and R5.

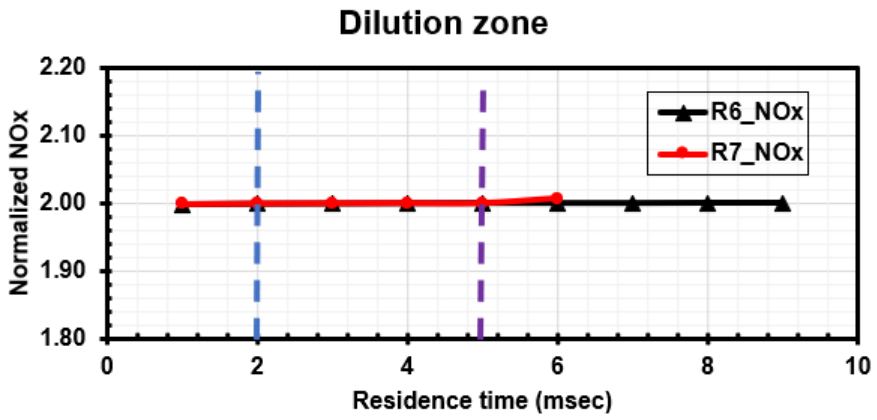

Figure 3.6 Residence time sensitivity analysis for dilution zone diesel-fueled gas turbine (blue and purple lines representing the chosen residence time for R6 and R7.

Table 6: Liquid fuel boundary conditions for Centaur 40 dry low emission (SoLoNOx) combustor.

Liquid fuel boundary conditions		
Variable	**Value**	**SI Unit**
T_amb	229.04	K
P_amb	101.01	kPa
Mass flowrate Air	17.83	Kg/s
Mass flowrate Fuel	0.276	Kg/s
AFR	58.79	-

The applied boundary conditions seen in Table 6 were selected to match those provided on the Centaur 40 dry low emission (SoLoNOx) liquid-fueled gas turbine test results. Notably, compressor discharge temperatures and pressures, i.e., the inlet conditions to the combustor, together with the total air and total fuel flow rates were chosen to match engine full load operation.

As noted earlier, the fuel/air was split into three inlet flow streams. The pilot and main flow split was chosen based on discussion with Solar turbines to stand for typical values during low NOx operation mode. The main flame was divided into two fuel/air flow streams when modeling the liquid fuel to capture the non-homogeneous mixing that can occur with injecting liquid fuels – details of this phenomenon and approach are described below.

3.2 Fuel Stratification

Designing a 0-D CRN simulation comes with some challenges when the fuel to be analyzed is a liquid fuel. Vaporization and mixing of the fuel before combustion need to be accounted for in the simulation process. The novel idea this thesis seeks to communicate is the use of a fuel stratification method in modeling CRN for liquid-fueled gas turbines. Fuel stratification is an existing phenomenon used to describe mixture inhomogeneity, due to uneven distribution of air-fuel mixtures inside a combustion chamber and associated combustion in internal combustion engines [115]. It can be based on a thermal gradient or mixture gradient which results in different localized equivalence ratios [116] [117]. To account for the non-homogeneous mixing with liquid fuels, many considerations were made accounting for impacts of residence time, number of PSRs, flow distribution of the combustion chamber, and air-fuel ratio. The conclusion was to split the main flame into two regions: 1. A lean premixed region accounting for the fuel and air that was able to mix ahead of the flame; and 2. A stoichiometric region representing the portion of the fuel that does not achieve perfect mixing with air and results in a local diffusion-like (stoichiometric) combustion process. The ratio of the fuel participating in the stoichiometric reactor to the total fuel feeding the main flame (i.e., the sum of the lean and stoichiometric fuel in the main flame section) is what I termed the fuel stoic fraction. It is recognized that liquid fuel often generates more NOx than gaseous fuels when used in a DLE combustion system because of the non-perfect mixing and

resultant localized elevated temperature flame regions [73][118]. The main flame fuel split between the lean and stoichiometric regions represents a knob that can be manipulated to achieve the desired results. A fuel stoichiometric fraction was selected to match the engine test data of Centaur 40 DLE liquid-fueled gas turbine with no EGR.

The energy for the vaporization of the fuel was also accounted for in the form of a sensible energy temperature reduction of the reactant streams, using:

$$Q = \dot{m}_{fuel} \times h_{fg} = \dot{m}_{air} \times C_{p,air} \times \Delta T \qquad \textit{Eq(3.4)}$$

Where Q(kJ/s) is the heat energy required, h_{fg}(kJ/kg) is the enthalpy of vaporization, $\dot{m}_{fuel}$(kg/s) is the mass flowrate of fuel, $\dot{m}_{air}$ is the mass flowrate of air, C_p(kJ/kg-K) is the heat capacity of air and ΔT(K) is the temperature change. This vaporization energy only equated to a sensible energy corresponding to a 3.6 K temperature term. The 3.6 K temperature was deducted from the incoming combustion air temperature.

Diesel fuel chemistry was modeled using a simple surrogate shown in

In this study, the boundary conditions for the combustor model, specifically, the compressor discharge pressure and temperature, as well as the total air and fuel flow rates were selected to reflect the gas turbine's full-load operating conditions. The objective was to capture representative behavior under steady-state, high-power scenarios. Accordingly, only full-load operation was considered in the thermodynamic and chemical reactor network (CRN) analysis presented in this thesis.

The fuel and air flows entering the combustor were split into two distinct inlet streams: the main flow and the pilot flow. These flow splits are crucial in defining flame stability, ignition characteristics, and emissions. The split ratios between the pilot and main flows were obtained from Solar Turbines (OEM) and represent typical operational values optimized for low-NOx performance. It is important to note that different pilot-to-main split values are used for natural gas and liquid (diesel) fuels, reflecting their distinct combustion characteristics.

For natural gas, the injection into the combustor facilitates homogeneous premixing with the incoming air, a critical requirement for lean-premixed combustion strategies such as those employed in the SoLoNOx combustor. This promotes uniform flame propagation, reduces flame temperature gradients, and significantly minimizes thermal NO_x formation. In contrast, diesel fuel, being a liquid, undergoes atomization and vaporization, resulting in a fundamentally different mixing and combustion behavior that necessitates a different fuel split strategy and zone-specific combustion modeling.

Table 3 while incorporating chemical reactions to predict NOx and CO emissions [119][120]. The oxidizer composition is also provided in

In this study, the boundary conditions for the combustor model, specifically, the compressor discharge pressure and temperature, as well as the total air and fuel flow rates were selected to reflect the gas turbine's full-load operating conditions. The objective was to capture representative behavior under steady-state, high-power scenarios. Accordingly, only full-load operation was considered in the thermodynamic and chemical reactor network (CRN) analysis presented in this thesis.

The fuel and air flows entering the combustor were split into two distinct inlet streams: the main flow and the pilot flow. These flow splits are crucial in defining flame stability, ignition characteristics, and emissions. The split ratios between the pilot and main flows were obtained from Solar Turbines (OEM) and represent typical operational values optimized for low-NOx performance. It is important to note that different pilot-to-main split values are used for natural gas and liquid (diesel) fuels, reflecting their distinct combustion characteristics.

For natural gas, the injection into the combustor facilitates homogeneous premixing with the incoming air, a critical requirement for lean-premixed combustion strategies such as those employed in the SoLoNOx combustor. This promotes uniform flame propagation, reduces flame temperature gradients, and significantly minimizes thermal NO_x formation. In contrast, diesel fuel, being a liquid, undergoes atomization and vaporization, resulting in a fundamentally different mixing and combustion behavior that necessitates a different fuel split strategy and zone-specific combustion modeling.

Table 3.

While maintaining the same airflow in the pilot system, the pilot fuel flow rate was increased by 10%, making the pilot equivalence ratio move from 0.515 to 0.686 and the effects of this increase in fuel are discussed in the result chapter.

3.3 Reactor network model for non-premixed combustion system (conventional combustor)

For the conventional combustor, a different approach was chosen. Conventional combustors exhibit a diffusion-like flame combustion at about stoichiometry or a little over stoichiometry as presented in Figure 2.8. With this system the oxidant and fuel come together in a reaction zone through molecular and turbulent diffusion [32] . Flames found in this kind of combustion are called a diffusion flame. In conventional combustors an equilibrium assumption is made where the chemical reactions occur faster than the diffusion and flow time scales [89]. The oxidizer and fuel mix at molecular level in the combustor and wherever there is stoichiometric mixing, a structure of flame is formed from the highest temperature [121]. The mixing is due to convection and diffusion of reactant species[32] . The fuel and oxidizer are introduced as seen in Figure 3.7.

For the conventional combustion system, some key assumptions were made, which are:

- Assuming the DLE liquid and conventional liquid combustor have the same combustor pressure.
- Assuming the liquid DLE and liquid conventional combustor have the same mass flowrates for air and fuel.
- Assuming the DLE liquid and liquid conventional combustor have the same residence time and beta value.

Figure 3.8 is a graphical representation of the CRN model for Centaur 40 conventional combustor that runs on liquid fuel (diesel). The model is comprised of fuel and air inlets that are connected to a gas mixture. The fuel and air are introduced as a stoichiometric mixture with an equivalence ratio of one. The gas mixture is connected to a PSR to model the primary zone of the combustor at 2200K. The PSR in the primary zone has a residence time of 3msec which was chosen based on flow patterns observed from CFD studies [91] on the DLE combustor of the same engine. The secondary zone is made up of two PSRs with a combined residence time of 23msec and temperature of 1800K for R2 and 1700K for R3. The stream is then mixed with the rest of the combustion air and passed through a final perfectly stirred reactor to model the dilution zone of the combustor at a temperature of 1500K and 3msec residence time. The total residence time set for the whole combustion process is 30msec which was also derived from **Eq(3.3**). The primary zone is the hottest region (2200K) in the reactor and the thermal NOx is highly influenced by temperature and time according to the Zeldovich mechanism [41].

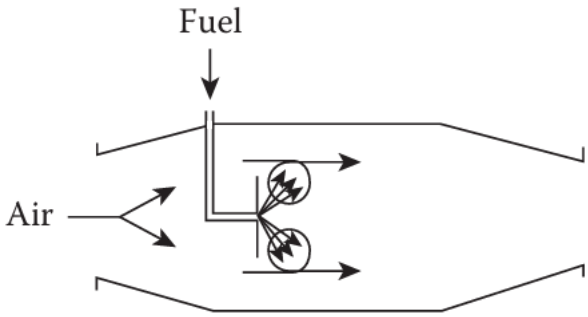

Figure 3.7 Conventional combustor fuel and air introduction. [32]

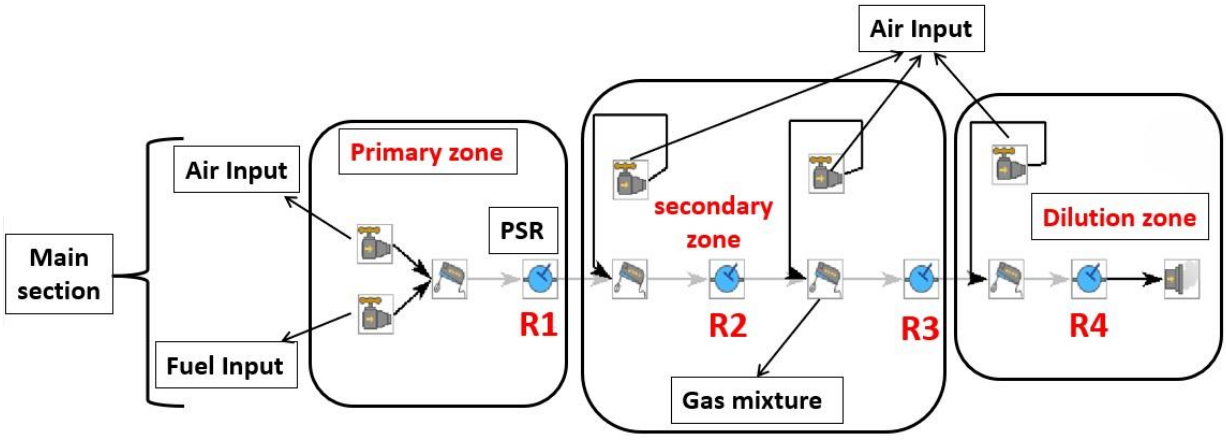

Figure 3.8 CRN model for Centaur 40 conventional liquid-fueled gas turbine.

3.4 Incorporating EGR into CRN models

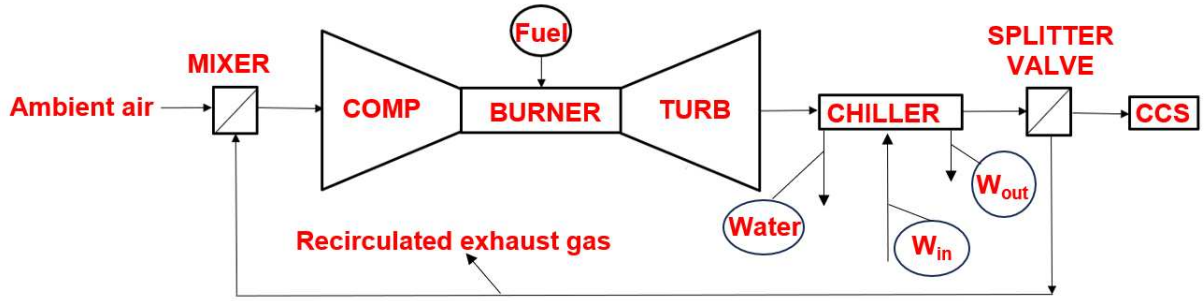

Figure 3.9 A schematic for exhaust gas recirculation that can be considered for gas turbine point source CCS.

For the CRN models incorporating EGR, it is required to use the correct inlet gas compositions that correspond to the varying levels of EGR. The EGR was done for both the DLE and conventional combustor. This was achieved by multiplying the EGR percentage by the moles of exhaust gas produced by the gas turbine. All EGR calculations were done based on the percentage volume. Exhaust gas composition was determined using chemical equilibrium calculations while allowing the fuel flow rate to vary to maintain a constant turbine rotor inlet temperature (TRIT – specified by the gas turbine manufacturer). The calculated product composition at 0% EGR was compared and validated with the engine test results of the centaur 40 DLE (SoLoNOx) gas turbine. This analysis and all the work for this thesis were done at full load of the Centaur 40 gas turbine design specs with all validation done with measured engine out emissions data [112]. The global equivalence ratio for the combustion process was defined in terms of oxygen available for combustion to fuel flow rate. And, finally, emissions from the CRN are reported by total parts per million (ppm) as well as ppm normalized to an oxygen content of 15%

by volume. An EGR sweep was performed to ascertain the thermodynamics of EGR on the centaur 40 gas turbine.

3.4.1 EGR thermodynamic Analysis

For the thermodynamic analysis, Engineering Equation Solver (EES) was utilized to perform all cycle and thermodynamic calculations. The introduction of EGR alters the composition of the oxidizer entering the combustor. This variation in oxidizer composition must be accurately accounted for in the modeling. For instance, in a case with 10% EGR, the gas turbine must operate through several cycles to reach a steady-state convergence, at which point the correct mole fractions of the oxidizer constituents are determined.

The central objective of this analysis is to maintain a constant Turbine Rotor Inlet Temperature (TRIT) across all EGR scenarios. Introducing EGR into the compressor initiates a cooling effect, primarily due to the elevated concentration of carbon dioxide, which has a higher specific heat capacity. This results in a lower TRIT. To compensate and maintain a constant TRIT, the fuel flow rate must be increased proportionally to the level of EGR. Consequently, the fuel input is adjusted to offset the cooling effect, ensuring consistent turbine inlet conditions.

At each EGR level, the oxidizer's mass flow rate and density were computed. The efficiencies of both the turbine and compressor were derived based on actual engine test data. To support the thermodynamic computations, reference properties such as enthalpy of formation, sensible enthalpy terms, specific heat capacities (Cp), specific heat ratio (γ), molecular weight, and specific gravity were sourced from the NIST Chemistry WebBook and Introduction to Combustion by Stephen R. Turns.

Given that the gas turbine operates on the Brayton cycle, key thermodynamic properties like enthalpy, entropy, pressure, and temperature were calculated for each state point in the cycle. The Lower Heating Value (LHV) of the fuels used, dodecane ($C_{12}H_{26}$) for liquid fuel and methane (CH_4) for gaseous fuel was also determined. These values, in conjunction with specific gravity, were used to calculate the Wobbe Index, which is a critical parameter for comparing the combustion performance of different fuels in the same gas turbine without modifying the fuel delivery system. This is particularly important when evaluating fuel flexibility between gaseous and liquid fuels.

The equivalence ratio for this analysis was defined in terms of the total moles of oxygen and fuel available for combustion. Both the stoichiometric oxygen-to-fuel ratio and the actual oxygen-to-fuel ratio were calculated to determine combustion conditions.

Based on the computed enthalpies and mass flow rates, the compressor work and turbine work were evaluated. As the level of EGR increases, so do the density and mass flow rate of the oxidizer, which directly impacts compressor performance. To better quantify this impact, the back work ratio was calculated. This ratio represents the percentage of the turbine's gross power output that is consumed by the compressor.

The combustion exhaust composition was analyzed using both the dry and wet methods. In the dry method, all water vapor is considered removed from the exhaust stream. As depicted in Figure 3.9 water content is assumed to be condensed and separated after passing through the chiller. However, for the CRN analysis, a more conservative approach was taken by retaining 1% water vapor in the exhaust stream to reflect operational conditions more accurately.

Finally, the vaporization of the liquid fuel was modeled as a sensible heat term, as described in **Eq**(3.4**)**. This accounts for the energy required to raise the liquid fuel to its vaporization

temperature before combustion occurs. The code used for the EGR thermodynamic analysis is provided in the Appendix.

CHAPTER 4 - RESULTS AND DISCUSSION

4.1 EGR thermodynamic analysis results

Prior to the incorporation of Exhaust Gas Recirculation (EGR) into the Chemical Reactor Network (CRN) model, a detailed thermodynamic analysis was conducted to determine the appropriate oxidizer mole fractions corresponding to various levels of EGR. This step was critical to ensure accurate representation of the modified combustion environment resulting from EGR implementation.

The analysis was conducted using Engineering Equation Solver (EES), a tool well-suited for performing thermodynamic and cycle-based computations. EES was utilized to determine the thermodynamic state points, maintain a constant adiabatic flame temperature across all EGR conditions, and compute the net power output of the gas turbine. Additionally, EES facilitated the evaluation of other key combustion parameters, such as fuel flow rates, oxidizer composition, and mass flow distribution, which were essential for accurately setting up the CRN model under varying EGR scenarios.

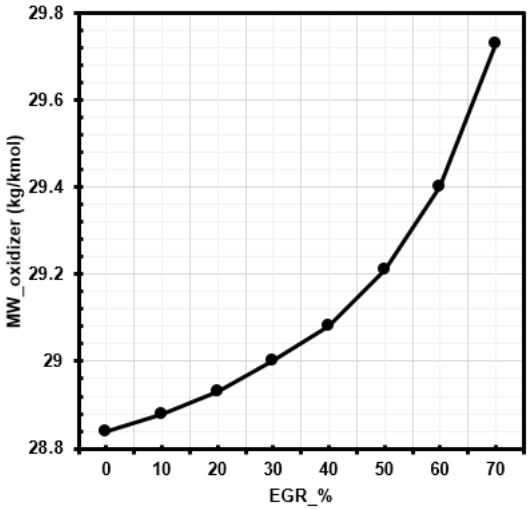

Figure 4.1 A graph of molecular weight of oxidizer at varying EGR percent.

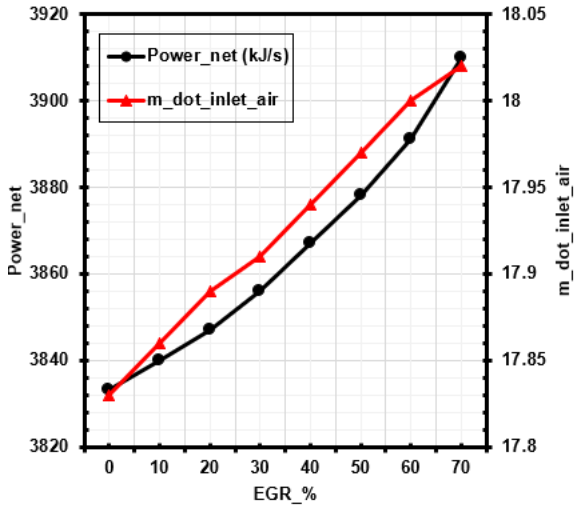

Figure 4.2 A graph of gas turbine power and mass flowrate of inlet air at varying EGR percent.

The cycle efficiency remained unchanged upon the introduction of EGR. This is primarily because additional fuel was supplied to maintain a constant turbine inlet temperature, thereby offsetting any potential thermal efficiency losses. Furthermore, the recirculated exhaust gas was cooled to ambient temperature before re-entering the system, which minimized its impact on the overall thermodynamic performance of the cycle.

4.2 Natural gas-fueled Centaur 40 DLE combustor CRN Results

The first phase of simulation studies conducted on the CSU Centaur 40 gas turbine model was aimed at creating a natural gas-fuel baseline for comparison with the NOx and CO emissions seen in [71].

The trends from this first phase are presented in Figure 4.3. Similarly, as seen in prior studies, the corrected NOx emissions steadily decreased with the addition of EGR [122] and CO emissions stayed low (less than 1 ppm) to approximately 50% EGR levels, which is when O_2 levels start to

affect flame stability. Corrected NOx emissions are predicted to fall near 0.47 (normalized value) to 50% EGR from the CRN modeling, which is about 53% reduction in the corrected NOx value at no EGR. From the simulation results, it was noticed that the uncorrected NOx emissions as seen in **Figure 4.3** do not change much as EGR levels are increased and this is because of the omission of the 15% O_2 correction factor. The uncorrected NOx was predicted to decrease as EGR levels increased up to 50% followed by an uptake in NOx as EGR levels increased further, a trend that was similarly observed D. Burnes et al [71]. This can be attributed to localized elevated temperatures caused by the reduction in O_2 available for combustion. The reduction in oxygen results in decreased flame stability [123][71]. It makes the flame less stable and uniform causing portions of the flame to have higher peak temperatures. This localized higher peak temperature is a catalyst for incomplete combustion, creating localized hot spots where more NOx can be formed.

The 15% O_2 NOx correction is performed to have a reference point to compare emissions between different gas turbines and operating conditions [89]. To achieve this, all water contents from the exhaust products are removed first before the correction is applied [32][124].

$$X_{dry} = \frac{X_{wet}}{1 - X_{H_2O,wet}} \qquad \textit{Eq(4.1)}$$

$$NOx_{z\%,O_2} = NOx_{dry}\frac{0.21 - Z\%}{0.21 - X_{O_{2,dry}}} \qquad \textit{Eq(4.2)}$$

Where Z% is typically 0.15.

With the addition of EGR, the dry O_2 mole fraction in the exhaust is reduced. **Eq(4.2)** confirms why the corrected NOx reduces less than that of the uncorrected NOx for the EGR cases, and why

there is a significant reduction in this value with added EGR in Figure 4.3. It also brings up the consideration of whether this correction is an appropriate means to report NOx emissions when EGR is utilized.

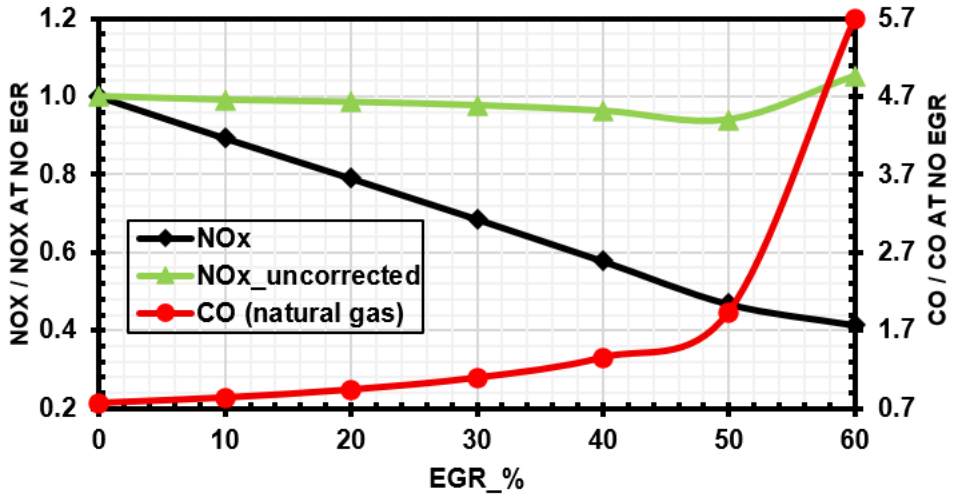

Figure 4.3 A graph of normalized CO and normalized NOx emissions (both corrected and uncorrected) at varying EGR percentages for natural gas-fueled Centaur 40 CRN. The 0% (no EGR case) was validated with engine test results.

4.3 Liquid- fueled Centaur 40 DLE combustor CRN results – Fuel Stratification

The validated CRN model with natural gas was then updated to model liquid fuels via the addition of the fuel stratification approach described in chapter 2. Initial calculations were performed by varying the stoichiometric fuel ratio, i.e., the amount of the main fuel flow taking part in the stoichiometric (non-premixed) flame region to the total main fuel flow. The results of this analysis are provided in Figure 4.4. NOx emissions, as expected, increased as the stoichiometric fuel fraction increased, accounting for more local hot regions within the flame. The overall adiabatic flame temperature remained constant across all stoichiometric fuel fractions (due to the total fuel/air flow remaining constant). A zero-fuel stoic fraction (assuming perfectly mixed

combustion process) results in NOx emissions that are much lower than those seen in actual engine operation.

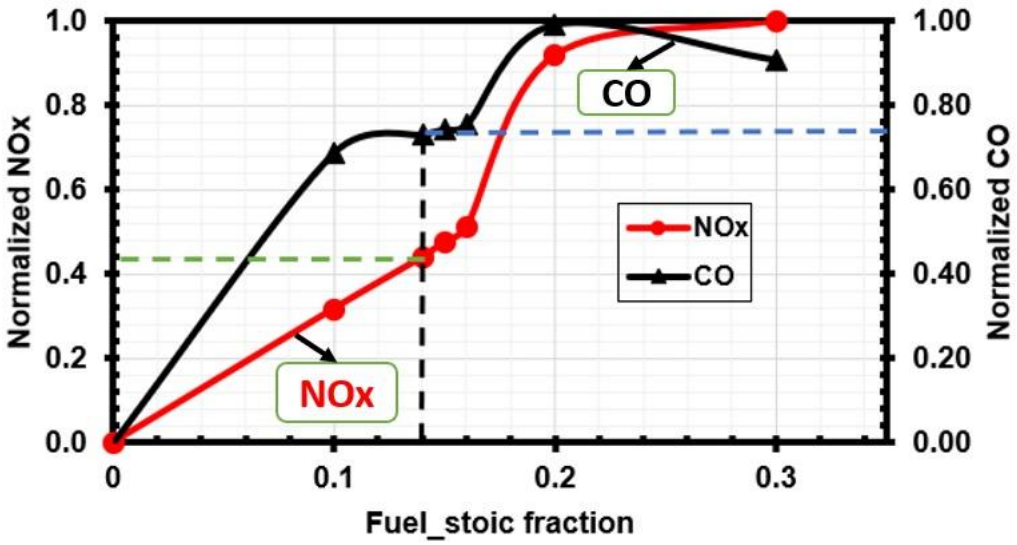

Figure 4.4 A graph of normalized NOx emissions at varying fuel stoichiometric fractions for the diesel-fueled Centaur 40 CRN with no EGR. The blue line represents the validated (engine test results) CO value, the green line is the validated (engine test result) NOx value, and the black line represents fuel stoic fraction required to model the multi-phase diesel combustion.

The fuel stratification approach provided an avenue of control within the diesel fuel reactor network to predict emissions levels which were compared and validated against Solar Turbines Centaur 40 DLE engine test emissions data. As seen in Figure 4.4, a stoichiometric fuel fraction of 0.14 provided the same NOx and CO emissions as a zero EGR full-load Centaur 40 engine test with diesel fuel. The blue line in Figure 4.4 is the validated normalized CO value, the green line is the validated normalized NOx value, and the black line is the fuel stoic fraction that resulted in these measured values. CO is relatively lower throughout the stoichiometric fuel fraction sweep but does increase due to the premixed regions becoming leaner as more fuel is added to the stoichiometric regions of the CRN.

4.3.1 Liquid-fueled Centaur 40 DLE combustor results – EGR Sweep

Results from the thermodynamic EGR calculations are presented in Figure 4.5, Figure 4.6, and Figure 4.7. Fuel flow rates steadily increased (Figure 4.5) with an increase in EGR rate. This increase in fuel flow rate contributed to an increase in the molecular weight of exhaust gases. The introduction of EGR into the combustor adds dilution that requires the addition of fuel to keep adiabatic flame temperature constant and causes a decrease in O_2 concentrations. The recirculation of EGR increases the exhaust (dry) CO_2 concentration routed to the CCS (Figure 4.7) at the expense of decreasing the inlet combustor O_2 levels (Figure 4.6). The exhaust molecular weight increased with increasing EGR rates which resulted in an increase in oxidizer density in Figure 4.8 causing added mass to be pulled through the engine. This explains the high-power outputs seen with EGR [71][125][126]. The power output presented in Figure 4.8 excludes all mechanical shaft losses, energy associated with fluid losses, and generator losses, explaining why it is a bit higher compared to the OEM rated power of 3,500 kJ/s at 0% EGR case. Trends are mild up to approximately 50 – 60% EGR where O_2 levels begin to rapidly decline, warranting supplemental oxygen. While the thermodynamic calculations show the potential of EGR to increase exhaust gas CO_2 concentrations, which would reduce the size and cost of CCS as shown in Figure 4.7, they do not show the impact of EGR on flame stability and emissions, which are rooted in chemical kinetics.

Leveraging the new fuel stratification approach, EGR is introduced into the liquid CRN model to understand the impact on emissions (CO and NOx) and flame-out conditions. The previously determined fuel stoichiometric fraction of 0.14 is implemented for all EGR CRN calculations. The

pilot to total fuel flow rate ratio is held constant throughout the EGR sweep and the results of the thermodynamic calculations were included as CRN inputs for the varying EGR levels.

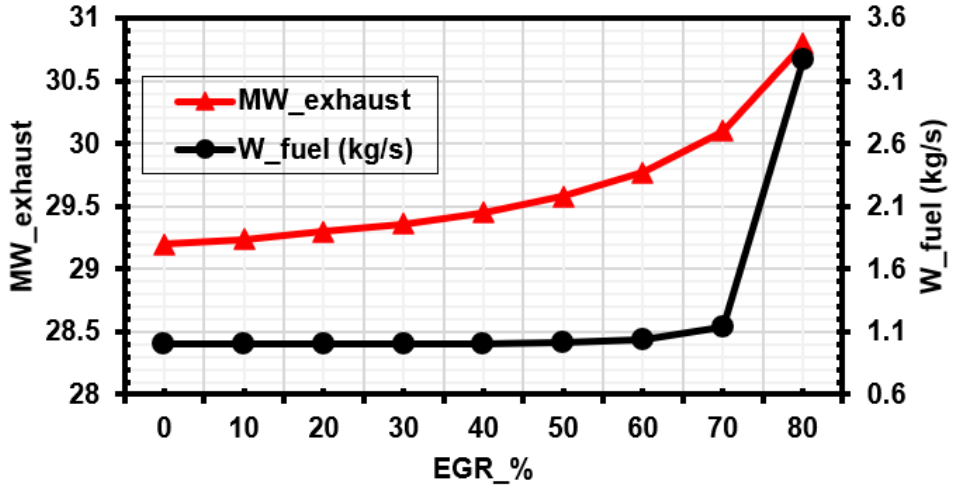

Figure 4.5 Calculated exhaust gas molecular weight and fuel flowrate trends.

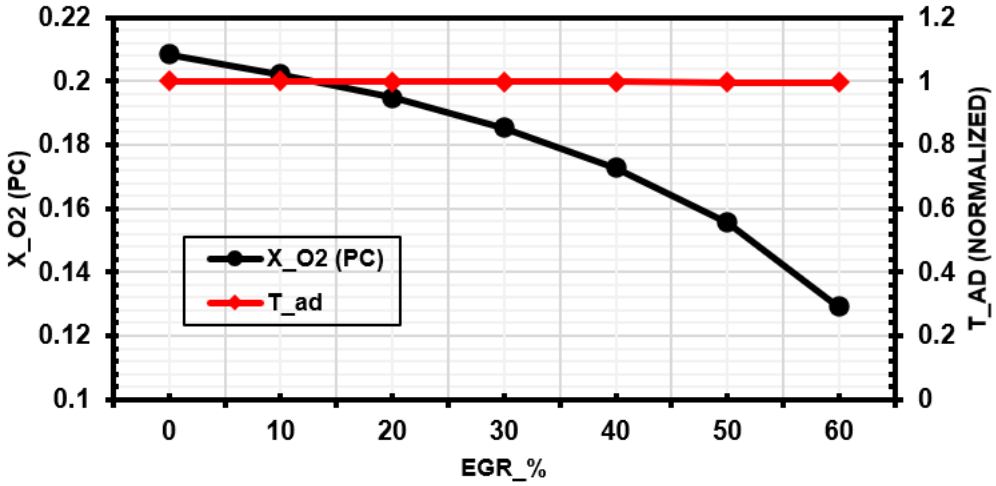

Figure 4.6 Calculated precombustion O_2 concentrations and calculated adiabatic temperature.

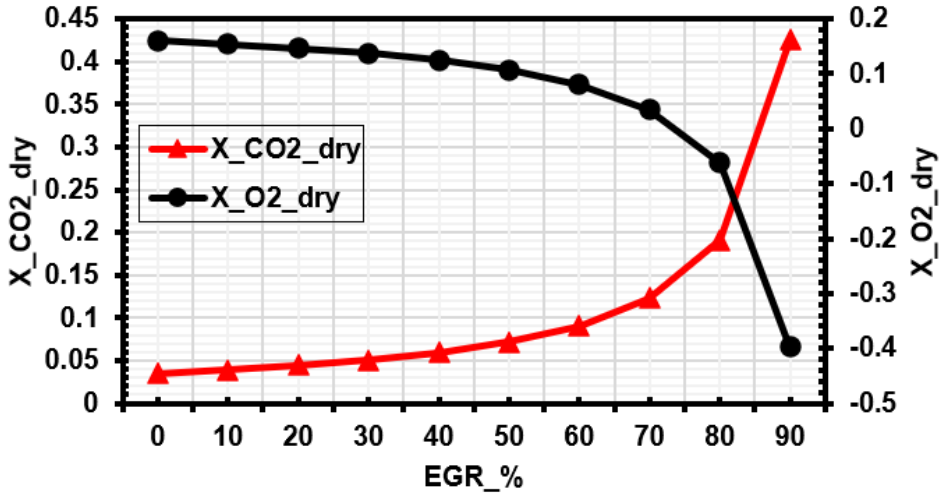

Figure 4.7 Exhaust dry (post chiller) CO_2 and O_2 levels for varying EGR levels for the liquid-fueled Centaur 40 DLE combustor.

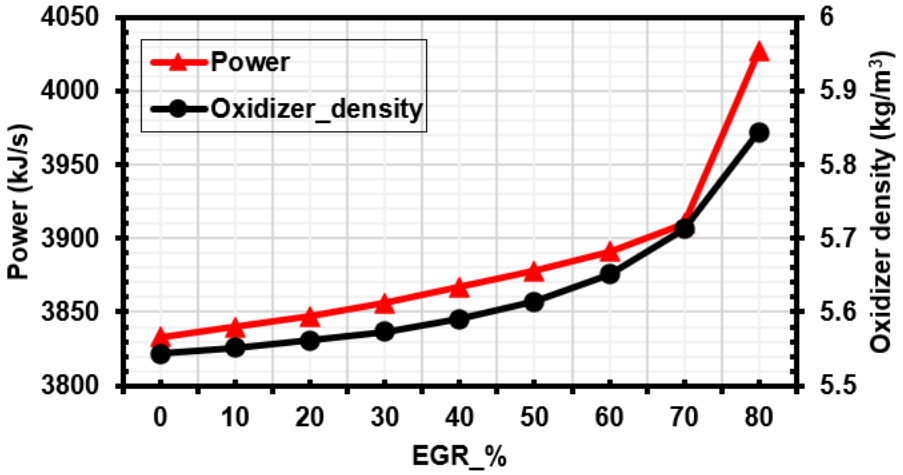

Figure 4.8 A graph of power output and oxidizer density for varying EGR levels for the liquid-fueled Centaur 40 DLE combustor.

Based on the results from Figure 4.4, an EGR sweep was performed on the diesel-fueled gas turbine DLE (SoLoNOx) combustor using the fuel stoic value of 0.14. The results are seen in Figure 4.9 and Figure 4.10. The liquid-fueled DLE (SoLoNOx) combustor is predicted to produce more NOx than the natural gas system due to the challenges associated with premixing the fuel

and air with liquid fuels. Predicted CO emissions also follow a similar trend to the natural gas CRN results, indicating the onset of combustion instabilities after 50% EGR.

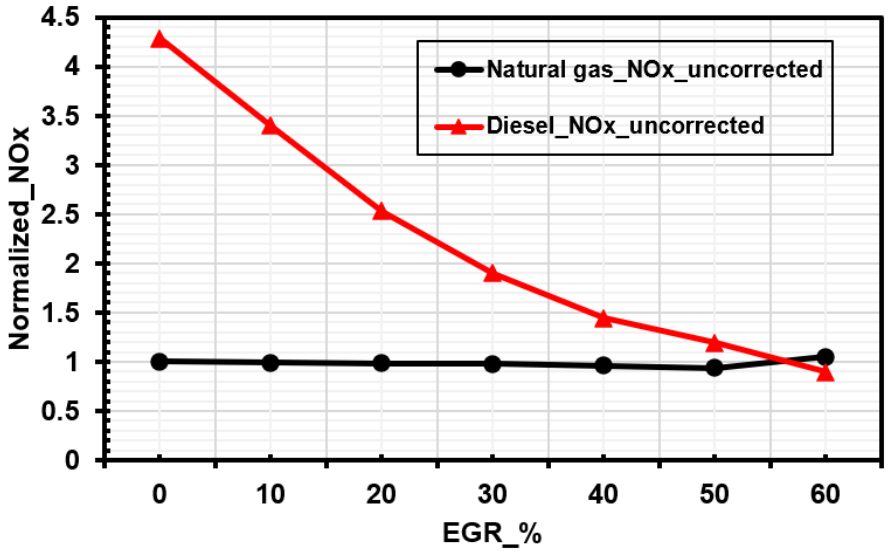

Figure 4.9 A graph of normalized uncorrected NOx at varying EGR percentages for the liquid-fueled Centaur 40 DLE CRN and the gas-fueled DLE CRN combustor. The 0% (no EGR case) was validated with engine test results.

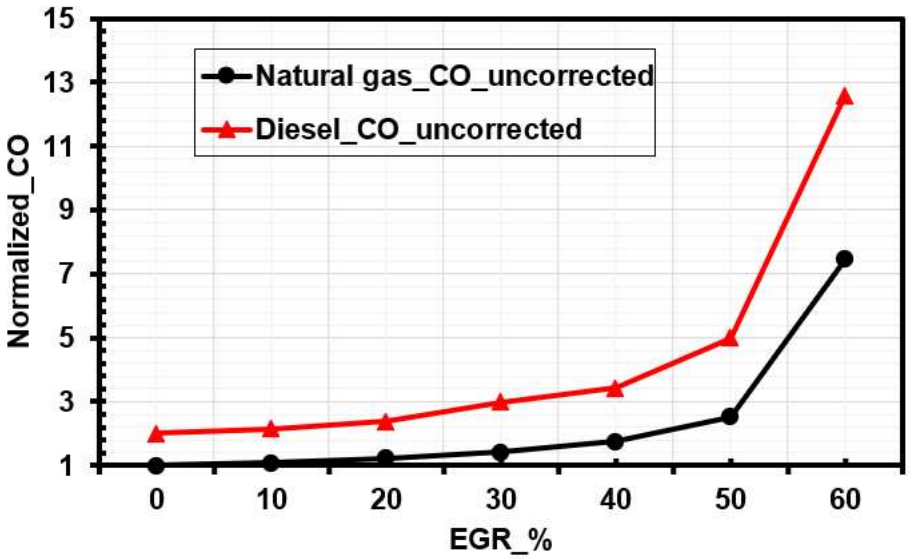

Figure 4.10 A graph of normalized uncorrected CO at varying EGR percentages for the liquid-fueled Centaur 40 DLE CRN and the gas-fueled DLE CRN combustor. The 0% (no EGR case) was validated with engine test results.

Although still low, CO emissions were higher for the diesel CRN compared to the natural gas-fueled turbine CRN. As previously discussed, this is expected given the lower equivalence ratio within the premixed regions of the main flame [89][106] and the thermal effect of the recirculated flue gas causing local flame quenching. For CO emissions, a slight upward trend was observed until 60% EGR where there was a sharp spike in CO emissions, likely to represent a sudden decrease in combustion efficiency as oxygen levels become too low to sustain desired combustion levels. At 70% EGR, the pre-combustion mole fraction for oxygen was 0.086. Operation at this EGR rate (or higher levels) would require supplemental oxygen. While not shown here, an elevated level of unburned hydrocarbons at this EGR level was also predicted as posited by General Electric [73].

4.3.2 Liquid-fueled Centaur 40 DLE Results – NOx and CO evolution and sensitivity Analysis.

A study investigated how NOx and CO emissions production evolve in each PSR reactor for both no EGR and 50% EGR cases by examining the uncorrected emissions. As seen in Figure 4.12 and Figure 4.12, R1 – stoic section in the primary zone is where most of the emission production happens in the model for both the no EGR case and the 50% EGR case. The calculated temperature of the stoic reactor (R1) for the 0% EGR case was approximately 500K more than the calculated temperature of the stoic reactor (R1) for the 50% EGR case. This temperature difference explains why there is a sharp decline in NOx in R1, where most of the NOx is produced, with the addition of EGR. Thermal NOx as the name suggests increases significantly as combustion temperature increases by the Zeldovich mechanism.

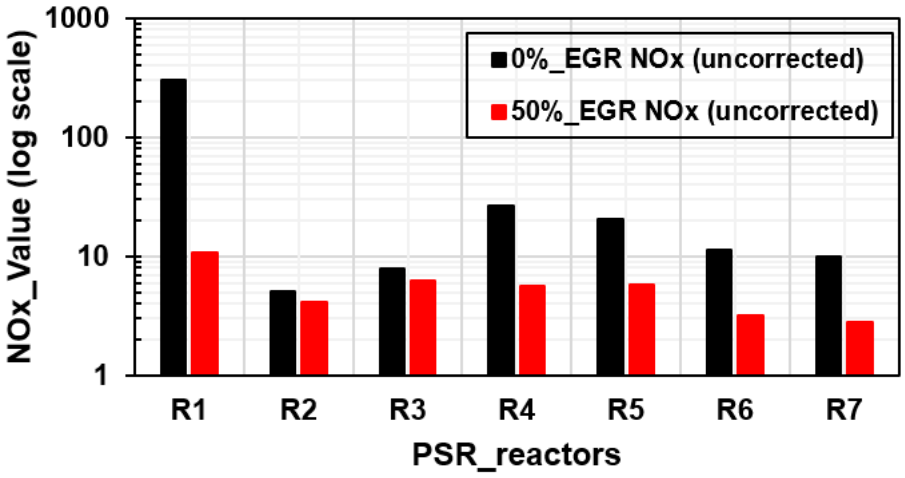

Figure 4.11 Evolving NOx production at 0% and 50% EGR in the various reactors, uncorrected values (diesel gas turbine).

On the contrary, CO production increased as EGR levels increased. This is due to two reasons: Firstly, as EGR levels increase the O_2 molecules available for combustion and oxidation of CO to CO_2 reduces as seen in Figure 4.7. **Eq(4.3)** Illustrates the oxidation of CO into CO_2 in the presence of O_2 molecules.

$$CO + O_2 \rightarrow CO_2 + O \qquad Eq(4.3)$$

Secondly, as EGR levels increase, higher CO_2 concentrations result in a cooling effect in the combustion chamber, reducing the rate at which OH radicals are produced. OH radicals play a significant role in the conversion of CO into CO_2 which is seen in **Eq(4.4)**

$$CO + OH \rightleftharpoons CO_2 + H \qquad Eq(4.4)$$

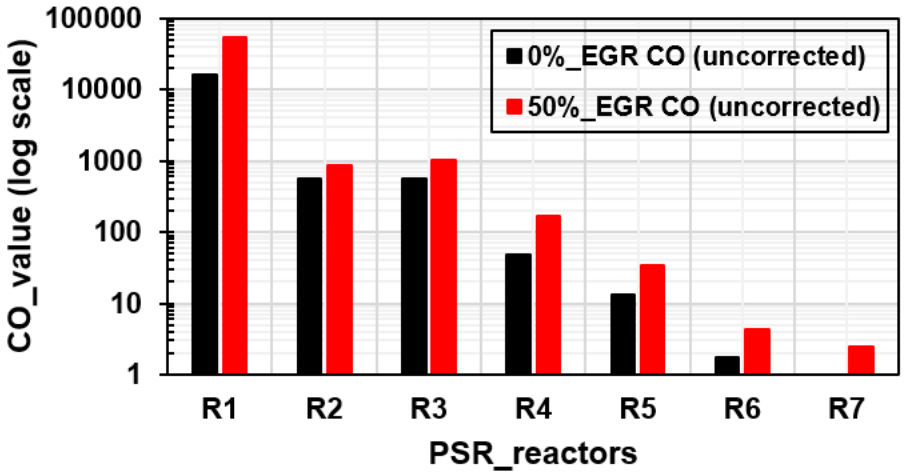

Figure 4.12 Evolving CO production at O% and 50% EGR in the various reactors, uncorrected values (diesel gas turbine).

A chemical sensitivity analysis was performed at the primary zone (stoic, lean, and pilot) of the reactor to study the various chemical reactions that contributed significantly to the production of NOx in the liquid-fueled gas turbine (DLE combustor). The primary zone was selected because these PSRs represent the hottest regions (1800K) in the reactor and thermal NOx production is highly influenced by temperature. The results of this analysis for 0% EGR and 50% EGR are shown in Figure 4.14, Figure 4.15, and Figure 4.15. In the 0% EGR stoichiometric PSR (R1 - Figure 4.13), the reaction $NO + N \rightleftharpoons N_2 + O$ had the most positive on NOx production. In the 50% EGR stoic PSR (R1), interestingly, a negative sensitivity to NO production was observed for this reaction, while $OH + N \rightleftharpoons H + NO$ had the most positive impact on NOx production. $N_2 + O \rightleftharpoons NO + N$ is the primary limiting step to thermal NOx production – the fact that the 0% and 50% EGR cases show different sensitivity relationship to this reaction points to the influence of EGR on its potential to reduce adiabatic flame temperatures (~500K reduction) and associated NOx

production pathways and explains the significant difference in the R1 NOx production between these cases (Figure 4.11).

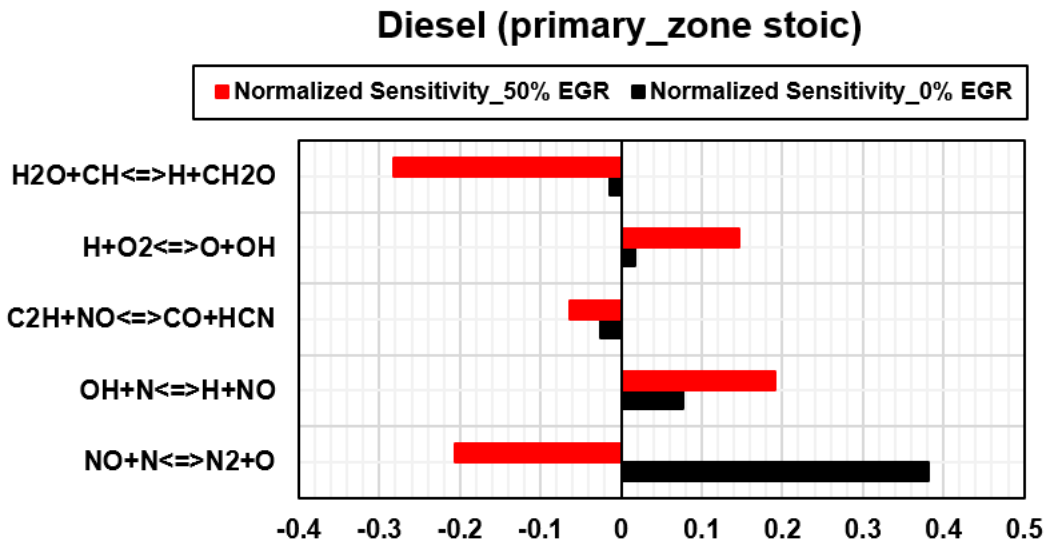

Figure 4.13 NOx normalized sensitivity analysis at 0% and 50% EGR at the stoic section of the main flame.

At both 0% and 50% EGR lean section (R2 - Figure 4.14), the reaction $O + N_2O \rightleftharpoons 2NO$ had the most positive impact on NOx production, whereas the reaction $H + N_2O \rightleftharpoons N_2 + OH$ had the most negative impact on NOx formation. In this reactor, the two EGR cases demonstrated similar behavior regarding NOx formation.

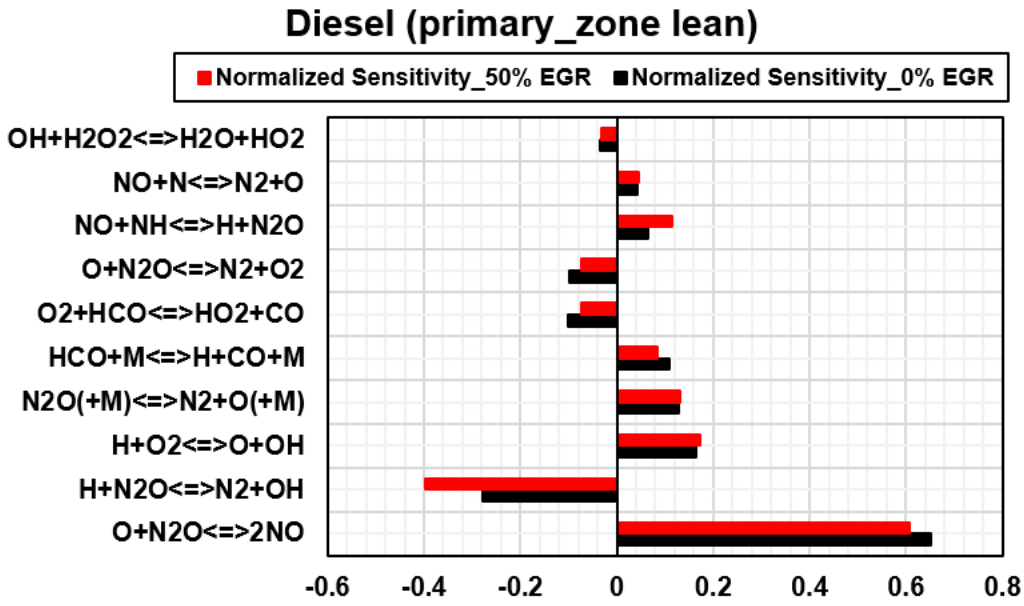

Figure 4.14 NOx normalized sensitivity analysis at 0% and 50% EGR at the lean section of the main flame.

At both 0% and 50% EGR pilot section (R3 - Figure 4.15), the reaction $O + N_2O \rightleftharpoons 2NO$ had the most positive impact on the formation of NOx while the reaction $H + N_2O \rightleftharpoons N_2 + OH$ had the most negative impact in NOx formation. In this reactor, both EGR cases show similar dependencies to one another on NOx formation.

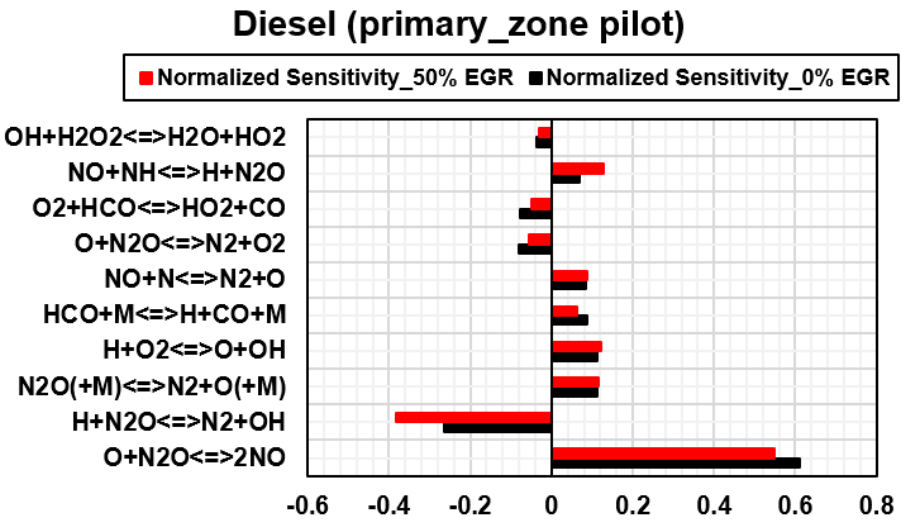

Figure 4.15 NOx normalized sensitivity analysis at 0% and 50% EGR at the pilot section of the flame.

As part of the studies on the liquid-fueled gas turbine (DLE combustor). I wanted to find out how the engine will respond to emissions and combustion stability if the pilot fuel flowrate increases by 10% while all other parameters stay the same. At the 10% Pilot fuel increase, an EGR sweep on liquid-fueled gas turbine (DLE combustor) was performed. According to the studies, the 10% pilot fuel increase yielded a 43.74% increase in NOx emissions when compared to the initial pilot fuel flowrate as seen in Figure 4.17. A normalized NOx and CO graph in Figure 4.16 shows the emission performance for the 10% pilot fuel flowrate increase and at about 70% EGR there is a sharp spike in CO emissions indicating the presence of combustion instabilities. It was around this same EGR percentage that the initial pilot flowrate saw a sharp spike. From, Figure 4.16 the corrected and uncorrected NOx emissions are not the same. This phenomenon was observed in all EGR runs and raises the concern of how EGR emissions should be reported.

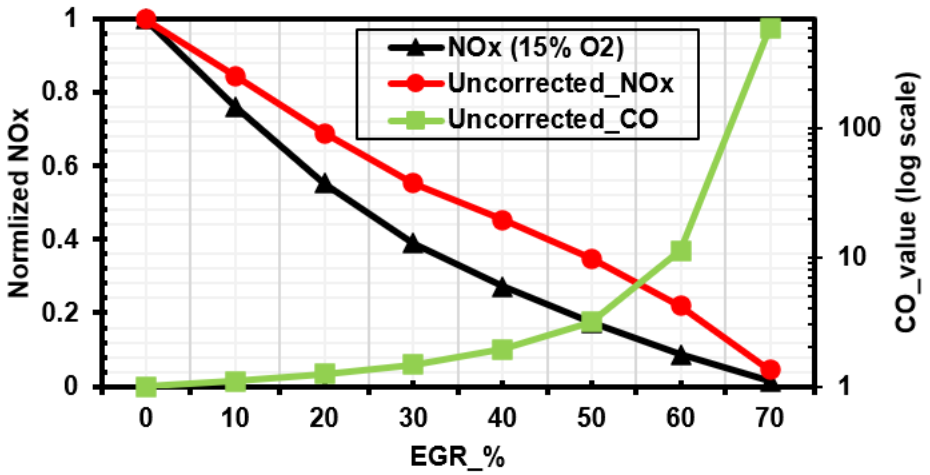

Figure 4.16 A graph of corrected, uncorrected NOx and uncorrected CO at 40% pilot EGR sweep of Centaur 40 SoLoNOx dual fuel (Liquid-fueled gas turbine).

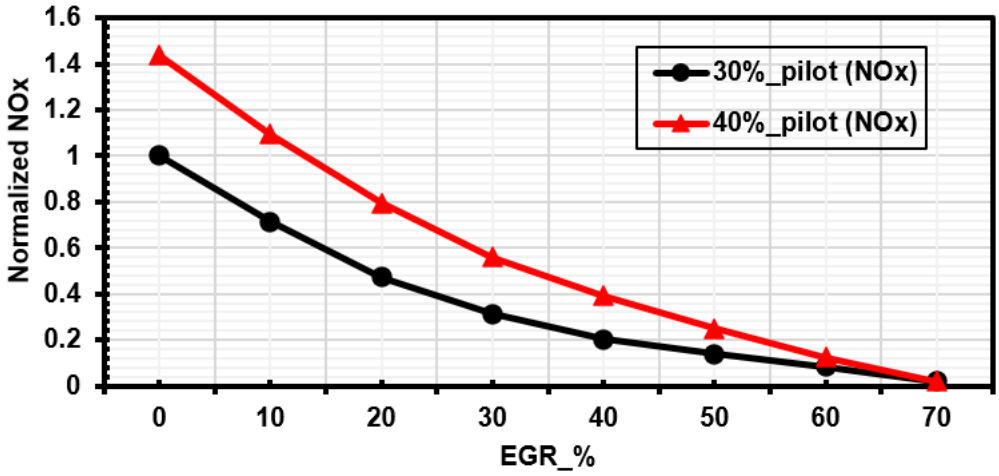

Figure 4.17 A graph of uncorrected NOx at 30% and 40% pilot Centaur 40 SoLoNOx dual fuel (liquid-fueled gas turbine).

From Figure 4.18, it is observed that increasing the pilot fuel flowrate by 10% doesn't really affect CO production that much. The trend observed in both scenarios is the same even to the point where combustion instability is becoming prominent.

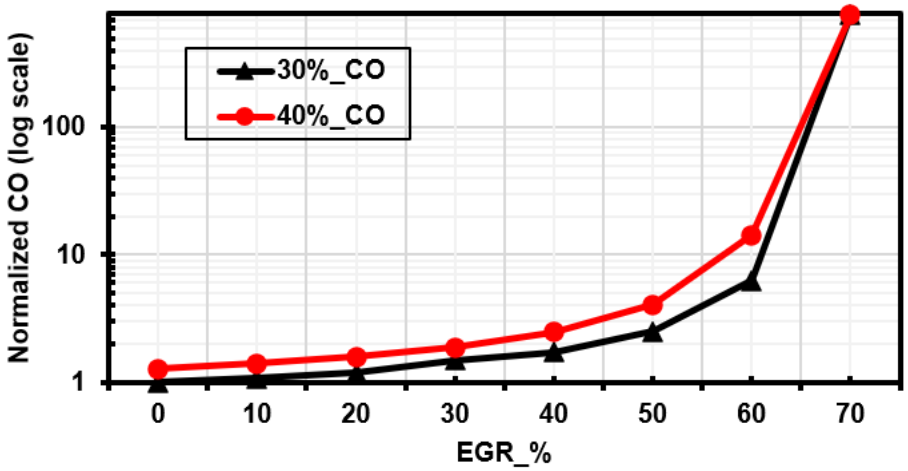

Figure 4.18 A graph of normalized CO emissions at 30% and 40% pilot fuel flowrate on the Centaur 40 SoLoNOx dual fuel (liquid-fueled gas turbine).

4.4 Conventional Centaur 40 combustor result

Figure 4.19, shows an EGR sweep performed on the conventional combustor of the Centaur 40 liquid-fueled gas turbine. From the graph a slight difference between the corrected and uncorrected NOx emissions as seen in previous EGR sweeps was observed. Also, at 30% EGR there is a sudden spike in CO emissions signifying combustion instabilities and inefficiencies. The conventional combustor exhibited similar trends like an increase in oxidizer mass flowrate, reduction in NOx emissions, increase in CO emissions, increase in equivalence ratio, etc. just like the DLE combustor. The only difference is the early sharp spike in CO emissions making the conventional combustor less tolerant to EGR.

Figure 4.21 and Figure 4.21 shows how NOx and CO emissions evolve through the reactor. At 0% EGR, the R1 reactor, where the reaction commenced produced most of the NOx. The addition of secondary and dilution air in the combustion system reduced the temperature of the reaction hence reducing the NOx production at the end of the combustion process. A similar trend is seen in the

production of CO. In the case of CO, there is a significant drop in CO emissions as the reaction moves from the primary zone in R1 to the secondary zone, R2. This is attributed to the presence of more oxygen molecules that help in the convention of CO into CO_2 as seen in Eq(4.3).

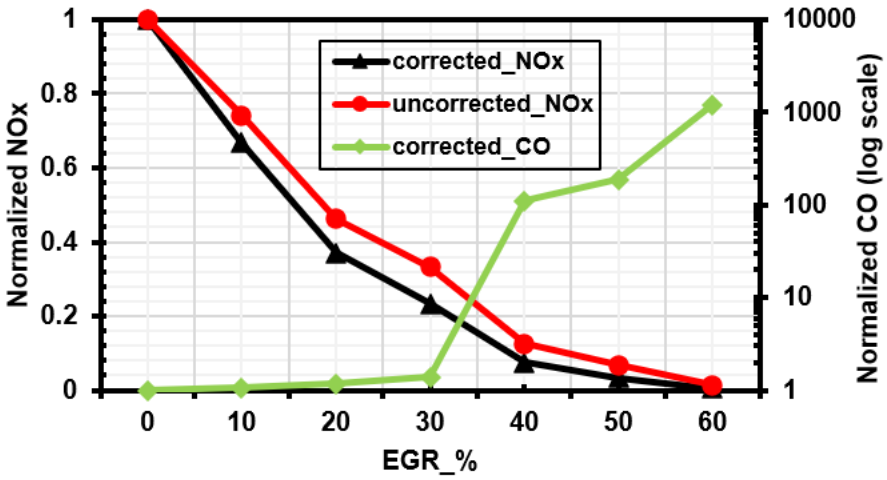

Figure 4.19 A graph of normalized CO and normalized emissions (both corrected and uncorrected) at varying EGR percentages for diesel conventional combustor.

At 50% EGR, the cooling effect of the recirculated flue gas strongly affects the combustion process. For NOx emissions, because of the cooling effects of EGR, NOx production in the primary zone, R1 almost reduced to 50% as compared to the 0% EGR case. The evolution of NOx emissions from R1 to R4 was not a significant one. Just a slight downward trend from R1 to the end of the combustion process, Figure 4.20.

For CO emissions at 50% EGR, there was just a slight increase in emissions at the primary zone, R1 as compared to the 0% EGR case. As the reaction proceeds into the secondary zone there is an almost 50% reduction in CO production.

From the two figures, it can be concluded that the primary zone, R1, is the most sensitive zone to emissions production in the conventional combustor.

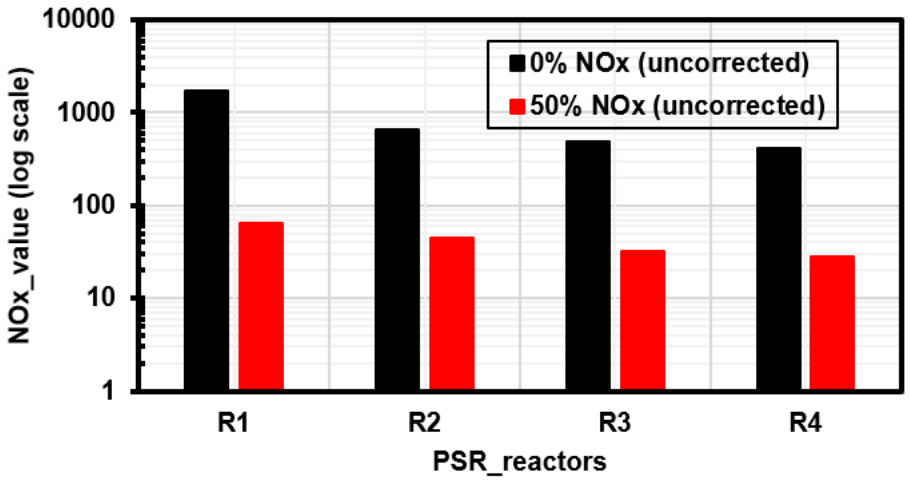

Figure 4.20 Evolving NOx production at 0% and 50% EGR in the various reactors, uncorrected values (diesel conventional combustor).

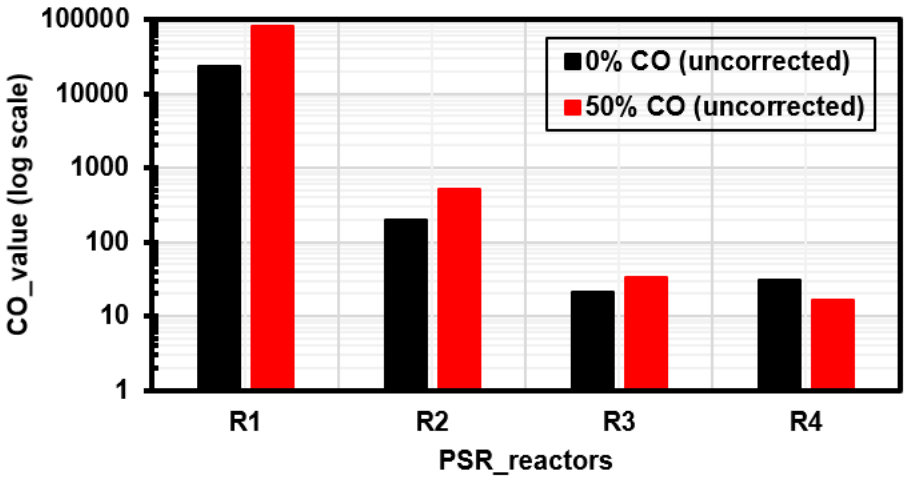

Figure 4.21 Evolving CO production at 0% and 50% EGR in the various reactors, uncorrected values (diesel conventional combustor).

To see how sensitive the dilution zone is to NOx emissions in terms of air flowrates, a study was conducted to see how an increase in the dilution zone air flowrate affects the production of NOx at the end of the combustion process in a conventional combustor. **Figure 4.22** shows the results for this study. Since the volume of the combustor is constant, as air is moved to the dilution zone, less air will be available in the primary zone for the combustion process. Since there is less air than

fuel, the equivalence ratio for the reaction leads to a way hotter flame (rich combustion) which is a precursor to higher thermal NOx production. The rise in NOx was slow and steady till a significant amount of air was moved to the dilution zone given rise to a remarkably high equivalence ratio in the primary zone.

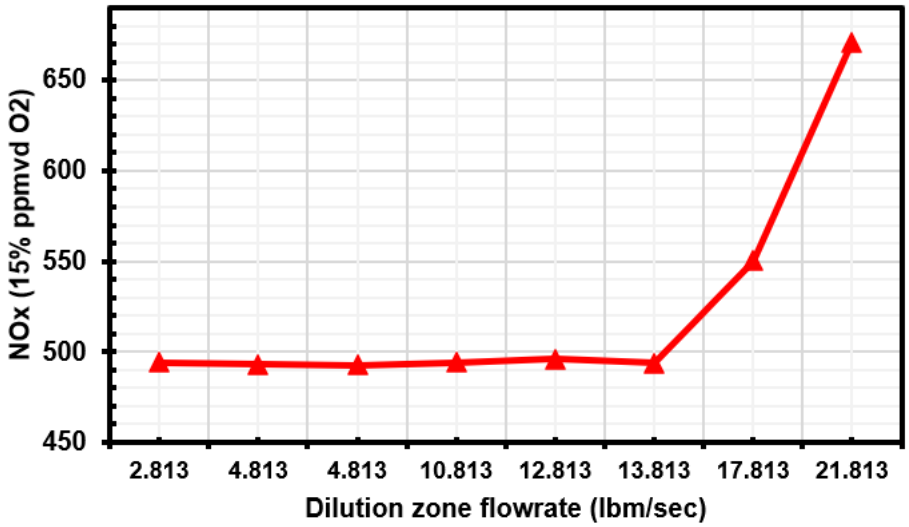

Figure 4.22 A graph of NOx and varying air flow rate in the dilution zone of a conventional combustor.

From the studies on both the DLE (SoLoNOx) and the conventional combustor of the Centaur 40 gas turbine, the results showed that the conventional combustor was less tolerant to EGR as seen in Figure 4.23. There are a couple of reasons why the conventional combustor is less tolerant to EGR, and these are:

- Firstly, the type of combustion. The DLE (SoLoNOx) is a lean premixed type of combustion with an equivalence ratio of about 0.52. With this type of combustion, the oxidizer is twice the amount of fuel been introduced which results in the dilution of the flame temperature leading to NOx emissions reduction. The conventional combustor

exhibits a diffusion type of combustion where both the oxidizer and fuel are introduced at the same flowrate resulting in an equivalence ratio of one (1). As EGR is introduced the amount of oxygen available for combustion reduces, in the case of the DLE (SoLoNOx) the effect of reduced oxygen takes a longer time before the impact is felt because in this combustion process there is more oxidizer. Thus, during reduction there is a shift towards stoichiometric combustion. The equivalence ratio gradually moves from 0.52 towards 1 as EGR is increased. In the case of a conventional combustor, since the combustion is a non-premixed, diffusion type flame at an equivalence ratio of 1, the moment EGR kicks in and the oxygen available for combustion reduces the equivalence ratio increases but this time over one (1) making the combustion process a rich one. With this, conventional combustors quickly start to get into higher equivalence ratio making them produce elevated levels of CO from unburned fuel since there is less oxygen available leading to quicker combustion instability. Figure 4.25 shows how the equivalence ratio from both the DLE and conventional combustor increases during an EGR sweep.

- Secondly, the conventional combustor is less tolerant of EGR because of flame stability features. DLE (SoLoNOx) combustors can maintain better flame stability and combustion efficiency under EGR because of the presence of swirlers, staged combustion and active combustion feedback systems that are absent in a conventional combustor. These features help DLE combustors better deal with leaner, slower-burning mixtures without blowout and flame instability.
- Mixing and temperature uniformity contributes to why conventional combustors are less tolerant to EGR. DLE (SoLoNOx) combustors are designed to achieve uniform temperature profiles under low oxidizer conditions by the incorporation of advanced

sensors and actuators to adjust fuel distribution and airflow dynamically without sacrificing performance. For conventional combustors, due to the diffusion type flame, they suffer from poor mixing under EGR leading to uneven temperature fields and flame lift-offs that cause increased emissions of CO and unburned hydrocarbons.

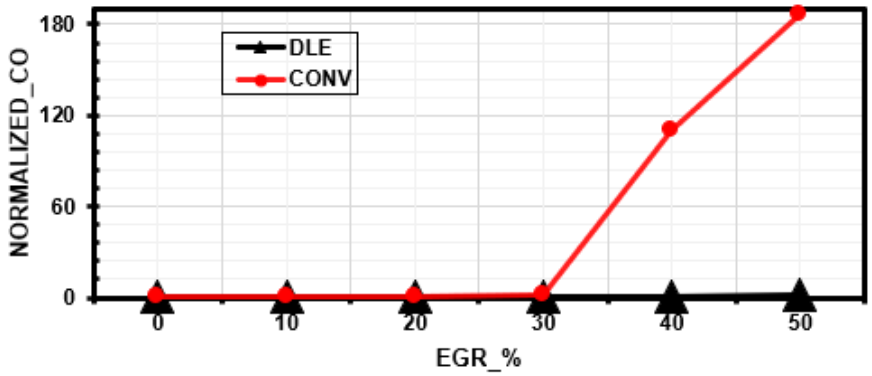

Figure 4.23 A graph of normalized CO values for both conventional and DLE combustors.

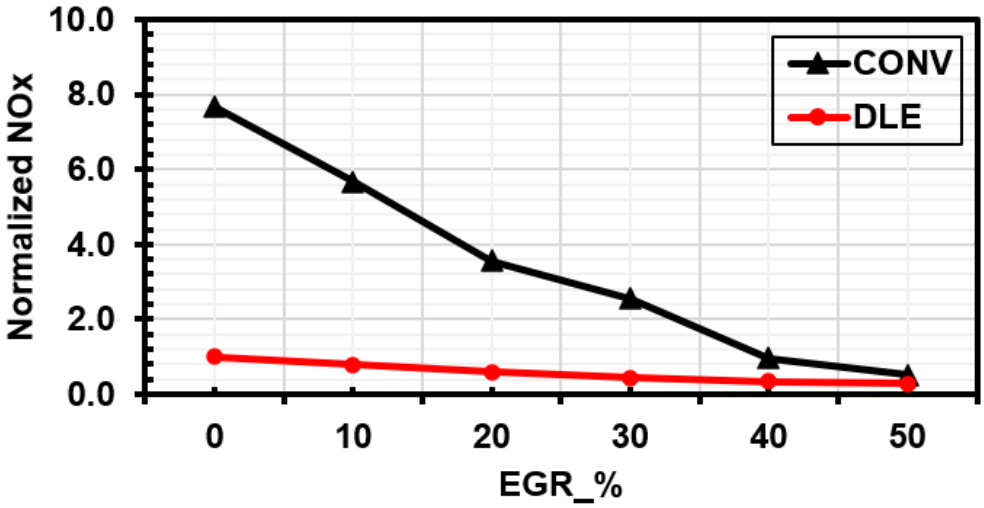

Figure 4.24 A graph of normalized NOx values for both conventional and DLE combustors.

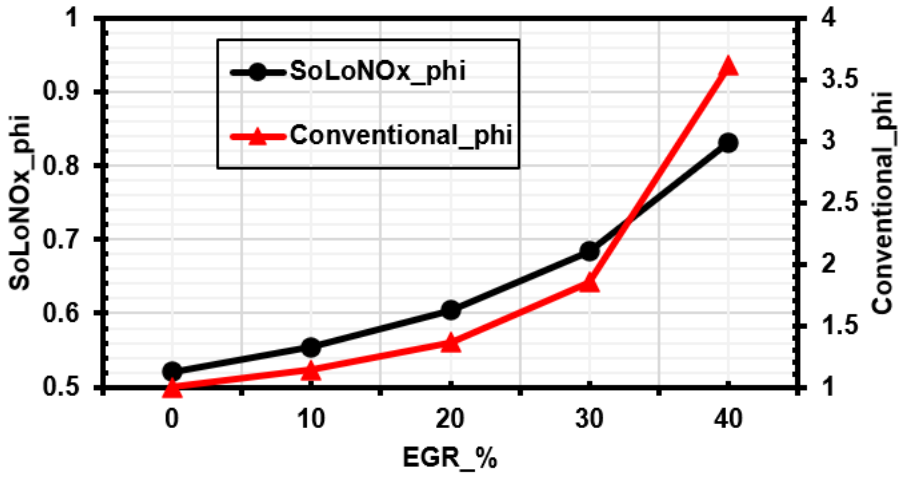

Figure 4.25 A graph of equivalence ratio of a conventional combustor and a SoLoNOx combustor of a Centaur 40 liquid-fueled gas turbine.

CHAPTER 5 - CONSTRUCTION AND SETUP OF THE CENTAUR 40 ENGINE

A dual-fuel Centaur 40 gas turbine equipped with a SoLoNOx combustor is currently being installed at the university's engine laboratory. This engine will serve as a critical testbed for the experimental validation of the EGR-enabled Combustion Reactor Network (CRN) model and the associated analytical results developed in this research. The installation and commissioning are being conducted by the Windom Research Group, of which I am an active contributing member.

The installation phase has been successfully completed, and the project has now entered the commissioning stage, where system functionality, instrumentation, and performance parameters are being systematically verified.

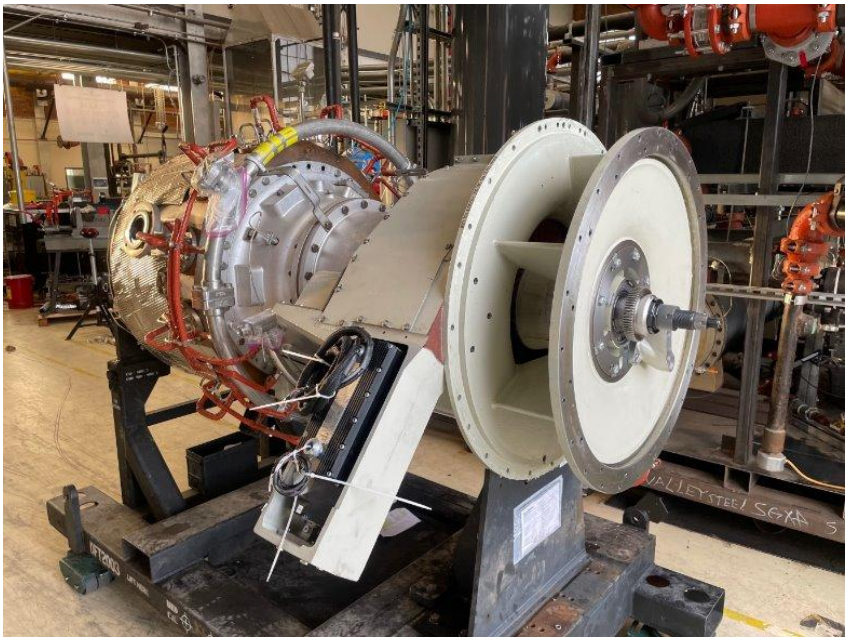

Figure 5.1 An image of the dual fuel Centaur 40 SoLoNOx engine.

During this project, I played a key role in several major subsystems:

5.1 Lube oil system.

The design, integration, and testing of the lubrication oil system for the dual-fuel Centaur 40 SoLoNOx gas turbine installation were guided primarily by Solar Turbines' engineering manuals ES9-224 and TPIM-1010E. These documents provided the detailed specifications and procedural steps necessary to ensure correct layout, component compatibility, flow integrity, and system reliability for the lubrication subsystem.

The lubrication system is a critical component, tasked with delivering continuous and reliable lubrication to all rotational equipment including the gas turbine bearings, generator bearings, and gearbox assemblies — to minimize friction, reduce wear, and maintain mechanical integrity under various operating conditions.

Due to spatial constraints within the engines lab, several modifications were made to the original equipment manufacturers (OEM) layout:

- The OEM lube oil demister had to be re-routed and repositioned to accommodate available floor space and ensure safe clearances for operation and maintenance.
- The OEM lube oil cooler was deemed unsuitable due to its size and orientation. To address this, a custom shell-and-tube heat exchanger was selected, sized, and installed. The replacement unit was designed to manage a maximum heat rejection load of 720,000 Btu/hr, exceeding the system requirement of 620,000 Btu/hr, thereby ensuring adequate thermal margin and improved cooling efficiency.

The final configuration of the lubrication oil system includes the following major components:

- Reservoir (365-gallon capacity at full operational level, plus an additional twenty gallons for filters and piping)
- Lube Oil Pump
- Hand-Operated Shutoff Valves
- Duplex Filter Assembly
- Electric Heater (for preheating the oil during cold starts)
- Oil Demister
- Custom Shell-and-Tube Oil Cooler
- Flame Arrestor (for safety in the vent line)

The fluid path and component arrangement were validated for proper flow rate, pressure drops, and temperature control. The system was also pressure-tested and leak-checked according to OEM and lab safety protocols to confirm operability under full-load conditions. These modifications and system upgrades were made with an emphasis on maintaining performance, safety, and serviceability within the physical constraints of the lab environment.

The lubricating oil selected for the gas turbine lubrication system is TurboFlo XL 32, a high-performance synthetic turbine oil manufactured by Petro-Canada. This lubricant was chosen due to its superior oxidative stability, excellent low-temperature flow properties, and enhanced wear protection characteristics, making it well-suited for high-speed, high-temperature applications typical of gas turbine operations.

TurboFlo XL 32 complies with industry standards for turbine-grade lubricants, including ISO VG 32 classification, and is specifically engineered for use in industrial gas turbines where both the

turbine and associated rotating equipment (e.g., generator and gearbox bearings) rely on consistent lubrication under dynamic load and temperature conditions. The detailed physical and chemical specifications of TurboFlo XL 32 including viscosity at standard temperatures, pour point, flash point, and Total Acid Number (TAN), are presented in Table 7. These properties ensure the oil maintains optimal performance throughout the full operating range of the lubrication system, supporting both thermal stability and long-term system reliability. Construction images are shown below.

Table 7: Lube oil physical and chemical properties.

Property	ASTM Test Method	TurboFlo XL 32
Viscosity cSt @ 40 °C/SUS @100 °F cSt @ 100 °C/SUS @210 °F	D445	33.9/175 5.6/45
Viscosity Index	D2270	101
Flash point, COC, °C / °F	D92	220/428
Pour point, °C/ °F	D5950	-30/-22
Acid number, mg KOH/g	D664	0.04

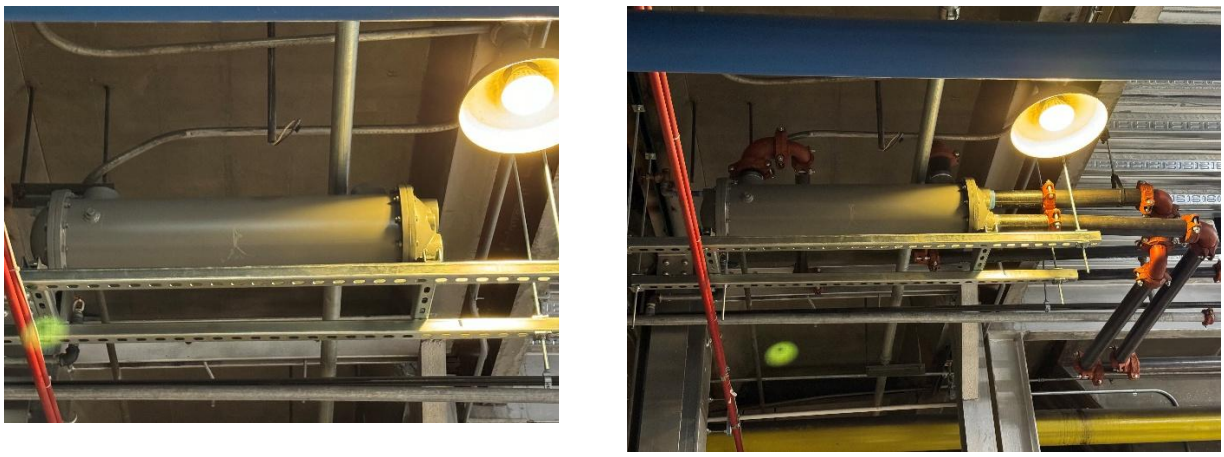

Figure 5.2 Heat exchanger for the lube oil system.

Figure 5.3 Piping to lube oil system heat exchanger.

Figure 5.4 A CAD image of the lube oil demister with the flame arrestor.

5.1.1 Lube oil polishing.

Prior to being introduced into the lubrication oil reservoir, the TurboFlo XL 32 turbine oil underwent a comprehensive oil polishing process to ensure it met the OEM-specified cleanliness and quality standards required for optimal gas turbine performance and component longevity.

The oil polishing procedure involved two key steps:

- Filtration: The lube oil was passed through a multi-stage filtration system to remove particulate contaminants. This included both coarse and fine filtration stages, designed to capture and eliminate suspended solids and debris.

- Thermal Conditioning: The oil was gently heated during the polishing process to enhance viscosity characteristics, promote flowability, and facilitate more effective contaminant removal.

The polishing process was conducted in strict accordance with Solar Turbines' technical requirements, achieving the following cleanliness criteria:

- ISO 4406 cleanliness code of 16/14/12, corresponding to particle counts of:
  - ≤16 for particles ≥4 microns,
  - ≤14 for particles ≥6 microns, and
  - ≤12 for particles ≥14 microns.
- A 25-micron filter bag inspection confirmed the presence of no more than five particles exceeding the minimum countable size of 0.010 inches (0.254 mm), thereby validating the effectiveness of the filtration process.

Meeting these standards is critical to ensuring the protection of precision components, such as journal bearings, thrust bearings, and high-speed rotating elements, which are sensitive to particulate contamination. Failure to meet these levels of cleanliness could result in accelerated wear, loss of lubrication film integrity, and premature component failure.

By adhering to these rigorous polishing standards, the lubricating oil was conditioned to provide maximum reliability, thermal stability, and protection, contributing to the overall performance and durability of the Centaur 40 SoLoNOx gas turbine system.

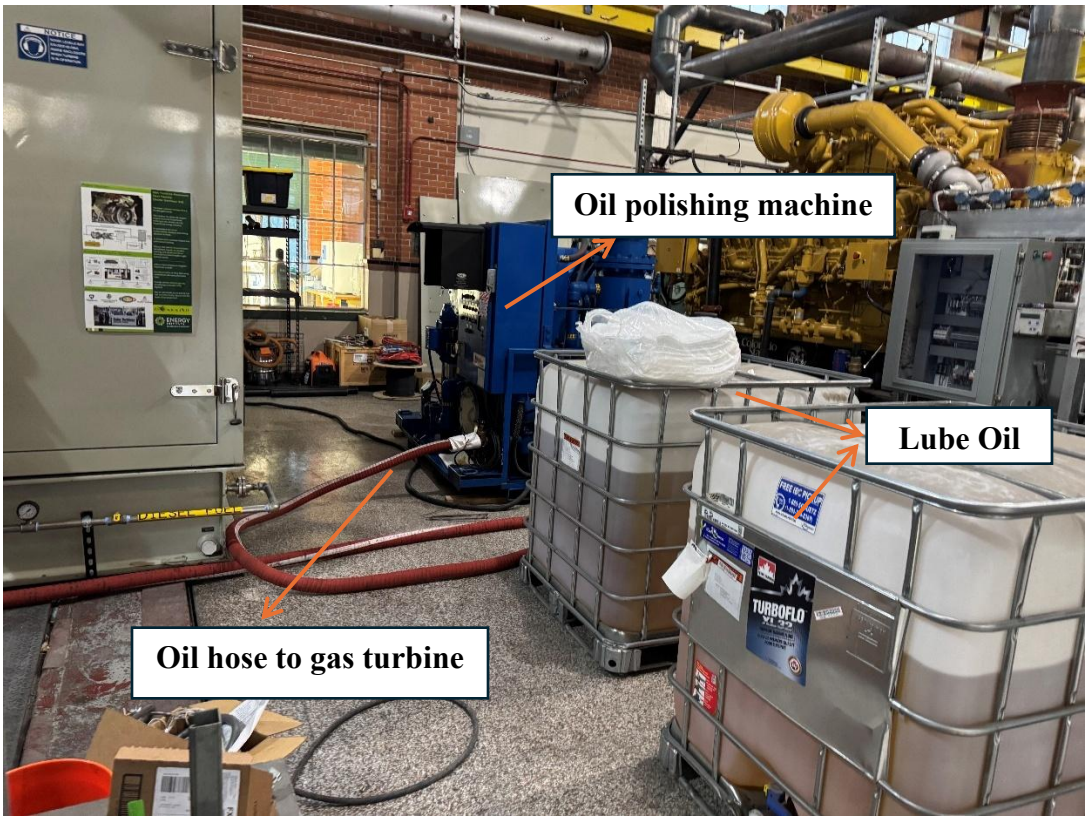

Figure 5.5 An image of the of oil polishing process.

Figure 5.6 Lube oil demister installation with the flame arrestor outside the building.

5.2 Fuel system

The Centaur 40 gas turbine is equipped with an internal fuel management system responsible for regulating and delivering the appropriate quantity of fuel to the injectors to sustain the combustion process. To support this, a dedicated external fuel transfer system was designed and implemented to supply diesel fuel from a 5,200-gallon, double-walled, ballistic-resistant storage tank to the inlet of the turbine's internal fuel system.

This engineered external transfer system was carefully designed to ensure operational reliability, fuel cleanliness, pressure integrity, and compliance with safety and performance standards. Key components of the external system include:

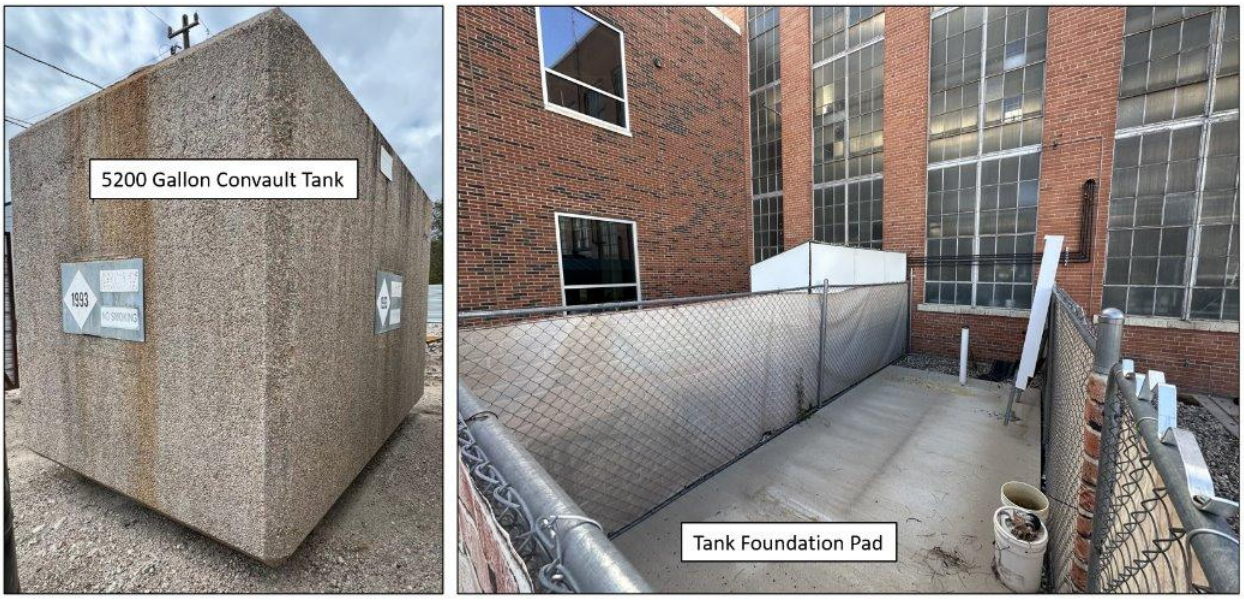

Figure 5.7 An image of 5200-gallon convault tank and foundation pad for the tank.

- A high-capacity stainless steel strainer to remove large particulates,
- A three-stage filtration system, where the final filter stage achieves a filtration threshold of 5 microns to protect sensitive turbine fuel components,
- An anti-siphon valve for backflow prevention and fire safety,
- Multiple pressure gauges for monitoring system pressure at critical points,
- A variable frequency drive (VFD)-controlled motor for precise pump speed control and operational flexibility,
- A positive displacement fuel pump selected and sized based on comprehensive hydraulic and thermodynamic calculations,
- A Morrison Bros float-type mechanical level gauge for real-time monitoring of fuel levels,
- A pressure relief valve to safeguard the system from over pressurization.

Stainless steel piping was utilized throughout the system to provide superior corrosion resistance, particularly critical given the long-term exposure to diesel fuel and environmental conditions.

The line sizing and pressure drop calculations were performed during the design phase to ensure the selected pipe diameter could deliver the required flow rate while minimizing losses. These calculations accounted for:

- Static head,
- Frictional losses due to pipe length and fittings,
- Minor losses across valves, strainers, and filters,
- Elevation differences and required net positive suction head (NPSH).

The fuel pump was carefully selected and sized using engineering principles, incorporating total dynamic head (TDH), flow rate requirements, and system backpressure into the pump selection criteria. All calculations, along with the Piping and Instrumentation Diagram (P&ID), and pump sizing methodology, are detailed in Table 8.

This external fuel delivery system ensures consistent, clean, and safe diesel fuel delivery to the turbine under all expected operating conditions, thereby supporting both commissioning activities and long-term engine testing under EGR conditions.

Table 8: A table indicating line sizing calculations and pump sizing.

PARAMETER	**UNIT**	**VALUE**	**REFERENCE**
Density of Diesel	lb/ft^3	53.06	
Volume flowrate	ft^3/s	0.0131	
Dynamic Viscosity @ 80F	lb/ft. s	0.00161	
Inside diameter	ft	0.17225	
Area	ft^2	0.02329	
Velocity	ft/s	0.562449	
Height	feet	7	
Kinematic velocity @ 80F			
Reynolds number		**3193**	
Length of piping	ft	140	
Reynolds suggests a transition to turbulent flow			
Outside diameter of pipe	mm	33.4	ASME B36.10M
Inside diameter of pipe	mm	26.6	ASME B36.10M
Maximum Design Pressure, P	ksi	1.4	Kingsley
Stress Value, S	ksi	20	ASME B31-3, TABLE A-1B
Weld joint Strength reduction Factor, W		1	TABLE 302.3.5
Quality Factor, E		1	ASME B31-3, TABLE A-1
Coefficient for t<D/6, Y		0.4	TABLE 304.1.1
Corrosion Allowance, c	mm	1	
Required thickness, t as per ASME 31.3 t =PD/2(SEW + PY)		**1.14**	

Required thickness, tm as per ASME 31.3 tm = t + c	mm	**2.14**	
Selected Pipe schedule, sch	sch	**40**	
Thickness per schedule	mm	3.91	ASME B36.10
T = thickness excluding mill tolerance (12.5%), T	mm	**3.42**	
Pass thickness T>tm	mm	1.28	
		APPROVED	
roughness for stainless steel	mm	0.03	
relative roughness		0.001128	
gravity due acceleration	ft/s^2	32.17	
Friction factor (using Churchill equation)		0.0441	
A		1.031E+18	
B		1.328E+17	
Straight line loses	feet	5	
h_minor	feet	0.04868	
Assumed loss from other equipment like pressure gauges	feet	1.00	
Total Line loss	feet	**6.5**	
height for static head	m	2.1336	
gravity due to acceleration	m/s^2	9.81	
Density of diesel	kg/m^3	850	
Static head	Pa	17791.0	
Static head	feet	6.0	
Total dynamic head	feet	12.4	
Total dynamic head	psi	5.4	
Discharge Pressure	psi	75	
Required Pump pressure	psi	**88.0**	
Absolute vapor pressure of diesel at 70°F	ft	0.007	
Velocity head	ft	0	
Atmospheric pressure	ft	33.898	

NPSH_available	ft	**22.5**	

The external fuel transfer system utilizes a Viking Spur Gear Pump, model SG-40711-G0V, selected for its high-pressure capability, compact design, and proven reliability in handling hydrocarbon-based fuels such as diesel. As part of Viking's SG Series, this external gear pump can deliver up to 16 GPM (60.6 L/min) at operating pressures reaching 2,500 psi (170 bar), depending on system configuration and viscosity.

For this application, the pump will be used to transfer diesel fuel from a 5,200-gallon double-walled external storage tank to the inlet of the gas turbine's internal fuel system. According to the manufacturer's guidelines, a discharge pressure range of 10 to 120 psi is recommended for optimal operation under steady-state conditions. The system is designed to operate within this pressure envelope to ensure adequate flow while avoiding cavitation or over-pressurization of downstream components.

The pump's robust construction (typically ductile iron) ensures chemical compatibility with diesel fuel, while its external spur gear configuration provides precise, pulse-free flow suited for stable combustion operation. Line sizing and pressure loss calculations were conducted in advance to ensure correct pipe diameter and to minimize system head losses. This ensures efficient fuel delivery and compatibility with the gas turbine's operating parameters.

Further design considerations such as suction head availability, motor sizing, and thermal effects were also incorporated into the system integration, as detailed in the design schematics and P&ID. The Viking SG-40711-G0V pump selection aligns with both the operational demands of the dual-fuel Centaur 40 SoLoNOx gas turbine and the stringent reliability requirements of continuous industrial gas turbine operations.

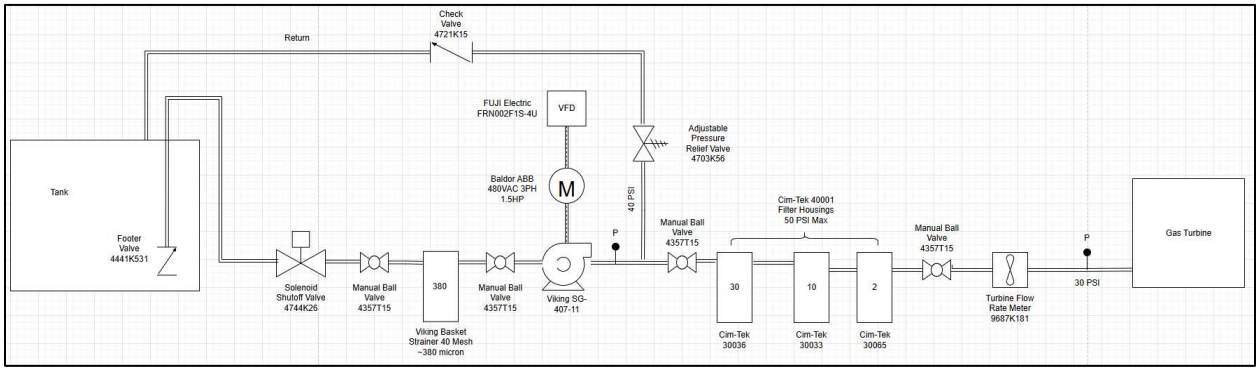

Figure 5.8 P&ID diagram for transfer fuel system.

5.3 Foundation works.

To ensure structural stability and vibration control during operation of the Centaur 40 SoLoNOx gas turbine, a robust foundation system was designed and implemented in accordance with manufacturer guidelines, specifically Solar Turbines' TPIM-1010E and document 9A381-14906 (which includes relevant Process and Instrumentation Diagrams, or P&IDs).

Proper foundation anchoring is essential for high-speed rotating equipment such as gas turbines. Inadequate support can lead to excessive vibration, shaft misalignment, bearing damage, and in severe cases, catastrophic failure of the turbine and generator systems. Therefore, the foundation design was developed to not only provide static support but also to ensure dynamic integrity under varying load and environmental conditions.

5.3.1 Mounting Configuration and Foundation Preparation

The gas turbine package consists of three main mounting points. Each of these was secured with high strength anchoring methods as follows:

- The east and west anchor points were secured using core-drilled holes into the concrete laboratory floor. Into each hole, a 1.5-inch diameter, 20-inch-long anchor bolt was inserted, with the embedded end tack-welded to the nut for enhanced mechanical integrity during installation. These holes were filled using Chockfast Gray, a precision epoxy grout engineered for high load rotating equipment. It provides excellent vibration damping and structural bonding.
- The south mounting point, located where concrete support was absent, was stabilized using a custom-fabricated steel plate and washer assembly. This solution enabled proper mechanical tensioning and ensured consistent contact pressure across the baseplate.
- The foundation pad was molded using Chockfast Orange, a heavy-duty epoxy compound ideal for machinery grouting. This material was used to cast the final pad surface and interface layer between the turbine package and floor.

5.3.2 Torquing and Alignment

Each of the anchor bolts was torqued to 1,460 lb-ft to ensure firm and uniform anchorage. This torque specification was based on OEM installation standards and verified against industry best practices for dynamic machinery mounting.

Precise mechanical alignment of the gas turbine package was critical to minimize rotational imbalance and prevent undue stress on couplings, bearings, and the drivetrain. Alignment was achieved using a precision engineer's leveler, which enabled accurate leveling of the entire turbine assembly in both lateral and longitudinal directions. This tool ensured the unit was properly leveled to within engineering tolerances before grout curing and bolt torquing were finalized.

5.3.3 Quality Control and Final Inspection

After the physical anchoring and leveling process, comprehensive quality checks were conducted, including:

- Verification of grout curing and bond integrity.
- Confirmation of bolt torque values.
- Visual and dimensional inspection of the foundation pad.

These measures ensured that the gas turbine was securely mounted, free of mechanical misalignment, and ready for commissioning. Images illustrating the installation sequence, core-drilled anchoring, and alignment process are included in Figure 5.9, 5.9, 5.10, and 5.11.

Figure 5.9 Foundation mounting pad (east side) with bolt.

The high-precision engineer's leveler, calibrated to an accuracy of 0.02 mm/m, was employed to verify the horizontal flatness of the turbine mounting interface. Measurements were taken across

designated reference pads located on the turbine skid to ensure that deviations in flatness remained within acceptable tolerances defined by OEM installation guidelines.

Figure 5.10 Foundation mounting pad (west side) with bolt.

In addition to horizontal leveling, vertical alignment was also performed to maintain proper orientation of the turbine relative to critical drivetrain components. Specifically, vertical level assessments were referenced to the main drive shaft that couples the gas turbine to the generator, as well as the interface with the accessory gearbox. This alignment was essential to:

- Prevent angular misalignment between rotating shafts,
- Minimize vibration and bearing load during operation,
- And ensure efficient power transmission and mechanical reliability.

Figure 5.11 South side foundation bottom plate.

All measurements were validated at multiple points to confirm consistency, and adjustments were made iteratively until both horizontal and vertical leveling met design specifications. This rigorous leveling process plays a crucial role in extending equipment life, improving performance, and reducing maintenance frequency.

Figure 5.12 Foundation pad mold making.

Figure 5.13 Precision Engineer's leveler.

These contributions are critical to the successful startup and operation of the gas turbine system and directly support the broader research goals of EGR implementation and model validation.

CHAPTER 6 -CONCLUSION AND FUTURE WORK

6.1 CONCLUSION

This thesis presents a novel approach to successfully modelling liquid-fueled gas turbine combustion using a CRN model and employing the fuel stoichiometric fraction technique to provide an avenue for control within the model. It also discusses the approach of modelling a liquid fuel conventional combustor using a CRN and how it performs with EGR. Key outcomes include:

- The natural gas Centaur 40 (SoLoNOx combustor) simulation results showed downward trends for the NOx and upward trends with CO emissions with the addition of EGR with a point of interest at 50% EGR where CO emissions began to increase exponentially signifying the onset of combustion instabilities.
- Corrected NOx and CO emissions from the liquid-fueled gas turbine (SoLoNOx combustor) simulation were reduced by approximately 41% and 10% respectively, as the fuel stoichiometric fraction was varied from 0.15 to 0.3. Compared to the natural gas combustor, the diesel SoLoNOx model predicted significantly higher NOx emissions due to increased localized hot regions within the flame typically associated with premixing the fuel/air with liquid fuels.
- Emissions corresponding to the test data collected on the liquid fuel operation of the Centaur 40 DLE (SoLoNOx) with no EGR were achieved at a fuel stoichiometric fraction of 0.14.
- With the introduction of EGR into the liquid fuel DLE (SoLoNOx) combustor model at a fuel stoichiometric fraction of 0.14, CO_2 concentrations in the exhaust stream more than doubled as EGR was increased up to 50%. This presents a wonderful opportunity for CCS.

At 50% EGR the CO_2 concentration in the exhaust stream increased to about 7%. A study by Hassan et al [70] showed that such an increase will result in a USD 33 reduction in tonnage capturing and compression when using the monoethanolamine (MEA) absorption which is the most widely used chemical solvent in the CCS industry as shown in Figure 6.1. However, O_2 levels started to decline rapidly at 60% EGR point which could be a precursor for flame and combustion instabilities. Past this 60% EGR levels, CO emissions were increased by multiple orders of magnitude as the combustor became increasingly oxygen-deficient and so, combustion efficiency degraded drastically, increasing the likelihood of flame blowout.

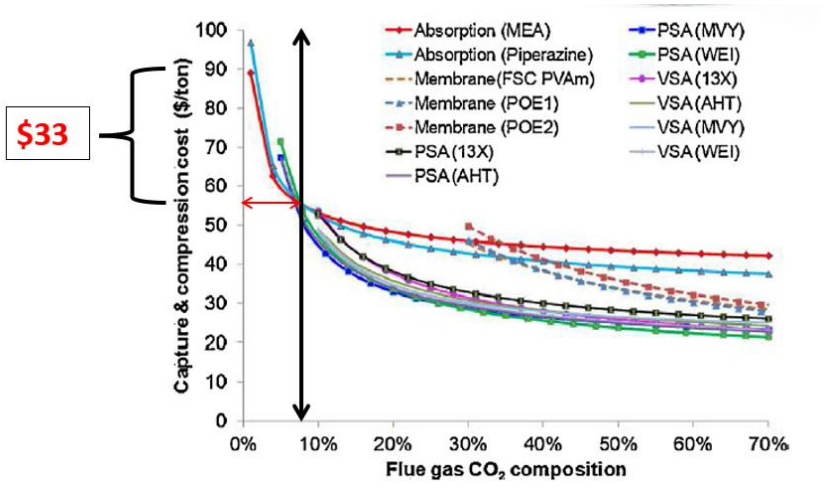

Figure 6.1 A graph of CCS capture cost vs flue gas CO2 concentration [70].

- The stoichiometric section (PSR - R1) of the primary zone (SoLoNOx combustor) contributed the most to final (CO and NOx) emissions outputs. Differences in thermal NOx pathways were found to be the primary reasons for more NOx emissions produced in this reactor between the 0% and 50% EGR cases.

- The actual NOx emissions for cases involving Exhaust Gas Recirculation (EGR) are represented by the uncorrected emission measurements, as they directly reflect the combustion conditions present during EGR operation. Applying a correction to normalize emissions to a reference oxygen concentration, typically 15% O_2 by volume, is inappropriate in EGR scenarios due to the inherent changes in the combustion product composition. In non-EGR combustion, post-flame oxygen levels typically approach the 15% O_2 reference value, making such normalization meaningful and standardized across various systems. However, in EGR enhanced combustion, a portion of the exhaust gas including CO_2, H_2O, and residual O_2 is recirculated into the combustion chamber, diluting the oxidizer stream and reducing the overall oxygen concentration in the flue gases. As a result, the oxygen mole fraction in the exhaust can fall well below 0.15, often reaching values significantly lower than those observed in non-EGR operations.

  When emissions are corrected to a standard 15% O_2 in EGR cases, the result is an artificially skewed and misleadingly low NOx emission value, due to the disproportionately low baseline oxygen level in the exhaust. Therefore, to accurately represent the environmental impact and combustion performance under EGR conditions, NOx emissions must be reported on an uncorrected basis. This approach ensures that the influence of EGR on flame temperature, reaction kinetics, and emission formation is properly captured without introducing distortion through conventional correction factors that are not applicable in diluted, oxygen-depleted exhaust streams.

- The conventional liquid-fueled combustor exhibits reduced tolerance to Exhaust Gas Recirculation (EGR), primarily due to its diffusion flame combustion characteristics. In

this configuration, fuel and oxidizer mix within the flame zone, and the overall equivalence ratio is typically near unity. With the introduction of EGR, the oxygen content in the oxidizer stream decreases, resulting in a locally richer mixture. As oxygen is displaced by inert exhaust gases, the equivalence ratio increases sharply, as illustrated in Figure 4.25. This shift toward richer combustion promotes incomplete oxidation, leading to elevated emissions of carbon monoxide (CO) and unburned hydrocarbons (UHCs). These conditions degrade combustion stability and thermal efficiency, making the combustor more susceptible to instability and potential flameout under high EGR levels.

- Studies investigating the effect of elevated pilot fuel flow rates in the liquid-fueled SoLoNOx combustor indicate that a 10% increase in pilot fuel flow rate does not significantly impact the combustor's tolerance to Exhaust Gas Recirculation (EGR). This suggests that the SoLoNOx configuration maintains stable operation under EGR conditions despite moderate variations in pilot fuel input.

6.2 FUTURE WORK

To comprehensively understand and implement Exhaust Gas Recirculation (EGR) in large-scale industrial gas turbines, the findings presented in this thesis serve as a foundational step but are not sufficient on their own. Further research and in-depth studies are required to address the complexities associated with full-scale application. Key areas of investigation that warrant additional focus include:

- The commissioning phase is currently underway for the installation of a dual-fuel Centaur 40 gas turbine equipped with a SoLoNOx combustor, which will serve as a critical platform for validating the computational models and analytical findings presented in this thesis. The

validation effort will encompass both the liquid-fueled SoLoNOx combustor configuration and the conventional liquid-fueled combustor, allowing for a comprehensive comparison of performance under various operating conditions, including the application of Exhaust Gas Recirculation (EGR).

This installation will not only support model verification but also enable extended experimental investigations into combustion stability, emissions behavior (NOx, CO, UHC), and overall thermodynamic performance under realistic field conditions. All validation activities will rely on actual engine test data obtained directly from the commissioned unit, ensuring high fidelity between simulated and real-world results. The insights gained from this work will further inform future design improvements and operational strategies for EGR implementation in industrial gas turbines.

- Developing a detailed performance model using the Numerical Propulsion System Simulation (NPSS) software toward evaluating the impact of EGR on gas turbine operation. This model will be designed to simulate and analyze both overall engine performance and individual subsystem behavior, including the compressor, combustor, turbine, and exhaust system, under various EGR conditions.

  By integrating thermodynamic and component-specific parameters, the NPSS model will enable a system-level assessment of EGR effects, such as changes in mass flow rate, pressure ratios, fuel flow requirements, turbine inlet temperature (TRIT), and exhaust gas composition. Furthermore, the model will provide insights into key performance metrics like thermal efficiency, specific fuel consumption (SFC), back work ratio, and emissions output.

This simulation tool will serve as a valuable complement to experimental validation efforts, offering predictive capabilities that support design optimization, control strategy development, and feasibility assessment for EGR implementation in industrial gas turbine systems.

- Comprehensive investigations into flame dynamics, specifically, flame stability, flame speed, and flashback tendencies, are essential when operating EGR-integrated systems, particularly in gas turbines such as the Centaur 40 equipped with the SoLoNOx combustor. These studies will focus on a wide range of fuels, including conventional hydrocarbons**,** alternative fuels, hydrogen, ammonia, and various fuel blends, each of which presents unique combustion characteristics under Exhaust Gas Recirculation (EGR) conditions. The objective will be to evaluate how EGR influences flame anchoring, propagation behavior, and potential flame flashback risks, especially when using high-reactivity fuels like hydrogen or low-carbon alternatives such as ammonia. These effects are highly dependent on the chemical kinetics of the fuel-air mixture, and as such, multiple detailed and reduced chemical mechanisms will be employed to accurately simulate and predict combustion behavior within the SoLoNOx configuration. Such studies will be vital in ensuring stable and safe operation of EGR-enabled gas turbines while also achieving low-emission combustion performance. These studies will also contribute to the broader goal of enabling fuel flexibility and decarbonization in industrial gas turbine applications.
- Performing systematic studies on the impact of load variations (load sweeps) and pilot-to-main fuel flow ratio adjustments (pilot fuel flow ratio sweeps) to understand the operational behavior of gas turbines under EGR conditions. These investigations will aim to assess how changes in

engine load and combustion staging influence thermal performance, combustion stability, emissions characteristics, and fuel efficiency in EGR-integrated systems.

Under varying load conditions, the gas turbine experiences shift in airflow, fuel demand, pressure ratios, and temperature profiles, all of which are further complicated by the dilutive and heat capacity effects introduced by EGR. Similarly, altering the pilot-to-main fuel flow ratio affects flame anchoring, ignition stability, and the distribution of heat release, which in turn influences emissions of NOx, CO, and unburned hydrocarbons (UHCs), as well as susceptibility to flame blowout or flashback.

These studies are particularly relevant for lean-premixed combustor architectures such as the SoLoNOx system in the Centaur 40 gas turbine, where maintaining combustion stability across a wide operating envelope is critical. By analyzing performance across these sweep conditions, optimal operating strategies can be developed to ensure reliable, low-emission performance under a variety of practical field conditions with EGR.

REFERENCES.

[1] D. C. Washington, “UNITED STATES SECURITIES AND EXCHANGE COMMISSION FORM 10-Q.” [Online]. Available: www.gevernova.com/investors/fls.

[2] G. Vernova, “GE Vernova 2024 Annual Report,” 2024.

[3] “Gas Turbine Market Size, Share | CAGR of 4.20%.” Accessed: Apr. 27, 2025. [Online]. Available: https://market.us/report/gas-turbine-market/#overview

[4] W. L. Stewart, W. J. Anderson, D. T. Bernatowicz, D. C. Guentert, D. R. Packe, and H. E. Rohlik, “V. BRAYTON CYCLE TECHNOLOGY.”

[5] H. Kurt, Z. Recebli, and E. Gedik, “Performance analysis of open cycle gas turbines,” *Int J Energy Res*, vol. 33, no. 3, pp. 285–294, Mar. 2009, doi: 10.1002/er.1472.

[6] W. Zhang, L. Chen, and F. Sun, “Power and efficiency optimization for combined Brayton and inverse Brayton cycles,” *Applied Thermodynamics Eng*, vol. 29, no. 14–15, pp. 2885–2894, Oct. 2009, doi: 10.1016/j.applthermaleng.2009.02.011.

[7] B. Zohuri, “Thermodynamics of Cycles,” in *Compact Heat Exchangers*, Springer International Publishing, 2017, pp. 291–313. doi: 10.1007/978-3-319-29835-1_6.

[8] Federal Aviation Administration, “Aircraft Systems Chapter 7,” 2023. Accessed: Apr. 24, 2025. [Online]. Available: https://www.faa.gov/sites/faa.gov/files/09_phak_ch7.pdf

[9] M. Grstein, “Fundamentals of gas turbine Combustion R ~ REHEEz!”

[10] B. Prade, “Gas turbine operation and combustion performance issues,” in *Modern Gas Turbine Systems: High Efficiency, Low Emission, Fuel Flexible Power Generation*, Elsevier Ltd., 2013, pp. 383–422. doi: 10.1533/9780857096067.3.383.

[11] A. H. Lefebvre, “Gas Turbine combustion,” 1983.

[12] W. Han *et al.*, “Aerodynamic design of the high pressure and low-pressure axial turbines for the improved coal-fired recompression SCO2 reheated Brayton cycle,” *Energy*, vol. 179, pp. 442–453, Jul. 2019, doi: 10.1016/j.energy.2019.05.016.

[13] K. Brun and R. Kurz, “Introduction to gas turbine theory,” 2019.

[14] J. Misiowiec, T. Mcelwee, and S. Dellavilla, “The American Society of Mechanical engineers’ evolution of gas turbines auxiliary systems designed for reliability,” 1993. [Online]. Available: http://asmedigitalcollection.asme.org/GT/proceedings-pdf/GT1993/78903/V03AT15A084/2403330/v03at15a084-93-gt-233.pdf

[15] F. G. Elliott, R. Kurz, C. Etheridge, and J. P. O'Connell, "Fuel system suitability considerations for industrial Gas Turbines," *J Eng Gas Turbine Power*, vol. 126, no. 1, pp. 119–126, Jan. 2004, doi: 10.1115/1.1619424.

[16] W. R. Loomis, D. P. Townsend, and R. L. Johnson, "Lubricants for inerted Lubrication Systems in Engines for Advanced Aircraft," 1968. [Online]. Available: https://www.jstor.org/stable/44565192?seq=1&cid=pdf-

[17] Aguero J.L., M. C. Beroqui, and H. Di Pasquo, "Gas turbine control. Modification for, Availability and limitation of spinning reserve and limitation of non-desired unloading," Jul. 2005.

[18] H. Asgari, X. Chen, and R. Sainudiin, "Considerations in modelling and control of gas turbines.," 2011.

[19] U. Unnikrishnan and V. Yang, "A review of cooling technologies for high temperature rotating components in gas turbine," Sep. 01, 2022, *Elsevier Ltd*. doi: 10.1016/j.jppr.2022.07.001.

[20] T. S. Chowdhury, F. T. Mohsin, M. M. Tonni, M. N. H. Mita, and M. M. Ehsan, "A critical review on gas turbine cooling performance and failure analysis of turbine blades," May 01, 2023, *Elsevier B.V.* doi: 10.1016/j.ijft.2023.100329.

[21] A. Nannarone and S. A. Klein, "Start-Up Optimization of a CCGT Power Station Using Model-Based Gas Turbine Control," *J Eng Gas Turbine Power*, vol. 141, no. 4, Apr. 2019, doi: 10.1115/1.4041273.

[22] G. Popov, V. Matveev, V. Zubanov, Y. Novikova, D. Kolmakova, and A. Korneeva, "Improving the start-up parameters of a gas turbine engine by adaptation the air turbine starter," in *IOP Conference Series: Materials Science and Engineering*, IOP Publishing Ltd, Aug. 2020. doi: 10.1088/1757-899X/904/1/012006.

[23] R. Pavri and G. D. Moore, "GE Power Systems Gas Turbine Emissions and Control."

[24] D. João Mário Burguete Botelho Cardoso Vogais and E. Celso Jacinto Branco Moreira Guerreiro Eng António Fernando dos Santos Rodrigues Mateus Doutor Rui Fernando dos Santos Pereira Martins, "Fatigue life assessment of exhaust systems for naval gas turbines," Sep. 2011.

[25] J. Liu, Z. Long, M. Bai, L. Zhu, and D. Yu, "A comparative study on fault detection methods for gas turbine combustion systems," *Energies (Basel)*, vol. 14, no. 2, Jan. 2021, doi: 10.3390/en14020389.

[26] W. G. Dukek, "Aviation and Other Gas Turbine Fuels," in *Kirk-Othmer Encyclopedia of Chemical Technology*, Wiley, 2000. doi: 10.1002/0471238961.0122090104211105.a01.

[27] L. S. Langston, “Introduction to Gas Turbines for Non-Engineers,” 1997.

[28] P. A. Pilavachi, “Power generation with gas turbine systems and combined heat and power,” Brussels, 2000. [Online]. Available: www.elsevier.com/locate/apthermeng

[29] S. Popli, P. Rodgers, and V. Eveloy, “Gas turbine efficiency enhancement using waste heat powered absorption chillers in the oil and gas industry,” in *Applied Thermal Engineering*, 2013, pp. 918–931. doi: 10.1016/j.applthermaleng.2012.06.018.

[30] C. B. Meher-Homji, B. Fellow, J. Zachary, T. Manager, M. Frederick, and A. F. Bromley, “Gas turbine fuels-system design, combustion and operability,” 2010.

[31] M. Welch, M. Welch, and B. M. Igoe, “Combustion, Fuels and Emissions for Industrial Gas Turbines,” 2016.

[32] A. H. Lefebvre and D. R. Ballal, “GAS Turbine Combustion: Alternative Fuels and Emissions,” 2010.

[33] J. B. Greenberg, “The Burke-Schumann Diffusion Flame Revisited-With Fuel Spray Injection,” 1989.

[34] L. O. Tomlinson and R. K. NH, “Economics of Heavy Fuels in Gas Turbines and Combined Cycles,” Houston, Dec. 1981. [Online]. Available: http://asmedigitalcollection.asme.org/GT/proceedings-pdf/GT1981/79627/V002T06A010/2393589/v002t06a010-81-gt-45.pdf

[35] A. N. Mustafa, O. M. Ali, and O. R. Alomar, “Effect of Heavy Fuel Combustion in a Gas Power Plant on Turbine Performance: A Review,” Feb. 01, 2022, *International Information and Engineering Technology Association*. doi: 10.18280/ijdne.170113.

[36] I. Gökalp and E. Lebas, “Alternative fuels for industrial gas turbines (AFTUR),” in *Applied Thermal Engineering*, Aug. 2004, pp. 1655–1663. doi: 10.1016/j.applthermaleng.2003.10.035.

[37] J. P. Longwell, “Synthetic fuels and combustion.”

[38] M. Overbaugh and V. Mcdonell, “Characterization of NOx Performance of Fuel Flexible Gas Turbine Combustors at Atmospheric Conditions,” Boston, Mar. 2025.

[39] M. Alhuyi Nazari, M. Fahim Alavi, M. Salem, and M. E. H. Assad, “Utilization of hydrogen in gas turbines: a comprehensive review,” 2022, *Oxford University Press*. doi: 10.1093/ijlct/ctac025.

[40] D. Pashchenko, “Hydrogen-rich gas as a fuel for the gas turbines: A pathway to lower CO2 emission,” *Renewable and Sustainable Energy Reviews*, vol. 173, Mar. 2023, doi: 10.1016/j.rser.2022.113117.

[41] S. R. Turns, “An introduction to combustion: Concepts and Applications,” 2000.

[42] A. H. Lefebvre and NASA Lewis Research center, “Lean Premixed/ Prevaporized combustion,” Jan. 1977.

[43] M. R. Kotal, S. De, S. Das, and S. Sen, “Characterization of laminar flame using high speed camera and spectrometer,” *Sadhana - Academy Proceedings in Engineering Sciences*, vol. 45, no. 1, Dec. 2020, doi: 10.1007/s12046-020-01465-4.

[44] G. G. Brown, “burke schumann 2002 diffusion flames,” Sep. 1928.

[45] S. K. Aggarwal, “Extinction of laminar partially premixed flames,” Dec. 2009. doi: 10.1016/j.pecs.2009.04.003.

[46] B. Paul and A. Datta, “Existence of Nano-Organic Carbon Particles below the Size Range of 10 nm in the Indoor Air Environment,” 2017. [Online]. Available: https://www.researchgate.net/publication/318778846

[47] A. A. V. Perpignan, A. Gangoli Rao, and D. J. E. M. Roekaerts, “Flameless combustion and its potential towards gas turbines,” Nov. 01, 2018, *Elsevier Ltd*. doi: 10.1016/j.pecs.2018.06.002.

[48] F. Biagioli and F. Güthe, “Effect of pressure and fuel-air unmixedness on NOx emissions from industrial gas turbine burners,” *Combust Flame*, vol. 151, no. 1–2, pp. 274–288, Oct. 2007, doi: 10.1016/j.combustflame.2007.04.007.

[49] M. Song, L. Zeng, X. Li, Z. Chen, and Z. Li, “Effect of Stoichiometric Ratio of Fuel-Rich Flow on Combustion Characteristics in a Down-Fired Boiler,” *Journal of Energy Engineering*, vol. 143, no. 3, Jun. 2017, doi: 10.1061/(asce)ey.1943-7897.0000415.

[50] B. Cuenot, “Gas Turbines and Engine Simulations,” in *Advances in marine biology. Volume 35*, Academic Press, 2016, pp. 273–285. doi: 10.1016/bs.ache.2016.09.004.

[51] A. S. Feitelberg, V. E. Tangirala, R. A. Elliott, R. E. Pavri, and R. B. Schiefer, “Reduced NOx diffusion flame combustors for industrial gas turbines,” *J Eng Gas Turbine Power*, vol. 123, no. 4, pp. 757–765, Oct. 2001, doi: 10.1115/1.1376722.

[52] A. N. Hayhurst and I. M. Vince, “Nitric oxide formation from N2 in flames, the importance of prompt NO,” vol. 6, pp. 35–51, 1980.

[53] A. N. Hayhurst and I. M. Vince, “The Origin and Nature of ‘Prompt’ Nitric Oxide in Flames,” 1983.

[54] J. W. Bozzelli and A. M. Dean, “O + NNH: A possible new route for NOX formation in flames,” *Int J Chem Kinet*, vol. 27, no. 11, pp. 1097–1109, 1995, doi: 10.1002/kin.550271107.

[55] S. J. Klippenstein, L. B. Harding, P. Glarborg, and J. A. Miller, “The role of NNH in NO formation and control,” *Combust Flame*, vol. 158, no. 4, pp. 774–789, Apr. 2011, doi: 10.1016/j.combustflame.2010.12.013.

[56] P. C. Malte and D. T. Pratt, “The Role of Energy-Releasing Kinetics in NOx Formation: Fuel-Lean, Jet-Stirred CO-Air Combustion,” 1974.

[57] D. G. Nicol, P. C. Matte, and R. C. Steele, “Simplified models for NO production rates in lean-premixed combustion,” 1994. [Online]. Available: http://asmedigitalcollection.asme.org/GT/proceedings-pdf/GT1994/78859/V003T06A037/2404610/v003t06a037-94-gt-432.pdf

[58] J. F. Driscoll, R.-H. Chen, and Y. Yoon, “Nitric Oxide Levels of Turbulent Jet Diffusion Flames: Effects of Residence Time and Damkohler Number,” 1992.

[59] D. Anderson, “Effects of Equivalence Ratio and Dwell Time on Exhaust Emissions from an Experimental Premixing Prevaporizing Burner Effects of Equivalence Ratio and Dwell Time on Exhaust Emissions from an Experimental Premixing Prevaporizing Liutiiri,” 1975. [Online]. Available: http://asmedigitalcollection.asme.org/GT/proceedings-pdf/GT1975/79771/V01BT02A007/2391349/v01bt02a007-75-gt-69.pdf

[60] D. Anderson, “Effects of Equivalence Ratio and Dwell Time on Exhaust Emissions from an Experimental Premixing Prevaporizing Burner Effects of Equivalence Ratio and Dwell Time on Exhaust Emissions from an Experimental Premixing Prevaporizing Liutiiri,” 1975. [Online]. Available: http://asmedigitalcollection.asme.org/GT/proceedings-pdf/GT1975/79771/V01BT02A007/2391349/v01bt02a007-75-gt-69.pdf

[61] Arthur H. Lefebvre, *Gas Turbine combustion*. Hemisphere Publishing Corporation, 1983.

[62] S. Bobi, P. Garai, R. K. Rahman, and S. S. Vasu, “Characteristics of counterflow diffusion flame of Ammonia-hydrogen blends under aviation turbines conditions,” Mar. 2025.

[63] L. S. Pedersen, P. Breithaupt, K. Dam-Johansen, and R. Weber, “Residence time distributions in confined swirling flames,” *Combustion Science and Technology*, vol. 127, no. 1–6, pp. 251–273, 1997, doi: 10.1080/00102209708935696.

[64] E. Emond, “Optimizing NOx emission reductions in industrial natural gas combustion processes | Informa-TECH.” Accessed: Apr. 27, 2025. [Online]. Available: https://informatech.energir.com/?p=8881&lang=en

[65] M. G. Talboom, “Chemical Kinetics Study of the Hybrid Combustion System.” [Online]. Available: http://repository.tudelft.nl/.

[66] Ø. Skreiberg, T. Li, L. Wang, M. Bugge, and T. Løvås, “An evaluation of effects of fuel parameters and flue gas recirculation on NOx emissions through detailed chemical

kinetics simulations," *Chem Eng Trans*, vol. 74, pp. 217–222, 2019, doi: 10.3303/CET1974037.

[67] K. Ajmani, K. M. Tacina, and T. R. Luginbuhl, "Parametric CFD Analysis of Low NOx Combustor Designs for Commercial Supersonic Aircraft," Mar. 2025.

[68] A. De Santis, D. B. Ingham, L. Ma, and M. Pourkashanian, "CFD analysis of exhaust gas recirculation in a micro gas turbine combustor for CO2 capture," *Fuel*, vol. 173, pp. 146–154, Jun. 2016, doi: 10.1016/j.fuel.2016.01.063.

[69] R. C. Robinson and J. L. Smialek, "SiC recession caused by SiO2 scale volatility under combustion conditions: I. Experimental results and empirical model," *Journal of the American Ceramic Society*, vol. 82, no. 7, pp. 1817–1825, 1999, doi: 10.1111/j.1151-2916.1999.tb02004.x.

[70] M. M. F. Hasan, E. L. First, F. Boukouvala, and C. A. Floudas, "A multi-scale framework for CO2 capture, utilization, and sequestration: CCUS and CCU," *Computer Chem Eng*, vol. 81, pp. 2–21, Oct. 2015, doi: 10.1016/j.compchemeng.2015.04.034.

[71] D. Burnes, P. Saxena, and P. Dunn, "STUDY OF USING EXHAUST GAS RECIRCULATION ON A GAS TURBINE FOR CARBON CAPTURE," 2020. [Online]. Available: http://asmedigitalcollection.asme.org/GT/proceedings-pdf/GT2020/84140/V005T06A034/6615759/v005t06a034-gt2020-16080.pdf

[72] L. Herraiz, E. S. Fernández, E. Palfi, and M. Lucquiaud, "Selective exhaust gas recirculation in combined cycle gas turbine power plants with post-combustion CO2 capture," *International Journal of Greenhouse Gas Control*, vol. 71, pp. 303–321, Apr. 2018, doi: 10.1016/j.ijggc.2018.01.017.

[73] A. T. Evulet, A. M. ELKady, A. R. Branda, and D. Chinn, "On the Performance and Operability of GE's Dry Low NOx Combustors utilizing Exhaust Gas Recirculation for Post Combustion Carbon Capture," in *Energy Procedia*, Feb. 2009, pp. 3809–3816. doi: 10.1016/j.egypro.2009.02.182.

[74] G. Di Lorenzo, P. Barbera, G. Ruggieri, J. Witton, P. Pilidis, and D. Probert, "Pre-combustion carbon-capture technologies for power generation: An engineering-economic assessment," *Int J Energy Res*, vol. 37, no. 5, pp. 389–402, Apr. 2013, doi: 10.1002/er.3029.

[75] M. A. Nemitallah *et al.*, "Oxy-fuel combustion technology: current status, applications, and trends," Oct. 10, 2017, *John Wiley and Sons Ltd*. doi: 10.1002/er.3722.

[76] C. Gough and P. Upham, "Biomass energy with carbon capture and storage (BECCS or Bio-CCS)," *Greenhouse Gases: Science and Technology*, vol. 1, no. 4, pp. 324–334, Dec. 2011, doi: 10.1002/ghg.

[77] N. McQueen, K. V. Gomes, C. McCormick, K. Blumanthal, M. Pisciotta, and J. Wilcox, "A review of direct air capture (DAC): Scaling up commercial technologies and innovating for the future," Jul. 01, 2021, *Institute of Physics*. doi: 10.1088/2516-1083/abf1ce.

[78] P. C. Psarras, S. Comello, P. Bains, P. Charoensawadpong, S. Reichelstein, and J. Wilcox, "Carbon Capture and Utilization in the Industrial Sector," *Environ Sci Technol*, vol. 51, no. 19, pp. 11440–11449, Oct. 2017, doi: 10.1021/acs.est.7b01723.

[79] B. Hoepke, S. Jannsen, E. Kasseris, and W. K. Cheng, "EGR Effects on Boosted SI Engine Operation and Knock Integral Correlation," *International Journal of Engines*, vol. 5, no. 2, pp. 547–559, 2012, doi: 10.2307/26278380.

[80] J. Lauber, T.-M. Guerra, and W. Perruquetti, "IC Engine: Tracking Control for an Inlet Manifold with EGR," 2002.

[81] T. Alger and B. Mangold, "Dedicated EGR: A New Concept in High Efficiency Engines," *Source: SAE International Journal of Engines*, vol. 2, no. 1, pp. 620–631, 2009, doi: 10.2307/26308421.

[82] Y. Lu, J. Que, Y. Xia, X. Li, Q. Jiang, and L. Feng, "A comparative study of the effects of EGR on combustion and emission characteristics of port fuel injection and late direct injection in hydrogen internal combustion engine," *Appl Energy*, vol. 375, Dec. 2024, doi: 10.1016/j.apenergy.2024.123830.

[83] N. X. Khoa and O. Lim, "A Review of the External and Internal Residual Exhaust Gas in the Internal Combustion Engine," *Energies (Basel)*, vol. 15, no. 3, Feb. 2022, doi: 10.3390/en15031208.

[84] M. Baratta, R. Finesso, D. Misul, and E. Spessa, "Comparison between Internal and External EGR Performance on a Heavy-Duty Diesel Engine by Means of a Refined 1D Fluid-Dynamic Engine Model," *Source: SAE International Journal of Engines*, vol. 8, no. 5, pp. 1977–1992, 2015, doi: 10.2307/26278096.

[85] D. Agarwal, S. K. Singh, and A. K. Agarwal, "Effect of Exhaust Gas Recirculation (EGR) on performance, emissions, deposits and durability of a constant speed compression ignition engine," *Appl Energy*, vol. 88, no. 8, pp. 2900–2907, 2011, doi: 10.1016/j.apenergy.2011.01.066.

[86] M. Hedge, P. Weber, J. Gingrich, T. Alger, and I. Khalek, "Effect of EGR on Particle Emissions from a GDI Engine," *Source: SAE International Journal of Engines*, vol. 4, no. 1, pp. 650–666, 2011, doi: 10.2307/26278177.

[87] P. E. Røkke and J. E. Hustad, "Exhaust Gas Recirculation in Gas Turbines for Reduction of CO 2 Emissions; Combustion Testing with Focus on Stability and Emissions," 2005.

[88] Ž. Rosec, T. Katrašnik, U. Žvar Baškovič, and T. Seljak, “Exhaust gas recirculation with highly oxygenated fuels in gas turbines,” *Fuel*, vol. 278, Oct. 2020, doi: 10.1016/j.fuel.2020.118285.

[89] A. Dastagir, “Impact of Exhaust Gas Recirculation on NOx emissions in non-premixed combusted Gas Turbines using CRN,” Sep. 2018. [Online]. Available: http://repository.tudelft.nl/.

[90] I. V. Novosselov, “Chemical reactor networks for combustion systems modeling,” Mar. 2006.

[91] P. C. Malte, I. V. Novosselov, J. C. Y. Lee, R. Srinivasan, and S. Yuan, “Chemical reactor network application to emissions prediction for industrial DLE gas turbine,” no. GT2006-90282, pp. 221–235, May 2006.

[92] B. Rosati, “Prediction of emissions from combustion systems using 0D and 1D reacting flow models Chemical Reactor Network modeling,” Dec. 2015. [Online]. Available: http://repository.tudelft.nl/.

[93] A. Y. Snegirev, “Perfectly stirred reactor model to evaluate extinction of diffusion flame,” *Combust Flame*, vol. 162, no. 10, pp. 3622–3631, Mar. 2015, doi: 10.1016/j.combustflame.2015.06.019.

[94] J. Swithenbank, I. Poll, M. W. Vincent, and D. D. Wright, “Combustion design fundamentals,” *Symposium (International) on Combustion*, vol. 14, no. 1, pp. 627–638, 1973, doi: 10.1016/S0082-0784(73)80059-1.

[95] V. Fichet, M. Kanniche, P. Plion, and O. Gicquel, “A reactor network model for predicting NOx emissions in gas turbines,” *Fuel*, vol. 89, no. 9, pp. 2202–2210, 2010, doi: 10.1016/j.fuel.2010.02.010.

[96] S. Liu, “Ideal Flow Reactors,” in *Bioprocess Engineering*, Elsevier, 2017, pp. 179–257. doi: 10.1016/b978-0-444-63783-3.00005-8.

[97] I. Ansys, “Chemkin-Pro chemistry simulation for more efficient designs,” 2016.

[98] R. C. Tolman, “The mechanism of chemical reaction,” UTC, Jun. 1925. [Online]. Available: https://pubs.acs.org/sharingguidelines

[99] Bragg. S.L., “Application of reaction rate theory to combustion chamber analysis,” Thornton, Sep. 1953.

[100] G. C. Williams, J. P. Longwell, M. A. WEISS Esso Research, and E. Co, “High temperature reaction rates in hydrocarbon combustion,” Aug. 1955. [Online]. Available: https://pubs.acs.org/sharingguidelines

[101] T. Rutar and P. C. Malte, “Nox formation in high-pressure jet-stirred reactors with significance to lean-premixed combustion turbines,” *J Eng Gas Turbine Power*, vol. 124, no. 4, pp. 776–783, Oct. 2002, doi: 10.1115/1.1492829.

[102] A. Schlegel, P. Benz, T. Griffin, W. Weisenstein, and H. Bockhorn, “Catalytic Stabilization of Lean Premixed Combustion: Method for Improving NO, Emissions,” 1996.

[103] G. J. Sturgess, S. P. Heneghan, M. D. Vangsness, and D. R. Ballal, “Lean Blowout in a Research Combustor at Simulated Low Pressures,” 1991. [Online]. Available: http://asmedigitalcollection.asme.org/GT/proceedings-pdf/GT1991/79009/V003T06A029/2400947/v003t06a029-91-gt-359.pdf

[104] G. Sturgess, “Studies of lean blowout in a research combustor,” May 1995.

[105] J. H. Tonouchi, “Macromixing and micromixing in lean premixed combustion,” Mar. 1996.

[106] J. Park, T. H. Nguyen, D. Joung, K. Y. Huh, and M. C. Lee, “Prediction of NOx and CO emissions from an industrial lean-premixed gas turbine combustor using a chemical reactor network model,” *Energy and Fuels*, vol. 27, no. 3, pp. 1643–1651, Mar. 2013, doi: 10.1021/ef301741t.

[107] I. V Novosselov, “Eight-Step Global Kinetic Mechanism on Methane Oxidation with Nitric Oxide Formation for Lean-Premixed Combustion Turbines,” 2001.

[108] A. B. Lebedev, A. N. Secundov, A. M. Starik, N. S. Titova, and A. M. Schepin, “Modeling study of gas-turbine combustor emission,” *Proceedings of the Combustion Institute*, vol. 32 II, no. 2, pp. 2941–2947, 2009, doi: 10.1016/j.proci.2008.05.015.

[109] B. F. Magnussen and B. H. Hjertager, “On mathematical modeling of turbulent combustion with special emphasis on soot formation and combustion.”

[110] O. Levenspiel, “Experimental search for a simple rate equation to describe deactivating porous catalyst particles octave LEVENSPIEL,” Oregon, Sep. 1972.

[111] “Combustor Design for Gas Turbine Engines Solar Turbines Incorporated James Blust,” 2024.

[112] Solar Turbines, “Caterpillar: Confidential Green,” DeSoto, Nov. 2024.

[113] J. F. Driscoll, R.-H. Chen, and Y. Yoon, “Nitric Oxide Levels of Turbulent Jet Diffusion Flames: Effects of Residence Time and Damkohler Number,” 1992.

[114] S. Dong *et al.*, “A new detailed kinetic model for surrogate fuels: C3MechV3.3,” *Applications in Energy and Combustion Science*, vol. 9, Mar. 2022, doi: 10.1016/j.jaecs.2021.100043.

[115] Y. Li, H. Zhao, and T. Ma, “Stratification of fuel for better engine performance,” *Fuel*, vol. 85, no. 4, pp. 465–473, Mar. 2006, doi: 10.1016/j.fuel.2005.08.005.

[116] S. Dong *et al.*, “Investigations on the effects of fuel stratification on auto-ignition and combustion process of an ethanol/diesel dual-fuel engine,” *Appl Energy*, vol. 230, pp. 19–30, Nov. 2018, doi: 10.1016/j.apenergy.2018.08.082.

[117] Y. Zhu, Y. Zhang, Z. He, Q. Wang, and W. Li, “A numerical investigation of gasoline/diesel direct dual fuel stratification (DDFS) combustion at high loads,” *Fuel*, vol. 312, Mar. 2022, doi: 10.1016/j.fuel.2021.122751.

[118] A. Al-Halbouni, A. Giese, E. Tali, J. Leicher, R. Albus, and K. Görner, “Combustor concept for industrial gas turbines with single digit NOx and CO emission values,” in *Energy Procedia*, Elsevier Ltd, 2017, pp. 134–139. doi: 10.1016/j.egypro.2017.07.146.

[119] A. M. Reiter, T. Wallek, A. Pfennig, and M. Zeymer, “Surrogate generation and evaluation for diesel fuel,” *Energy and Fuels*, vol. 29, no. 7, pp. 4181–4192, Jul. 2015, doi: 10.1021/acs.energyfuels.5b00422.

[120] C. J. Mueller *et al.*, “Diesel Surrogate Fuels for Engine Testing and Chemical-Kinetic Modeling: Compositions and Properties,” *Energy and Fuels*, vol. 30, no. 2, pp. 1445–1461, Feb. 2016, doi: 10.1021/acs.energyfuels.5b02879.

[121] D. Sebastian Pérez-Gordillo, J. M. Mantilla-González, and J. P. Gore, “An Evaluation of Combustion Models for Turbulent Diffusion Flames,” Boston, Mar. 2025.

[122] A. Elkady, A. Evulet, A. Brand, and C. Vandervort, “GE Global Research Technical Information Series Exhaust Gas Recirculation Performance in Dry Low Emissions Combustors Public (Class 1),” 2010.

[123] Ž. Rosec, T. Katrašnik, U. Žvar Baškovič, and T. Seljak, “Exhaust gas recirculation with highly oxygenated fuels in gas turbines,” *Fuel*, vol. 278, Oct. 2020, doi: 10.1016/j.fuel.2020.118285.

[124] A. De Toni, T. Hayashi, and P. Schneider, “A reactor network model for predicting NOx emissions in an industrial natural gas burner,” *Journal of the Brazilian Society of Mechanical Sciences and Engineering*, vol. 35, no. 3, pp. 199–206, Oct. 2013, doi: 10.1007/s40430-013-0039-5.

[125] A. M. Elkady, A. Evulet, A. Brand, T. P. Ursin, and A. Lynghjem, “Exhaust gas recirculation in DLN F-class gas turbines for post-combustion CO2 capture,” 2008. [Online]. Available: http://asmedigitalcollection.asme.org/GT/proceedings-pdf/GT2008/43130/847/4577337/847_1.pdf

[126] J. Hachem, T. Schuhler, D. Orhon, M. Cuif-Sjostrand, A. Zoughaib, and M. Molière, “Exhaust gas recirculation applied to single-shaft gas turbines: An energy and exergy approach,” *Energy*, vol. 238, Jan. 2022, doi: 10.1016/j.energy.2021.121656.

The turbine inlet temperature is 1665 deg F at full load.

Assumptions

Gamma & specific heat Cp_air are constant.

No losses due to fluid friction, therefore compression and expansion are isentropic.

T_{ref} = 298 [K]

$T_{ref,C}$ = **ConvertTemp** (K, C, $T_{ref,C}$)

T_{fuel} = 300 [K] **Dodecane temperature, 76.3 deg F**

$T_{fuel,C}$ = **ConvertTemp** (K, C, T_{fuel})

P_{ref}= 101.34 [kPa]

T_{prod} = 1180.4 [K]

$T_{cp,avg,fuel} = \frac{(T_{ref} + T_{fuel})}{2}$

$T_{cp,avg,fuel,C}$ = **ConvertTemp** (K, C, $T_{cp,avg,fuel}$)

$T_{cp,avg,react} = \frac{T_{ref} + T_{combustion,air}}{2}$

$T_{cp,avg,react,C}$ = **ConvertTemp** (K, C, $T_{cp,avg,react}$)

$T_{cp,avg,prod} = \frac{T_{ref} + T_{prod}}{2}$

$T_{cp,avg,prod,C}$ = **ConvertTemp** (K, C, $T_{cp,avg,prod}$)

$\dot{m}_{dodecane}$ = 0.276 [kg/s] **Total mass flowrate of fuel at full load,2190 pph**

$\dot{m}_{air}$ = 17.83 [kg/s] **Total mass flowrate of air at full load, 39.3 pps**

$Combustion_{air} = 0.91 \cdot \dot{m}_{air}$ **9% of air goes into secondary flow**

P_2 = 140.4 [psi] **Compressor exit pressure, 125.7 psig**

$P_{2,kPa} = P_2 \cdot (6.895 \cdot \frac{kPa}{psi})$

$T_{air,input}$ = 608.48 [K] **Compressor discharge temperature, 635.6 deg F from test data**

$T_{exhaust}$ = 718.76 [K] **From engine test**

change in temperature for fuel evaporation calculation below.

$P_{fuel,supply}$ = 272.3 [psi]

$P_{fuel,supply,kPa} = P_{fuel,supply} \cdot (6.895 \cdot \frac{kPa}{psi})$

$Cp_{dodecane}$ = $\boldsymbol{Cp}$ (n–Dodecane, T = $T_{fuel,C}$, P = $P_{2,kPa}$)

$Q_f = \dot{m}_{dodecane} \cdot \Delta_{vap,dodecane}$ **Heat energy required**

$\Delta_{vap,temp} = \frac{Q_f}{Combustion_{air} \cdot Cp_{dodecane}}$

$T_{combustion,air} = T_{air,input} - \Delta_{vap,temp}$ **Temperature after dodecane vaporization**

$LHV_{dodecane}$ = 44.15 [MJ/kg] **25 degrees celsius**

$\Delta_{vap,dodecane}$ = $\boldsymbol{Enthalpy}_{vaporization}$ (n–Dodecane, T = $T_{fuel,C}$)

$Low_{heating\ value}$ = 44150 [kJ/kg]

$\Delta h_{fuel} = \frac{\dot{m}_{dodecane}}{\dot{m}_{air}} \cdot Low_{heating\ value}$

γ = 1.4

SG = 0.835 **specific gravity for diesel**

WI = $\frac{LHV_{dodecane}}{\sqrt{SG}}$ **Wobbe Index**

Cp_{air} = $\boldsymbol{Cp}$ (Air_{ha}, T = $T_{ref,C}$, P = P_{ref}) **At reference point**

Cp values of reactants @ 450 K

$Cp_{O_{2,react}}$ = 30.662 [kJ/kmol-K]

$Cp_{N_{2,react}}$ = 29.478 [kJ/kmol-K]

$Cp_{CO_{2,react}}$ = 42.923 [kJ/kmol-K]

$Cp_{H_2O,react}$ = 34.887 [kJ/kmol-K]

Cp values of products @ 740 K

$Cp_{N_{2,prod}}$ = 30.968 [kJ/kmol-K]

$Cp_{O_{2,prod}}$ = 33.26 [kJ/kmol-K]

$Cp_{H_2O,prod}$ = 37.853 [kJ/kmol-K]

$Cp_{CO_{2,prod}}$ = 50.39 [kJ/kmol-K]

Enthalpy of formation @ 298 K

$\Delta H_{O_2,ref}$ = 0 [kJ/kmol]

$\Delta H_{N_2,ref}$ = 0 [kJ/kmol]

$\Delta H_{H_2O,ref}$ = – 241845 [kJ/kmol]

$\Delta H_{CO_2,ref}$ = – 393546 [kJ/kmol]

$\Delta H_{dodecane,ref}$ = – 292162 [kJ/kmol]

Molecular weights

$MW_{dodecane}$ = 170.337 [kg/kmol]

MW_{N_2} = 28 [kg/kmol]

MW_{O_2} = 32 [kg/kmol]

MW_{CO_2} = 44 [kg/kmol]

MW_{H_2O} = 18 [kg/kmol]

MW_{air} = 28.84 [kg/kmol]

MW_C = 12 [kg/kmol]

MW_H = 1 [kg/kmol]

MW_{AR} = 39.9 [kg/kmol]

Reactant sensible heat terms

$\Delta_{sensible,CO_2}$ = 12899 [kJ/kmol]

$\Delta_{sensible,O_2}$ = 9254 [kJ/kmol]

$\Delta_{sensible,N_2}$ = 8905 [kJ/kmol]

$\Delta_{sensible,H_2O}$ = 10528 [kJ/kmol]

Fuel molecule

X = 12 **Number of carbon atoms**

Y = 26 **Number of hydrogen atoms**

Z = 0.0003 **Number of carbon dioxide in the atmosphere**

K = 0.005 **Number of carbon dioxide in the atmosphere**

EGR fraction input

a = $X + \frac{Y}{4}$

$$AFR_{stoic} = \frac{4.76 \cdot a \cdot MW_{air}}{MW_{dodecane}}$$

$$AFR_{actual} = \frac{Combustion_{air}}{\dot{m}_{dodecane}}$$

$$OF_{stoic} = \frac{a \cdot MW_{O_2}}{MW_{dodecane}}$$

$$OF_{actual} = \frac{\dot{m}_{O_2,intake}}{\dot{m}_{dodecane}}$$

$$a_{new} = \frac{AFR_{actual} \cdot MW_{dodecane}}{4.76 \cdot MW_{air}}$$

$$a_{OF} = \frac{OF_{actual} \cdot MW_{dodecane}}{MW_{O_2}}$$

Mole fraction

$$X_{O_2,atm} = \frac{0.992}{4.76}$$

$$X_{N_2,atm} = \frac{3.698}{4.76}$$

$$X_{H_2O,atm} = \frac{0.024}{4.76}$$

$$X_{CO_2,atm} = \frac{0.00143}{4.76}$$

$$X_{AR,atm} = \frac{0.0443}{4.76}$$

Atmospheric air mass

$$mass_{O_2,air} = \frac{X_{O_2,atm} \cdot MW_{O_2}}{MW_{air}}$$

Mass fraction

$$Y_{O_2,atm} = \frac{X_{O_2,atm} \cdot MW_{O_2}}{MW_{air}}$$

$$Y_{N_2,atm} = \frac{X_{N_2,atm} \cdot MW_{N_2}}{MW_{air}}$$

$$Y_{H_2O,atm} = \frac{X_{H_2O,atm} \cdot MW_{H_2O}}{MW_{air}}$$

$$Y_{CO_2,atm} = \frac{X_{CO_2,atm} \cdot MW_{CO_2}}{MW_{air}}$$

$$Y_{AR,atm} = \frac{X_{AR,atm} \cdot MW_{AR}}{MW_{air}}$$

$$\phi_{AFR} = \frac{AFR_{stoic}}{AFR_{actual}}$$

$$\phi_{OF} = \frac{OF_{stoic}}{OF_{actual}}$$

$$N_{combustion,air} = \frac{combustion_{air}}{MW_{air}}$$

$$N_{dodecane} = \frac{dodecane_{consumption}}{MW_{dodecane}}$$

R_u = 8.315 [kJ/kmol-K] **Universal gas constant**

After compression condition

$$\rho_{air} = \frac{P_{2,kPa}}{\frac{R_u}{MW_{air}} \cdot T_{combustion,air}}$$

$$\dot{V}_{combustion,air} = \frac{combustion_{air}}{\rho_{air}}$$

EGR convergence

$$\boldsymbol{C_X H_y + a_{new}\,(O_2 + 3.76 * N_2) + EGR_{frac} * (D + F + G) \rightarrow D * CO_2 + E * H_2O + F * N_2 + G * O_2}$$

Water has been dropped in this equation.

G represents mole fraction of excess water in combustion products

D represents mole fraction of carbon dioxide in combustion products.

E represents mole fraction of water in combustion products

F represents mole fraction of Nitrogen in combustion products

EGR convergence calculation.

$$a_{egr,frac} = (1 - EGR_{frac}) \cdot a_{new}$$

Carbon balance

$$D = X + EGR_{frac} \cdot D + Z \cdot a_{egr,frac}$$

Hydrogen balance

$$E = \frac{Y}{2} + K \cdot a_{egr,frac}$$

Oxygen balance

$$2 \cdot a_{egr,frac} + EGR_{frac} \cdot D \cdot 2 + EGR_{frac} \cdot G \cdot 2 + Z \cdot 2 \cdot a_{egr,frac} = D \cdot 2 + E + G \cdot 2$$

Nitrogen balance

$$a_{egr,frac} \cdot 3.76 + EGR_{frac} \cdot F = F$$

Argon balance

$$J = 0.0093 \cdot a_{egr,frac} + EGR_{frac} \cdot J$$

Mole fraction of wet exhaust products

$$Total_{moles,wet} = D + E + F + G + J$$ **Total moles**

$$X_{CO_2,wet} = \frac{D}{Total_{moles,wet}}$$

$$X_{H_2O,wet} = \frac{E}{Total_{moles,wet}}$$

$$X_{N_2,wet} = \frac{F}{Total_{moles,wet}}$$

$$X_{O_2,wet} = \frac{G}{Total_{moles,wet}}$$

$$X_{AR,wet} = \frac{J}{Total_{moles,wet}}$$

Mole fraction of dry exhaust products

$$Total_{moles,dry} = D + F + G + J$$

$$X_{CO_2,dry} = \frac{D}{Total_{moles,dry}}$$

$$X_{N_2,dry} = \frac{F}{Total_{moles,dry}}$$

$$X_{O_2,dry} = \frac{G}{Total_{moles,dry}}$$

$$X_{AR,dry} = \frac{J}{Total_{moles,dry}}$$

Compressor inlet mole fraction

$$X_{O_2,EGR} = EGR_{frac} \cdot X_{O_2,wet}$$

$$X_{CO_2,EGR} = EGR_{frac} \cdot X_{CO_2,wet}$$

$$X_{N_2,EGR} = EGR_{frac} \cdot X_{N_2,wet}$$

$$X_{AR,EGR} = EGR_{frac} \cdot X_{AR,wet}$$

$$X_{H_2O,EGR} = 0.06 \cdot X_{H_2O,wet}$$ **6% water saturation after cooling**

Compressor inlet mass fraction

$$Y_{O_2,EGR} = \frac{X_{O_2,EGR} \cdot MW_{O_2}}{MW_{EGR}}$$

$$Y_{CO_2,EGR} = \frac{X_{CO_2,EGR} \cdot MW_{CO_2}}{MW_{EGR}}$$

$$Y_{N_2,EGR} = \frac{X_{N_2,EGR} \cdot MW_{N_2}}{MW_{EGR}}$$

$$Y_{AR,EGR} = \frac{X_{AR,EGR} \cdot MW_{AR}}{MW_{EGR}}$$

$$Y_{H_2O,EGR} = \frac{X_{H_2O,EGR} \cdot MW_{H_2O}}{MW_{EGR}}$$

$$X_{O_2,intake} = X_{O_2,atm} \cdot \left(1 - EGR_{frac}\right) + X_{O_2,EGR}$$

$$X_{N_2,intake} = X_{N_2,atm} \cdot \left(1 - EGR_{frac}\right) + X_{N_2,EGR}$$

$$X_{CO_2,intake} = X_{CO_2,atm} \cdot \left(1 - EGR_{frac}\right) + X_{CO_2,EGR}$$

$$X_{AR,intake} = X_{AR,atm} \cdot \left(1 - EGR_{frac}\right) + X_{AR,EGR}$$

$$X_{H_2O,intake} = X_{H_2O,atm} \cdot (0.94) + X_{H_2O,EGR}$$

$$Y_{O_2,intake} = \frac{X_{O_2,intake} \cdot MW_{O_2}}{MW_{oxidizer}}$$

$$Y_{N_2,intake} = \frac{X_{N_2,intake} \cdot MW_{N_2}}{MW_{oxidizer}}$$

$$Y_{CO_2,intake} = \frac{X_{CO_2,intake} \cdot MW_{CO_2}}{MW_{oxidizer}}$$

$$Y_{AR,intake} = \frac{X_{AR,intake} \cdot MW_{AR}}{MW_{oxidizer}}$$

$$Y_{H_2O,intake} = \frac{X_{H_2O,intake} \cdot MW_{H_2O}}{MW_{oxidizer}}$$

$$\dot{m}_{prod} = \dot{m}_{air} + \dot{m}_{dodecane}$$

$$\dot{m}_{recirc} = EGR_{frac} \cdot \dot{m}_{prod}$$

$$\dot{m}_{inlet,air} = \dot{m}_{recirc} + (1 - EGR_{frac}) \cdot \dot{m}_{air}$$

$$\dot{m}_{exhaust} = \left(1 - EGR_{frac}\right) \cdot \dot{m}_{air} + \dot{m}_{recirc} + dodecane_{consumption}$$

$$\dot{m}_{O_2,intake} = Y_{O_2,intake} \cdot \dot{m}_{inlet,air}$$

$$massflow_{exhaust} = MW_{EGR} \cdot N_{EGR} \quad \textbf{[kg/s]}$$

$$massflow_{air,input} = \dot{m}_{air} - \left(EGR_{frac} \cdot \dot{m}_{air}\right) + (EGR_{frac} \cdot massflow_{exhaust})$$

EGR thermodynamic calculations

$Rel_{hum} = 0.75$

T_1 = 25 [C]

$T_{1,K}$ = **ConvertTemp** (C, K, T_1)

T_2 = 332.55 [C]

$T_{2,K}$ = **ConvertTemp** (C, K, T_2)

T_3 = 966.85 [C]

$T_{3,K}$ = **ConvertTemp** (C, K, T_3)

T_4 = 445.65 [C]

$T_{4,K}$ = **ConvertTemp** (C, K, T_4)

$$T_{2,calculated} = T_{ref} \cdot \left[\frac{PR^{\left[\frac{\gamma-1}{\gamma}\right]}-1}{\eta_{comp}} + 1\right]$$

$$T_{4,calculated} = T_{ad,EGR} \cdot \left[1 - \frac{\eta_{turb}}{PR^{\left[\frac{\gamma-1}{\gamma}\right]}}\right]$$

$$PR = \frac{P_{2,kPa}}{P_{ref}}$$

$comb_{drop} = 0.05$ **5% combustion pressure drop**

$P_1 = P_4 = 101.34$ [kPa]

$P_2 = PR \cdot P_1$

$P_3 = P_2 - (P_2 \cdot comb_{drop})$

$P_{combustor} = 0.95 \cdot P_{2,kPa}$

$\dot{V}_{air} = (1 - EGR_{frac}) \cdot \dot{V}_{combustion,air}$

$\dot{V}_{EGR} = \dot{V}_{air} \cdot EGR_{frac}$

$$MW_{EGR} = (X_{CO_2,wet} \cdot MW_{CO_2}) + (X_{O_2,wet} \cdot MW_{O_2}) + (X_{N_2,wet} \cdot MW_{N_2}) + (X_{AR,wet} \cdot MW_{AR}) + (X_{H_2O,wet} \cdot MW_{H_2O})$$

$$MW_{oxidizer} = \left(1 - EGR_{frac}\right) \cdot MW_{air} + (EGR_{frac} \cdot MW_{EGR})$$

$$\rho_{oxidizer} = \frac{P_{2,kPa}}{\frac{R_u}{MW_{oxidizer}} \cdot T_{combustion,air}}$$

$\dot{m}_{EGR} = \dot{V}_{air} \cdot \rho_{oxidizer}$

$$N_{EGR} = \frac{\dot{m}_{exhaust}}{MW_{EGR}}$$

$N_{total,intake} = N_{combustion,air} + N_{EGR}$

$h_1 = \boldsymbol{h}\,(Air_{ha}, T = T_1, P = P_1)$

$h_2 = \boldsymbol{h}\,(Air_{ha}, T = T_2, P = P_2)$

$h_3 = \boldsymbol{h}\,(Air_{ha}, T = T_3, P = P_3)$

$h_4 = \boldsymbol{h}\,(Air_{ha}, T = T_4, P = P_4)$

$s_1 = \boldsymbol{s}\,(Air_{ha}, T = T_1, P = P_1)$

$s_2 = \boldsymbol{s}\,(Air_{ha}, T = T_2, P = P_2)$

$$s_3 = \boldsymbol{s}\,(Air_{ha}, T = T_3, P = P_3)$$

$$s_4 = \boldsymbol{s}\,(Air_{ha}, T = T_4, P = P_4)$$

$$Cp_1 = \boldsymbol{Cp}\,(Air_{ha}, T = T_1, P = P_1)$$

$$Cp_2 = \boldsymbol{Cp}\,(Air_{ha}, T = T_2, P = P_2)$$

$$Cp_3 = \boldsymbol{Cp}\,(Air_{ha}, T = T_3, P = P_3)$$

$$Cp_4 = \boldsymbol{Cp}\,(Air_{ha}, T = T_4, P = P_4)$$

$$\eta_{comp} = \frac{h_2 - h_1}{h_{2a} - h_1}$$

$$\eta_{combustor} = \frac{\dot{m}_{inlet,air} \cdot Cp_{air} \cdot (h_3 - h_2)}{Low_{heating\ value}}$$

$$\eta_{turb} = \frac{h_3 - h_{4a}}{h_3 - h_4}$$

$$W_{in} = h_{2a} - h_1$$

$$W_{out} = h_3 - h_{4a}$$

$$Q_{in} = h_3 - h_{2a}$$

$$Q_{out} = h_4 - h_1$$

$$\dot{Q}_{comb} = dodecane_{consumption} \cdot \eta_{combustor} \cdot Low_{heating,value}$$

$$T_{ad,EGR} - T_{exhaust} = \eta_{turb} \cdot T_{ad,EGR} \cdot \left[1 - \left[\left[\frac{P_{ref}}{P_{combustor}}\right]^{\frac{\gamma-1}{\gamma}}\right]\right]$$

$$T_{air,input} - T_{ref} = \frac{T_{ref}}{\eta_{comp}} \cdot \left[\left[\frac{P_{2,kPa}}{P_{ref}}\right]^{\left[\frac{\gamma-1}{\gamma}\right]} - 1\right]$$

$$W_{compressor} = \frac{Cp_{air} \cdot T_{1,k}}{\eta_{comp}} \cdot \left[\left[\left[\frac{P_2}{P_1}\right]^{\left[\frac{\gamma-1}{\gamma}\right]} - 1\right]\right] \cdot \dot{m}_{inlet,air}$$

NB: Using the Cp of air in the combustor and not the Cp of the mixture.

$$W_{turbine} = \eta_{turb} \cdot Cp_3 \cdot T_{ad,EGR} \cdot \left[1 - \left[\left[\frac{P_4}{P_3}\right]^{\left[\frac{\gamma-1}{\gamma}\right]}\right]\right] \cdot (dodecane_{consumption} + \dot{m}_{inlet,air})$$

$$Work_{in} = Cp_{air} \cdot (T_{air,input} - T_{ref})$$

$$Combustor = Cp_{air} \cdot (T_{ad,EGR} - T_{combustion,air})$$

$$Turbine = Cp_{air} \cdot (T_{exhaust} - T_{ad,EGR})$$

$$Q_{combustor} = (dodecane_{consumption} + \dot{m}_{inlet,air}) \cdot (h_3 - h_{2a})$$

$$W_{net} = W_{turbine} - W_{compressor}$$

$$Back_{work\ ratio} = \frac{W_{compressor}}{W_{turbine}}$$

EGR fuel consumption

$$X_{fuel,use} = \frac{1 - N_{fuel}}{a_{egr,frac} + a_{egr,frac} \cdot 3.76 + X_{O_2,EGR} + X_{CO_2,EGR} + X_{N_2,EGR} + N_{fuel}}$$

$$Fuel_{needed} = X_{fuel,use} \cdot \dot{m}_{dodecane}$$

$$Dodecane_{consumption} = Fuel_{needed} + \dot{m}_{dodecane}$$

Net power available

$$Power_{net} = massflow_{air,input} \cdot Cp_{air} \cdot (T_{ad,EGR} - T_{4,K}) - massflow_{air,input} \cdot Cp_{air} \cdot (T_{combustion,air} - T_{1,K})$$

Combustion product analysis

$$N_{prod,CO_2} = N_{EGR} \cdot X_{CO_2,EGR} + (X \cdot N_{dodecane})$$

$$N_{prod,H_2O} = E \cdot N_{dodecane}$$

$$N_{prod,O_2} = \left(N_{combustion,air} \cdot X_{O_2,atm}\right) + \left(N_{EGR} \cdot X_{O_2,EGR}\right) - \left(N_{prod,CO_2} + \frac{N_{prod,H_2O}}{2}\right)$$

$$N_{prod,N_2} = \left(N_{combustion,air} \cdot X_{N_2,atm}\right) + \left(N_{EGR} \cdot X_{N_2,EGR}\right)$$

$$N_{prod,AR} = \left(N_{combustion,air} \cdot X_{AR,atm}\right) + \left(N_{EGR} \cdot X_{AR,EGR}\right)$$

$$N_{prod,total} = N_{prod,CO_2} + N_{prod,H_2O} + N_{prod,O_2} + N_{prod,N_2} + N_{prod,AR}$$

$$X_{CO_2,prod} = \frac{N_{prod,CO_2}}{N_{prod,total}}$$

$$X_{H_2O,prod} = \frac{N_{prod,H_2O}}{N_{prod,total}}$$

$$X_{O_2,prod} = \frac{N_{prod,O_2}}{N_{prod,total}}$$

$$X_{N_2,prod} = \frac{N_{prod,N_2}}{N_{prod,total}}$$

$$X_{AR,prod} = \frac{N_{prod,AR}}{N_{prod,total}}$$

$$\dot{m}_{prod,CO_2} = N_{prod,CO_2} \cdot MW_{CO_2}$$

$$\dot{m}_{prod,H_2O} = N_{prod,H_2O} \cdot MW_{H_2O}$$

$$\dot{m}_{prod,O_2} = N_{prod,O_2} \cdot MW_{O_2}$$

$$\dot{m}_{prod,N_2} = N_{prod,N_2} \cdot MW_{N_2}$$

$$\dot{m}_{prod,AR} = N_{prod,AR} \cdot MW_{AR}$$

$$\dot{m}_{prod,sum} = \dot{m}_{prod,CO_2} + \dot{m}_{prod,H_2O} + \dot{m}_{prod,O_2} + \dot{m}_{prod,N_2} + \dot{m}_{prod,AR}$$

Turbine inlet temperature (TRIT) calculation

$$H_{react,EGR} = N_{fuel} \cdot (\Delta_{H_{dodecane,ref}} + X_{CO_2,EGR} \cdot \left(\Delta_{H,CO_2,ref} + \Delta_{sensible,CO_2}\right) + Cp_{CO_2,react} \cdot \left(T_{combustion,air} - T_{ref}\right) + X_{N_2,EGR} \cdot \left(\Delta_{H,N_2,ref} + \Delta_{sensible,N_2}\right) + Cp_{N_2,react} \cdot \left(T_{combustion,air} - T_{ref}\right) + X_{O_2,EGR} \cdot \left(\Delta_{H,O_2,ref} + \Delta_{sensible,O_2}\right) + Cp_{O_2,react} \cdot \left(T_{combustion,air} - T_{ref}\right) + a_{egr,frac} \cdot \left(\Delta_{H,O_2,ref} + \Delta_{sensible,O_2}\right) + Cp_{O_2,react} \cdot \left(T_{combustion,air} - T_{ref}\right) + a_{egr,frac} \cdot 3.76 \cdot \left(\Delta_{H,N_2,ref} + \Delta_{sensible,N_2}\right) + Cp_{N_2,react} \cdot \left(T_{combustion,air} - T_{ref}\right))$$

$$H_{prod,EGR} = D \cdot \left(\Delta_{H,CO_2,ref} + Cp_{CO_2,prod} \cdot \left(T_{ad,EGR} - T_{ref}\right)\right) + E \cdot \left(\Delta_{H,H_2O,ref} + Cp_{H_2O,prod} \cdot \left(T_{ad,EGR} - T_{ref}\right)\right) + F \cdot \left(\Delta_{H,N_2,ref} + Cp_{N_2,prod} \cdot \left(T_{ad,EGR} - T_{ref}\right)\right) + G \cdot (\Delta_{H,O_2,ref} + Cp_{O_2,prod} \cdot \left(T_{ad,EGR} - T_{ref}\right))$$

$$H_{react,EGR} = H_{prod,EGR}$$